THE UNIVERSITY OF QUEENSLAND

AUSTRALIA

Neonatal EEG source localization

Maryam Odabaee

Bachelor of Science (Electronic Engineering),

Master of Science (Telecommunication Engineering)

A thesis submitted for the degree of Doctor of Philosophy at

The University of Queensland in 2015

School of medicine

Abstract

Knowledge of the relationship between functional brain activity and its anatomical source is vital in many clinical situations. A multidisciplinary research approach is necessary to enhance understanding of the basic mechanisms of normal and pathological brain functions. Although functional neuroimaging techniques such as functional Magnetic Resonance Imaging (fMRI) facilitate non-invasive access to the active brain, the low temporal resolution necessitates using alternative techniques to study brain dynamics. Electroencephalography (EEG) is a non-invasive method for acquiring neural information with high temporal resolution which measures electric potential over the scalp corresponding to neural activity. EEG source localization (ESL) is a technique applied to EEG to localize the sources of the measured potentials. This technique has been applied to EEG in adults in the studies of physiological, psychological, pathological, and functional brain abnormalities such as tumours and epilepsies.

There are indications of the early brain developmental roots of specific abnormalities such as autism, Williams syndrome and schizophrenia that are observed in certain developmental and neuropsychiatric disorders. However, these observations have been performed only in adults. Indeed, despite the necessity of research in neonatal brain functional analysis for medical care of preterm and ill infants, there is limited research in neonatal ESL due in part to limitations in acquiring the relevant parameters of the neonatal head.

The overall objective of this thesis is to improve neonatal health care through enhancing non-invasive neonatal brain monitoring by developments in neonatal ESL. The accuracy of neonatal ESL is critically dependant on the quality of the head model whose main components, conductivity, thickness, and homogeneity of different layers have not been established. The number of electrodes needed to capture neonatal EEG in full spatial detail is another missing parameter of importance in extracting information about functional brain activity from neonatal scalp recordings. The last step to achieve this objective, neonatal ESL development, is proposing and applying an accurate algorithm to estimate neural currents from scalp potentials, i.e., to solve the inverse EEG problem.

This thesis proposes methodologies for estimating the required neonatal head model parameters and then solves the inverse EEG problem in newborns. This has been completed in three steps by: (i) estimating the source depth and spatial resolution of neonatal EEG, (ii) estimating appropriate head model conductivity values including the effect of fontanelles on neonatal skull conductivity, and (iii) fitting an inverse solution to the neonatal ESL problem. Solving EEG inverse problem in this thesis refers to computing the inverse solution in a particular case. After completing these steps, the procedure is validated and evaluated through simulated and real EEG datasets.

Parameters such as neonatal skull conductivity cannot be directly calculated in newborns due to ethical constraints. Therefore, tasks I and II were completed by applying empirical methods along with simulations using the Boundary Element method (BEM) and Finite Element Method (FEM) to indirectly estimate the unknown in vivo neonatal head model parameters.

The last task was completed through applying subspace separation and time-frequency signal processing techniques to solve the inverse EEG problem. Time Frequency MUltiple Signal Classification (TF-MUSIC), which uses the orthogonality between estimated noise subspace and the Lead Field Matrix (LFM) to find the best source locations / orientations, was enhanced by applying image processing techniques to substitute subjective steps in the prior implementations of the TF-MUSIC algorithm.

The major findings of this study are:

A) The amount of unique information in neonatal scalp EEG is much richer than has been commonly assumed. The Nyquist frequency for spatial EEG sampling is (~0.5-0.8 c/cm) that is equivalent to a wavelength of 1.25-2 cm which would translate to the need for interelectrode spacing of about 3-5mm to capture full spatial detail.

B) Source depth strongly affects spatial power spectral density (PSDx) as does skull conductivity. Simulation experiments support previous suggestions that the depth of the dipole representing the cortical source is about 10 mm.

C) Fontanelles of the neonatal skull have conductivity that is not statistically significant different from other areas of the skull.

D) Comparing different skull conductivities from 0.003 to 0.3 S/m in models shows that the spatial decay of real neonatal EEG data is best reproduced when skull conductivity values 0.06-0.2 S/m are used. These conductivity values are orders of magnitude higher than used in adult head models.

E) The TF-MUSIC algorithm reconstructed original source distribution even in low signal to noise situations where it was applied to a range of realistic simulated neonatal EEGs with different time-frequency domain signatures. The realistic simulated neonatal EEGs were generated using the realistic neonatal head model which was produced based on segmented neonatal brain MRI and the estimated parameters. The performance of the TF-MUSIC algorithm was calculated using an introduced performance metric.

F) Visually evoked potentials (VEP) EEG data was selected to evaluate the TF-MUSIC algorithm in its application to the real neonatal EEG. The maximum of the TF-MUSIC output, i.e. the source location determined by the algorithm, was in the occipital lobe, the expected site of cortical representation of VEP data.

The observation of highly varying spatial patterning is consistent with the idea that the development of infant cognition may be able to be studied by analysis of the formation of spatiotemporal patterns like cinematic frames that in some respects resemble “neural avalanches”. Capturing these with novel dense array EEG devices, may open a novel window to capturing the details. The implication of these outcomes is important: from opening a new opportunity for source level connectivity analysis of emerging large scale brain processes involved in the development of perception and cognition through to providing an important tool to study pathological conditions such as neonatal brain seizures and the effectiveness of interventions to improve brain outcomes.

Declaration by author

This thesis is composed of my original work, and contains no material previously published or written by another person except where due reference has been made in the text. I have clearly stated the contribution by others to jointly-authored works that I have included in my thesis.

I have clearly stated the contribution of others to my thesis as a whole, including statistical assistance, survey design, data analysis, significant technical procedures, professional editorial advice, and any other original research work used or reported in my thesis. The content of my thesis is the result of work I have carried out since the commencement of my research higher degree candidature and does not include a substantial part of work that has been submitted to qualify for the award of any other degree or diploma in any university or other tertiary institution. I have clearly stated which parts of my thesis, if any, have been submitted to qualify for another award.

I acknowledge that an electronic copy of my thesis must be lodged with the University Library and, subject to the policy and procedures of The University of Queensland, the thesis be made available for research and study in accordance with the Copyright Act 1968 unless a period of embargo has been approved by the Dean of the Graduate School.

I acknowledge that copyright of all material contained in my thesis resides with the copyright holder(s) of that material. Where appropriate I have obtained copyright permission from the copyright holder to reproduce material in this thesis.

Publications during candidature

a) Peer-reviewed Journal Articles

[1]. **M. Odabaee**, A. Tokariev, S. Layeghy, M. Mesbah, P. B. Colditz, C. Ramon and S. Vanhatalo, "Neonatal EEG At Scalp Is Focal And Implies High Skull Conductivity In Realistic Neonatal Head Models," Neuroimage, vol. 96, pp. 73-80, 2014.

[2]. **M. Odabaee**, W. J. Freeman, P. B. Colditz, C. Ramon, and S. Vanhatalo, "Spatial Patterning Of The Neonatal EEG Suggests A Need For A High Number Of Electrodes," Neuroimage, vol. 68, pp. 229-235, 2013.

b) Conference Articles

[1]. **M. Odabaee**, S. Layeghy, M. Mesbah, G. Azemi, B. Boashash, P. Colditz and S. Vanhatalo, "EEG Amplitude And Correlation Spatial Decay Analysis For Neonatal Head Modelling," in Information Science, Signal Processing and their Applications (ISSPA), 2012 11th International Conference on, 2012, pp. 882-887.

Publications included in this thesis

a) Peer-reviewed Journal Articles

[1]. **M. Odabaee**, A. Tokariev, S. Layeghy, M. Mesbah, P. B. Colditz, C. Ramon and S. Vanhatalo, "Neonatal EEG At Scalp Is Focal And Implies High Skull Conductivity In Realistic Neonatal Head Models," Neuroimage, vol. 96, pp. 73-80, 2014.

Contributor	Statement of contribution
Maryam Odabaee	- contributed to the concept, design of study and analysis (60%), - performed the literature survey (100%), - implemented the codes (100%), - contributed to the first drafts (40%), - contributed to editing the manuscript (40%), - contributed to the technical work (70%).
Anthon Tokariev	- contributed to the technical work (10%).
Siamak Layeghy	- contributed to the technical work (10%).
Mostefa Mesbah	- contributed to the concept, design of study and analysis (10%), - contributed to editing the manuscript (10%).
Paul Colditz	- contributed to editing the manuscript (10%).
Ceon Ramon	- contributed to the technical work(10%).
Sampsa Vanhatalo	- contributed to the concept, design of study and analysis (30%), - contributed to the first drafts (60%), - contributed to editing the manuscript (40%).

[2]. **M. Odabaee**, W. J. Freeman, P. B. Colditz, C. Ramon, and S. Vanhatalo, "Spatial Patterning Of The Neonatal EEG Suggests A Need For A High Number Of Electrodes," Neuroimage, vol. 68, pp. 229-235, 2013.

Contributor	Statement of contribution
Maryam Odabaee	- contributed to the concept, design of study and analysis (60%), - performed the literature survey (100%), - implemented the codes (100%), - contributed to the first drafts (40%), - contributed to editing the manuscript (50%), - contributed to the technical work (80%).
Walter Freeman	- contributed to the technical work (10%).
Paul Colditz	- contributed to editing the manuscript (10%).
Ceon Ramon	- contributed to the technical work (10%).
Sampsa Vanhatalo	- contributed to the concept, design of study and analysis (40%), - contributed to the first drafts (60%), - contributed to editing the manuscript (40%).

b) Conference Articles

[1]. **M. Odabaee**, S. Layeghy, M. Mesbah, G. Azemi, B. Boashash, P. Colditz and S. Vanhatalo, "EEG Amplitude And Correlation Spatial Decay Analysis For Neonatal Head Modelling," in Information Science, Signal Processing and their Applications (ISSPA), 2012 11th International Conference on, 2012, pp. 882-887.

Contributor	**Statement of contribution**
Maryam Odabaee	- contributed to the concept and design of study (50%), - performed the literature survey and analysis (100%), - implemented the codes (100%), - wrote the first drafts (80%), - contributed to editing the manuscript (50%). - contributed to the technical work (90%)
Siamak Layeghy	- contributed to the technical work (10%).
Mostefa Mesbah	- contributed to the concept and design of study (20%), - contributed to editing the manuscript (10%).
Ghasem Azemi	- contributed to editing the manuscript (10%).
Boualem Boashash	- contributed to editing the manuscript (10%).
Paul Colditz	- contributed to editing the manuscript (10%).
Sampsa Vanhatalo	- contributed to the concept and design of study (30%), - contributed to the first drafts (20%), - contributed to editing the manuscript (10%).

Contributions by others to the thesis

The following researchers contributed to this thesis in terms of the concept and design of the studies; technical work; analysis and interpretation of the results:

- Dr Sampsa Vanhatalo
- Dr Mostefa Mesbah,
- Dr Ghasem Azemi,
- Prof Ceon Ramon
- Prof Walter Freeman
- Siamak Layeghy
- Anthon Tokariev
- Prof Paul Colditz
- Prof Boualem Boashash

Statement of parts of the thesis submitted to qualify for the award of another degree

None

Acknowledgements

The accomplishment of my PhD was made only possible by continuous support of my family and directions of my advisory team.

I would like to extend my sincere appreciation to Dr Sampsa Vanhatalo for his great enthusiasm, inspiration and supportive guidance throughout my research project. I would like to express my deepest gratitude to him for opening the door of EEG signal processing to me and letting me experience the brain research. He not only taught me these valuable academic skills, but also the value of ethics and support in the research environment.

I sincerely thank Dr Mostefa Mesbah, Dr Ghasem Azemi and Prof Paul Colditz for their encouragement and insightful comments throughout my research. I appreciate the efforts they made to make the drafts of my manuscripts and thesis proofread, as English is my second language. I would like also to sincerely thank Dr Julie Wixey and Dr Benjamin Wallace long for reading my thesis drafts and providing their comments. I also deeply appreciate Prof Sabine Van Huffel from KU Leuven who supported my scholar visit to KU Leuven and provided the neonatal EEG datasets for my research project.

I thankfully acknowledge my sole financial support in this PhD, the Australian Postgraduate Award.

I am appreciative to Prof Michael Breakspear, Prof Stephen Wilson, Dr Simon Finnigan and Dr Tracey Bjorkman, who provided me their precious feedbacks during my PhD milestones. I would like also to express my appreciation to my fellow colleagues at UQ Steph, Shannon, Amir, Amir Hossein Ansari from KU Leuven, and others who their names will make a long list. I am also grateful to my friends in Australia and Iran who made a lot of memorable moments for me and all the good times we have had together outside of the research environment, Dr Hossein Elahi Ghomshei, Dr Parvin Zandi, Dr Hamidreza Amindavar, Dr Sirous Mobini and Alexandra McDonald.

Last but not least, my deepest appreciations and thanks goes to my mother, my husband, my son, my two brothers and my sister, for their support and inspiration during my PhD.

Keywords

Electroencephalogram, neonatal brain, neonatal head model, spatial patterning of EEG, neonatal skull conductivity, EEG source localization, time-frequency analysis, spatial time frequency distribution, multiple signal classification, region of interest.

Australian and New Zealand Standard Research Classifications (ANZSRC)

ANZSRC code: 090609, Signal Processing, 40%

ANZSRC code: 090399, Biomedical Engineering not elsewhere classified, 60%

Fields of Research (FoR) Classification

FoR code: 0906, Electrical and Electronic Engineering, 40%

FoR code: 0903, Biomedical Engineering, 60%

Table of content

List of figures

List of tables

List of Abbreviations used in the thesis

ANOVA: Analysis of Variance

ASA: Advanced Source Analysis

BEM: Boundary Element Method

BESA: Brain Electric Source Analysis

CAR: Common Average Reference

CSF: Cerebrospinal Fluid

CNS: Central Nervous System

CW: Choi-Williams distribution

DIS: Distributed Inverse Solutions

dSPM: dynamic Statistical Parametric Maps

ECD: Equivalent Current Dipole

EDF: European Data Format

EEG: Electroencephalography

EMBD: Extended Modified B-Distribution

ESL: EEG source localization

ERP: Event Related Potentials

FEM: Finite Element Method

FIR: Finite Impulse Response

fMRI: functional Magnetic Resonance Imaging

FOCUSS: Focal Underdetermined System Solution

GA: Gestational Age

hdEEG: high density Electroencephalography

IES-MUSIC : Improved Sequential MUSIC

LAURA: Local Auto Regressive Average

LCMV: Linearly constrained minimum variance

LFM: Lead Field Matrix

LORETA: Low Resolution Electrical Tomography

MEG: Magnetoencephalography

MLP: Median Low Pass

MNE: Minimum Norm Estimate

MRI: Magnetic Resonance Imaging

MUSIC: Multiple signal classification

nEEG: Neonatal Electroencephalography

nESL: Neonatal EEG Source Localization

NICU: Neonatal Intensive Care Unit

PET: Positron Emission Tomography

PSDx: spatial Power Spectral Density

PWVD: Pseudo Wigner-Ville Distribution

R-MUSIC: Recursive Multiple signal classification

RAP-MUSIC: Recursively Applied and Projected Multiple signal classification

RIO: Region of Interest

SAT: Spontaneous Activity Transient

SD: Standard Deviation

SLOFO: Shrinking LORETA-FOCUSS

SNR: Signal to Noise Ratio

SPECT: Single Photon Emission Computer Tomography

SSLOFO: Standardized shrinking LORETA-FOCUSS

STFD: Spatial Time Frequency Distribution

STFT: Short Time Fourier Transform

SVD: Singular Value Decomposition

TF-MUSIC: Time-Frequency Multiple signal classification

TFD: Time Frequency Distribution

VEP: Visually Evoked Potentials

WGN: White Gaussian Noise

wMNE: Weighted Minimum Norm Estimate

WT: Wavelet Transform

WVD: Wigner-Ville Distribution

CHAPTER 1: THESIS BACKGROUND

1.1 Introduction

Knowledge of the relationship between functional brain activity and its anatomical source, i.e. functional organization of the brain, is important in many clinical situations that include diagnosis and treatment of pathologies that impair normal brain function such as intractable epilepsy, schizophrenia, depression, and Parkinson's and Alzheimer's diseases [1, 2]. This is of necessity a multidisciplinary research field that enhances our understanding of the basic mechanisms of cognitive processes, processes that underlie normal and pathological brain functions [3, 4].

Functional neuroimaging techniques such as Single Photon Emission Computer Tomography (SPECT), Positron Emission Tomography (PET), and functional Magnetic Resonance Imaging (fMRI) have made it possible to non-invasively access the active brain [5]. Cognitive tasks activate several large-scale brain regions which determine the dynamic interactions with the others [5, 6]. These functional imaging techniques exploit physiological changes that fluctuate in the scale of several hundreds of milliseconds at best. Their temporal resolution is limited and rapid brain dynamics cannot be studied using these techniques [7]. Methods such as covariance-based analysis of PET images [8] and the hemodynamic response of single-trial event-related fMRI [9] have been proposed to improve previous methods and solve this problem, but they have been only partly successful [5].

Electroencephalography (EEG) is a non-invasive method for acquiring neural information with a high temporal resolution. It measures electrical potential corresponding to neural activities over the scalp by means of sensors directly attached to the scalp. EEG as a clinical tool has had widespread application to examining different abnormal electrical behaviour in neurons [1]. The millisecond-range temporal resolution of EEG [10] has made it possible to obtain evidence about some brain states such as epileptic state during seizure that cannot be provided by other modalities [11]. Another advantage of EEG over other modalities except Magnetoencephalography (MEG) is its capability to

determine causality within the neural assemblies in addition to detecting them [10]. MEG is EEG's complementary technique that measures the magnetic induction outside the head generated by the electrical brain activity [1]. However, due to its higher cost and lesser flexibility, MEG is a less desired option.

EEG signals can also be utilized to extract the functional organization of the brain. This procedure is realized in the form of a mathematical analysis known as the EEG source localization (ESL). This technique has been widely applied on adult EEG. However, due to limitation of acquiring the relevant parameters of the neonatal head, there is no report of successful application of this technique to neonatal EEG. This dissertation investigates the functional organization of the neonatal brain and proposes novel methodologies for studying newborn brain functionality through scalp EEG analysis and Magnetic Resonance Imaging (MRI). Three aspects of the neonatal EEG source localization (nESL) problem have been investigated: i) appropriate head model conductivity values, ii) spatial resolution of neonatal EEG and source depth and iii) fitting the inverse solution. Empirical methods were applied to indirectly estimate the unknown *in vivo* neonatal head model parameters. These parameters were then employed to establish a realistic neonatal head model that was used both in the generation of simulated realistic EEG and later in the validation of the proposed source localization method.

This approach has been enhanced through replacing the subjective stages of legacy ESL methods by applying image processing techniques to the time-frequency transformation of the EEG signals. A new ESL performance metric is also introduced which not only measures the dipole localization error, but the effect of the presence of other sources. The approach is evaluated by applying it to event related potentials (ERP) and visually evoked potentials (VEP) EEG recordings of healthy term, and preterm infants. This chapter describes the background and the rationale of the thesis which precedes a description of the significance, objectives and overall contributions of the work. It concludes with an outline of the whole thesis.

1.2 Background of Neonatal EEG Source Localization

Despite its superior temporal resolution, the spatial resolution of EEG is less than other functional brain imaging methods because of the separation between EEG electrodes and current sources inside the head, i.e. neurons, by several layers with different conductivity values [12]. Moreover, since various source arrangements inside the brain or cortex can result in a similar potential distribution on the scalp, the visual interpretation of EEG cannot result in the accurate location of neural generators [11, 13]. Accordingly, inferring the underlying generator source distribution in the brain for a potential distribution on the scalp is ambiguous and the only approved method to sensibly estimate the corresponding sources with more detailed spatial information is to apply a mathematical procedure referred to as the inverse problem solution [13, 14].

ESL techniques attempt to estimate the current sources within the brain that produced the EEG signals from electrodes. ESL is an important tool used to estimate the intracerebral generators of the potentials observed on the scalp in both clinical neuroscience and cognitive neuroscience research [13, 15]. The clinical applications of ESL in neurology have been mainly focused on the epilepsy and yet there is an increasing interest in studying motor evoked potentials by means of ESL as well. Similarly, cognitive neuroscience studies have used ESL to investigate temporal information in the ERP. In addition, psychiatry and psychopharmacology have employed ESL to study sources in specific frequency bands [13].

In view of the fact that there are an infinite number of different compositions of current sources that can give rise to an identical potential distribution over the scalp, there are an infinite number of equivalent inverse solutions for a single potential distribution. This necessitates applying some prior assumptions or extra information to determine the appropriate solution [1]. Consequently this further information / constraint describe a main characteristic of each individual ESL method. This additional information / *a priori* assumption / s can be introduced in the form of source modelling / distribution or the volume conductor's constraints [11, 13]. Accordingly, as long as new knowledge of creation of source signal or the volume conductor is generated which can be incorporated as *a priori*

constraints in the inverse problem, new solutions to the inverse problem exist that can be formulated in the form of a new source localization method [13].

Based on recent works in neuroimaging [16-18] and in developmental neurobiology [19-21], it is clear that brain functions are already highly specialized at early developmental stages. Functional assessment of neonatal brain has been encouraged by the increasing interest in medical care of preterm and ill infants as well as recent advances in developmental neuroscience. Neonatal brain activity can reliably be recorded with neonatal EEG, in a manner similar to that used in the adult, [22]. However, the neonatal EEG (nEEG) includes numerous features such as focal or multi-focal transients [23, 24] which are normal and differentiate it from adult EEG. These are relatively sharp fluctuations in the scalp potentials that are likely to be produced by focal sources within the brain.

Despite the wide range of methods currently applied in adult EEG source localization, no specific method has been proposed to address the nESL problem. This is mainly because of differences in electrostatic parameters and head geometry [25, 26]. There is no agreement on which methods may be most appropriate for nESL. The accuracy of source localization is critically dependent on the quality of the head model [27]. The two essential and critical components of the head volume conductor model include the geometry and conductivity profile of different layers. The accuracy of both parameters has a direct impact on the accuracy of source localization [28, 29]. Lack of accurate knowledge about these parameters in the neonatal head model has been the main obstacle in applying the existing adult source localization techniques. Fitting a head model for newborns requires data relating to conductivity, thickness, and homogeneity of different layers especially the skull, and the effect of the fontanelles. Neither direct nor indirect information is currently available about the conductivity of the cartilage layer and the fontanelles. The development of a proper neonatal head model requires that this lack of knowledge is dealt with effectively and this will then allow the assessment of whether adult source localization techniques are well-adapted to neonates [25].

Another key parameter that needs to be considered in an accurate nESL is the proper range of source depth in the neonatal head model. The effect of source depth has been successfully investigated in

adult ESL techniques but it has not been sufficiently studied in neonates [30]. Since electrical and magnetic signals are attenuated by distance based on the inverse square law, the distance between EEG electrodes and the brain/cortex is another key variable in the accuracy of each ESL method. However, there is insufficient knowledge of variation of brain-scalp distance in different cortical regions in neonates and children [31, 32]. Consequently, each prospective source model needs to carefully consider the neonatally relevant range of tissue conductivities and source depths when source localizing cortical activity in neonates [30].

The number of electrodes needed to capture neonatal EEG in full spatial detail is another parameter of importance in extracting information about the functional brain activity from neonatal scalp recordings. It is not clear how much information can be obtained from the neonates scalp. This richness in amplitude texture can be perceived as "spatial patterning", i.e. spatial distribution of the neonatal scalp EEG and it has been measured in adults by estimating the spatial frequency content of the scalp EEG [33-35]. Since the number of actual sources that create the potential distribution over scalp is much more than the number of receivers (EEG electrodes), increasing the number of receivers will enhance the accuracy of ESL. The functional assessment of neonatal brain activity is currently thoroughly hampered by the poor spatial resolution provided by conventional neonatal EEG recording with about 10 electrodes that ignores most of the spatial content of neonatal EEG [22]. Accordingly a genuine nESL approach should observe the spatial patterning of the neonatal EEG and determine the value of satisfactory EEG electrode density.

The final stage of a neonatal EEG source localization method is to choose an appropriate inverse solution which will be possible only when all the required information is already present. The inverse problem is to estimate the distribution of sources that fits the given recorded EEG signal from the scalp. The best choice of the inverse solution is strongly dependent on the source model [1, 10, 11, 13, 36]. The main approaches of ESL include Equivalent current dipole (ECD) [37-39] and imaging methods [5, 13, 40, 41]. The assumption of *a priori* knowledge about the number of sources to model the neural generators is the main difference between the two categories. While ECD assumes a limited

known number of dipoles can produce a sufficient approximate of scalp EEG, a huge number of dipoles (normally ~10000 or more) is required producing an adequate approximation of scalp potentials in imaging methods. There is no limitation in this case on the number of current dipoles used to model the source of electrical activity in brain. There is another intermediate approach to approximate the sources that generated the scalp potentials. These are a subcategory of ECD approaches that do not need *a priori* knowledge about the exact number of sources, similar to the distributed sources approach, they scan through the whole brain / cortex volume for a handful of fitting dipoles. These scanning methods constitute an alternative approach in EEG source localization [37, 42].

Selecting an appropriate localization approach for the neonatal EEG inverse problem includes several prerequisites that need to be considered concisely. This choice clearly determines how we interpret the data and every selected approximation will reflect the accepted assumptions or the prior knowledge implemented in the methodology chosen for solving the problem [10]. These assumptions include *a priori* knowledge about the source distribution and number of sources (single/ multiple sources), location of the sources (cortical/deeper sources), source expansion (focal and sparse sources), and time dependent/independent source/s. Based on previous works on adult EEG source localization, methods based on equivalent current dipoles generate more accurate results in somatosensory stimulation [43], in the analysis of epileptic brain activity [44], and interictal spike localization [45, 46] where brain activity is highly focused in a small area. Imaging methods, on the other hand, are more appropriate for the case where large areas of the brain may be involved in the activity and it is not possible to predict the number of active regions in the brain such as in cognitive experiments [10].

1.3 A short review of inverse solutions

The general form of the relationship between the EEG measurements and its generator current sources for the discrete signals can be stated as [36]

$$V = \boldsymbol{L}S + N \quad (1)$$

in which V is the measurement vector, S is the source vector, $\boldsymbol{L}$ is the Lead Field Matrix (LFM) and N is the noise vector introduced into the measurements. Under this notation, the ESL is the procedure to estimate S when V (EEG) and $\boldsymbol{L}$ (LFM) are known. The LFM is the gain value from each source location to the measurement positions and hence, is dependent on the characteristics of the media between the source and destination. As it is a prerequisite for solving the inverse problem, it should be worked out in advance.

Practically, the LFM is calculated in the procedure which is called forward problem solution. Consequently, the inverse solution practically starts with solving the forward problem. In the forward problem, a given electrical source distribution is assumed in order to calculate the potentials on the scalp. Poisson's differential equation along with Neumann and Dirichlet boundary conditions can be used to describe the potentials in a volume conductor generated by the extracellular current from cells. Then the next step is to determine the boundaries to calculate the solution of the pertaining electromagnetic boundary problems [47]. Selecting the volume model and its physical / electrical parameters will determine the method for solution of these equations. In other words, the choice of the head model geometry determines which of the forward solution techniques is applicable. The two main options for the head model include spherical and realistic head models.

The first volume conductor model is a homogeneous spherical head model with three or four concentric layers. In this model, the inner sphere, the intermediate layer and outer layer represent the brain, skull, and scalp respectively. The main advantage of this model is that it accommodates an analytical solution for Poisson's equations when the surface integrals are computed over the simplified geometry of the spherical head model [1]. However, spherical models that can reasonably approximate the superior regions of the brain do not generate satisfactory results in terms of the overall localization accuracy. This is because the head is roughly spherical in this part and therefore realistically shaped models are necessary to represent the whole head [10, 48]. These models are

generated by incorporating anatomical information / imaging to the forward problem. For instance, MRIs are segmented into different regions to identify different tissues such as brain, cerebrospinal fluid (CSF), skull and scalp. The segmented MRI is then used to construct a 3D mesh.

This information makes it possible to find the surface boundaries for brain, CSF, skull and scalp which determine the boundary conditions of the electromagnetic equations [1]. These are surfaces that separate regions of different conductivities. There are two broadly applied numerical methods for solving these equations. The first method, Boundary Element Method (BEM), assumes homogeneity and isotropy over the entire region within boundaries and is computationally more efficient than the other. In the second method, Finite Element Method (FEM), the entire volume conductor is digitized in small elements as tetrahedrons and the Poisson equation is solved for each element [49]. Both methods need knowledge of the conductivity of the head tissues. However, since the exact conductivity of elements is not known, applying the piecewise constant conductivity instead of a spatially varying anisotropic conductivity model, generates similar results in terms of accuracy of the solution [8].

Once the forward problem's equations are solved and the LFM is calculated, the inverse problem can be solved for a given EEG dataset. There are a variety of inverse solutions that are currently applied in the adult ESL problem. These methods can be broadly divided into three major categories, as mentioned above: (i) equivalent current dipole (ECD) or parametric methods, (ii) distributed source or imaging or non-parametric methods, and (iii) intermediate methods [13]. All these methods use a current dipole as an elemental source model to represent an idealized point source. The main characteristic of every localization method depends on the choice of the *a priori* assumptions / extra information implemented in the source distribution or the volume conductor's properties to solve the ill-posed ESL problem. Accordingly the above approaches are the result of different assumptions about the source distribution.

1.3.1 Equivalent current dipole (ECD) approaches

In the first approach, ECD known as dipole fitting or parametric methods, it is assumed that potential measurement over the scalp is generated by a few current dipoles of unknown location and moment parameters. The ESL method then attempts to estimate these unknown parameters through a non-linear numerical method. A solution will exist only if the number of unknown parameters is less than or equal to the number of electrodes. Once some estimates of these unknown parameters are acquired, a potential distribution is calculated by solving the forward problem and the result is compared with the true measurements. The trivial solution to find the best fitting parameters is an exhaustive search through the whole solution space with any possible location and orientation of the sources. This is very demanding and if more than one dipole is assumed it is nearly impossible [50]. Hence, non-linear optimization processes based on directed search algorithms are usually used to find the parameters that generate the potential distribution over the scalp with the *least* difference from the actual EEG measurements. There is a risk of undesirable local minima in these methods in which the algorithm accepts a certain location in the source space because moving in any direction increases the error of the fit [51]. Although the theoretical number of sources is determined by the number of EEG electrodes, the practical number of sources that can be reliably localized by these methods is limited by the complexity of the directed search algorithms and the problem of local minima. The main parametric approaches are non-linear least-squares solvers, Brain Electric Source Analysis (BESA), simulated annealing and finite elements. [1, 10, 11, 13, 36].

1.3.1.1 Least-Squares:

The earliest and most straightforward strategy is to fix the number of sources and use a nonlinear estimation algorithm to minimize the squared error between the EEG data and the fields computed from the estimated sources using a forward model. A key problem with the least-squares method is that the number of sources to be used must be decided *a priori*. Estimates can be obtained by looking

at the effective rank of the data using singular value decomposition (SVD) or through information-theoretic criteria, but in practice several model orders are run and the results are selected based on physiological plausibility. Caution is obviously required since a sufficiently large number of sources can be made to fit any data set, regardless of its quality. Furthermore, as the number of sources increases, the nonconvexity of the cost function results in increased chances of trapping in undesirable local minima [1].

1.3.1.2 Brain electric source analysis (BESA):

It has been shown that the practical limitation of the number of sources can be relaxed if the temporal domain is incorporated in the dipole fitting procedure [52]. The BESA software has implemented this spatio-temporal multiple source analysis technique. In this method, dipoles are assumed to have fixed position and fixed or varying orientation over a given time interval and then the whole block of data is used in the least square fit [53]. It is essential to assume the correct number of initial sources in this method similar to other ECD approaches.

1.3.1.3 Simulated annealing and finite elements:

This is a global optimization approach that uses simulated annealing [54] for the optimization [1]. The basis for optimization is an objective function based on the current-density boundary integrals rather than potential differences in other ECD approaches. It is associated with standard finite-element formulations in two dimensions. The user is also able to define target search regions. Thus, by approaching current density at each electrode to zero, the modelled dipole is varied in such a way that the Neumann and Dirichlet boundary condition is satisfied [55].

1.3.2 Distributed sources approaches

The imaging approaches on the other hand, are based on the assumption that a large number of current dipoles distributed within the brain or on the cortical surface give rise to the potential measurements on the scalp. Imaging methods or non-parametric optimization methods are also referred to as Distributed Source Models, or Distributed Inverse Solutions (DIS). In these methods, there is no need to know the exact number of sources. The brain / cortex in this approach is converted to a mesh of points which is called the source space and a current dipole is supposed to be fixed in each point of this source space (with possibly fixed orientations). However, there is a major difference between the assumptions made on dipoles in the two methods. The dipoles in parametric methods can be localized everywhere in the brain / cortex and can take any orientation. However, in the non-parametric approaches the location / orientation of dipoles are supposed to be known beforehand and the localization method tries to estimate the amplitude of each dipole. In this case, since the only unknowns are the amplitudes of the dipole, the source localization is linear. These methods henceforth approximate the 3D current distribution in the brain.

In the noise free conditions it will be possible to find a current distribution that can exactly produce the measured potential distribution over the scalp. However, it is not the only possible solution that exactly reproduces the measured potentials and there are an infinite number of distributions of current dipoles in the source space with equivalent generated potentials [13, 36]. The non-parametric methods are designed for the localization of brain activities generated by a large number of sources (around 10,000) such as cognitive experiments that cannot be modelled by the few limited number of dipoles of the parametric methods. Alternatively if non-parametric techniques are used to localize highly focal sources such as somatosensory stimulation or epilepsies, these methods lack the precision of parametric methods and show the activity over a large portion of the brain / cortex surface. This is because in these methods a limited number of detectors (e.g. ~ 100) are mapped to a large number of generators (e.g. 10000) and the problem is severely underdetermined [1, 10, 36]. The three main trends in non-parametric ESL include Bayesian framework such as Minimum norm estimates (MNE)

and Low resolution electrical tomography (LORETA), the weighted resolution optimization such as Local Auto Regressive Average (LAURA), and Shrinking and multiresolution methods such as Shrinking LORETA-FOCUSS [10, 11, 13, 36].

1.3.2.1 Bayesian Framework

The Bayesian approach uses the Bayes posterior probability theorem to incorporate *a priori* information about the current source distribution S into the estimation of the sources given the measurements V [1, 36]

$$P(S/V) = \frac{P(V/S) \times P(S)}{P(V)} \quad (2)$$

where $P(S/V)$ is the posterior probability for the current distribution given the potential V and $P(S)$ is *a prior* current distribution which reflects our *a prior* knowledge about it. Practically this is estimated by maximization of the posterior probability [1]

$$\hat{S} = \arg\max_{S}\{P(V/S) \times P(S)\} \quad (3)$$

in which $\hat{S}$ is the estimated current distribution and $P(V/S)$ is the term that depends on the forward model and the true source distribution. The type of *a priori* knowledge $P(S)$ that is incorporated results in different methods. Minimum norm estimate (MNE) and Low resolution electrical tomography (LORETA) are the most famous techniques in this group.

Minimum norm estimates (MNE):

MNE is the estimate of this current distribution without incorporating almost any *a priori* information [56]. It only assumes that the current distributions should have minimum overall power and is

achieved through regularization method [36, 57]. Also a more general assumption in MNE is that the noise and current are normally distributed [58]. The MNE requires minimal assumptions and hence is suitable for the localization of poorly known activity distributions and for tracking activity changes between brain areas as a function of time [59]. However, there is no physiological validation on the MNE's assumption for selecting the solution with the minimum power. In other words, in the activities where there are a large number of active points in the brain, MNE favours superficial sources. This is because less activity is required in superficial areas to generate a certain surface voltage distribution than deeper sources which can lead to erroneous interpretations [13].

- Low resolution electrical tomography (LORETA)

The tendency of MNE to select superficial sources is modified in later methods such as weighted MNE (WMNE) by applying various weighting strategies. In the simplest form, the norm of columns of the LFM, which corresponds to the source space points, are used for the weighting. In the Focal Underdetermined System Solution (FOCUSS) algorithm [60], weights are iteratively modified according to the solutions estimated in the previous step, leading to a non-linear solution. LORETA [61, 62] assumes that the spatial distribution of sources is smooth and hence tries to minimize the Laplacian of the weighted sources. Consequently it gives the depth-compensated inverse solution [36]. In other words, superficial or deeper sources have a similar opportunity to be reconstructed.

The physiological assumption of LORETA is that activity is correlated among the neurons in neighbouring areas of cortex. Although this assumption is generally correct, it has been criticized in that it leads to a spatial scale where such correlations can no longer be reasonably expected [13]. Indeed, there are anatomically close areas of brain such as the medial parts of the two hemispheres with distinct functionality which do not comply with this assumption. Furthermore, the assumption of correlation over relatively large distances has caused LORETA to provide rather blurred, over-smoothed, solutions. Consequently, this technique is not well suited for focal source estimation and some false activities may appear[61].

1.3.2.2 Weighted resolution optimization approaches

This approach is composed of a family of linear distributed solutions such as Local Auto Regressive Average (LAURA) [36, 63] and EPI-FOCUS [64] in which physical constraints into the solution are realized in the form of a local autoregressive average. These are (quasi) linear inverse solutions especially suitable for single, but not necessarily point-like generators, in realistic head models [65].

1.3.2.3 Shrinking methods and multi resolution methods

A concentrated source solution may be obtained by applying suitable iterations to the solution of a distributed source model. This is the basis in the inverse solutions based on the Shrinking and multi resolution methods.

- Shrinking LORETA-FOCUSS (SLOFO)

To reduce computation time and increase source resolution, SLOFO combines the ideas of LORETA and FOCUSS and makes iterative adjustments [36]. The weighting matrix and the solution space are both adjusted in this method [66]. It enhances the strength of some prominent dipoles in the solution and decays the strength of other dipoles. The starting point of the algorithm is the smooth LORETA solution.

- Standardized shrinking LORETA-FOCUSS (SSLOFO)

This procedure is similar to the Shrinking LORETA-FOCUSS. Features of high resolution (FOCUSS) and low resolution (WMN, Shrinking LORETA (sLORETA)) methods are used to extract regions of dominant activity as well as to localize multiple sources within those regions. SSLOFO gives better results than FOCUSS when there are many extended sources [36]. It also reconstructs different source configurations better than WMN and sLORETA [14].

1.3.3 Scanning methods

The last approach is the intermediate alternative approach in which the presence of an equivalent current dipole is scanned in the entire source space without the necessity of *a priori* knowledge of the number of sources. In other words, while these methods can localize sources with a high resolution similar to ECD approaches, they do not need the exact number of sources to be determined beforehand [1]. In these methods a metric, which is an estimator of the contribution of each putative source location to the data, is derived either via spatial filtering techniques or signal classification indices (subspace separation). Source locations in these methods are assumed the whole points of a 3D grid or mesh that constitutes the source space spanned over the whole brain or cortical surface. The ESL in these methods finds the best performing location (orientation) among the whole points of source space [1, 38, 42]. Consequently, the output of ESL in these methods is comprised of a matrix of values for the whole grid points. Distributed source methods similarly generate an output value for each grid point that resembles the output of dipole scan methods. Though, the interpretation of the outputs of the two methods is different. For a small number of sources, the location of the maximum metric in dipole scanning methods is comparable with the location of the dipole with maximum amplitude in distributed source approaches. The major techniques based on scanning method include linearly constrained minimum variance (LCMV) beamformer and multiple signal classification (MUSIC) and their variations.

1.3.3.1 Linearly constrained minimum variance (LCMV):

The main idea in beamforming is to discriminate between signals arriving from a location of interest and those originating elsewhere by means of spatial filtering on data from a sensor array. The LCMV beamformer was developed in the array signal processing community as a means for combining the outputs of multiple antennae to produce a single output with the characteristics of a single larger antenna. [1, 67].

In the application of LCMV beamformer in MEG and EEG it is used as a virtual depth electrode. It minimizes the contribution from all other sources to monitor a single point in the brain by forming a linear combination of the EEG channels. In this way all possible source locations in the brain are monitored by scanning the location of this virtual depth electrode throughout the brain.

The performance of the LCMV beamformer is limited by the transient and often correlated nature of neural activation in different parts of the brain. This is because the process of minimization of the effect of other sources is affected by cancellation of the signal of interest that is correlated to other sources. Consequently, the LCMV beamformers can only be suitable for the cases where there is a limited number of strongly correlated independent components in the data [1, 10].

1.3.3.2 Multiple signal classification (MUSIC)

MUSIC was developed in the array signal processing community and then applied in the EEG signal processing [68]. It can be used to localize single or multiple simultaneous sources from an EEG signal. Fixed orientation dipoles as well as the rotating dipoles or a mixture of both can be used to model the current sources. This is a spatio-temporal approach which incorporates the temporal domain to estimate the signal subspace and use it for localizing the sources. The signal subspace is estimated in the SVD [36] of the covariance matrix of EEG signals. First a part of EEG signals are selected in time domain according to the research question in hand and the desired physiological features. Next the covariance matrix of this part of the signal is calculated and then its singular value decomposition is found as

$$M = U\Sigma V^T \tag{4}$$

in which U is known as the left singular vectors and the signal subspace is estimated to be spanned by U_S the p (the number of sources) first left most columns of U. The algorithm scans through a three-dimensional (3-D) head volume and computes projections onto an estimated signal subspace.

In other words, columns of LFM that are corresponding to a particular dipole are scanned for finding the maximum projection to signal subspace.

Although the MUSIC method can estimate the sources with a high accuracy in the cases where the number of sources is not large, its performance reduces for a large number of sources that can happen in activities such as cognitive brain actions. Errors in the estimation of the signal subspace can affect the performance of the localization of multiple sources. Moreover, when the dimension of the source space increases it becomes difficult to find several local maxima in the MUSIC metric. When the projection to signal subspace is computed only at a finite set of grid points, some problems may also occur [1, 69].

Several variants of MUSIC such as Recursive MUSIC (R-MUSIC) [70], recursively applied and projected (RAP-MUSIC) [42], and Time-Frequency MUSIC (TF-MUSIC) [71-74] have been proposed to modify the shortcomings of the MUSIC method. TF-MUSIC approach uses the time domain and frequency domain simultaneously to estimate the signal subspace. It has been shown that neuronal activities in a human brain and their electrophysiological data such as EEG are basically nonstationary signals [75] and therefore can be better characterized and analysed by means of time-frequency analysis [76]. It is possible to use time-frequency distribution [77] of signals to identify a region of interest (ROI) including the desired bio-physiological features [74]. This will enhance the signal to noise ratio (SNR) effectively and the performance of the localization method effectively will be improved. However, the subjectivity in the identification of ROI can affect the performance in low SNR values and result in inaccurate source arrangements.

To summarize, use of the ECD based methods is most appropriate when the source of the brain activity is expected to be focal and there is a prior knowledge of exact number of sources. The distributed sources methods are more appropriate to study complex brain activities which include spatially extended sources or unpredicted active regions of the brain [10, 11]. The scanning methods, on the other hand, must be used when the application of EEG includes focal sources but there is no prior knowledge about the exact number of sources. The inverse solution of an individual ESL

problem is selected upon the requirements and the conditions of the problem. Accordingly, the specific prerequisites of the neonatal EEG research question should be utilized to limit the selection criteria for nESL approach. The selection criteria in the neonatal EEG source localization problem can be summarised in two major necessities.

First, the method should be fitted to localize focal sources precisely. The focal fluctuations in the amplitude of neonatal EEG are the common features of normal and abnormal neonatal EEG with the prominent occurrence [22, 78, 79]. Since these features, which differentiate neonatal EEG from the adult EEG, are assumed to be generated by the focal sources, the candidate inverse method for nESL should be selected from the approaches adapted to fulfil this condition. In addition to normal neonatal EEG, the prospective method should be fitted for accurate localization of sources in ERP and pathologic studies in neonates such as seizure. These conditions are better satisfied by the approaches that use a small number of dipoles to model the current sources i.e. the ECD and the scanning methods.

Secondly, the selected method should be able to discriminate between the separate EEG events seen in the dense array EEG recordings in terms of their sources. The recordings of neonatal EEG with 64 channels display many EEG events that look like they are distinct events. Any proposed neonatal source localization technique should be able to separate these distinct events in time and frequency domains and disclose their differences in terms of the sources accordingly. This can be realized through using techniques which take into the account time and frequency domains simultaneously. It is possible to use features of signal in both domains to identify a ROI which includes the desired events. Methods such as TF-MUSIC has been suggested and applied on adult MEG signals to fulfil this necessity [72-74].

There are also minor priorities in the selection of a neonatal EEG source localization scheme which can be satisfied according to the individual research project. It is specially the case when the nESL output is used as an input to other neonatal EEG research projects. In this case, the specific requirements of the research study needs to be included in the corresponding selection criteria. For

instance as a valuable research project, nESL can be utilized to establish a brain level connectivity analysis tool for the neonatal EEG. The method then must be able to localize multiple simultaneous sources, a feature present in MUSIC-based methods [14, 37, 71, 80, 81]. Another example of this type of prerequisites is the ability to locate oscillations from the scalp level signal onto the cortical surface which will be employed in the study of the oscillatory activities in the neonatal EEG. Since the ECD approaches require *a priori* knowledge of the exact number of dipoles, which is not the case in many of above mentioned applications, the scanning methods are preferred to ECD approaches. The selection procedure includes more criteria and particulars that will be covered in full details in chapter 5 of this thesis.

1.4 Motivation and significance

Independent extrauterine living and breathing necessitates a state of maturity of the fetus and its developmental processes that is only achieved after about 37 weeks gestational age (GA). More than 50% of infants born earlier, i.e. preterm infants [82, 83], face immaturity of vital functions of the brain [83]. Most preterm babies only survive with the continuous special care given in neonatal intensive care units (NICU). Although the survival rate for all but the most extremely preterm infants now surpasses 85%, they may experience later neurobehavioral impairments, including motor incoordination, cognitive impairment, attention deficits, or behavioural problems [84]. Preterm birth is associated with increased risk of psychiatric disorders such as bipolar disorder, depression and psychosis [85].

In Australia approximately 2600 very-low-birth weight (<1500g) or very preterm infants (<30 weeks GA) are born per annum [84]. Around 8% of infants are born preterm in Australia each year and approximately 15% of infants are admitted to NICUs [82]. Owing to the increasing rate of preterm birth during the last two decades [86] in Australia [87, 88] the development of early intervention tools is required to improve neurodevelopmental outcomes. The broad aim of this thesis is to improve the neonatal health care by enhancing the non-invasive neonatal brain monitoring. This enhancement is realized through applying time-frequency signal processing techniques to the task of neonatal EEG source localization. The major significance of this thesis includes:

A) Automatic non-invasive neonatal brain monitoring through EEG:

The lack of apparent clinical symptoms such as muscle spasms or sporadic eye movements makes the detection of neurological abnormalities in neonates challenging. EEG recording is the mere detection method in some situations such as neonatal seizure [89], with early predictive potential for long-term neurological outcomes. Although the neurophysiologist's assessment of the severity of newborn encephalopathy still serves as the gold standard, it requires high levels of expertise and is time consuming. In addition, studies [90, 91] have shown that the interpretation of EEG is very subjective and challenging for the majority of neonatologists [89, 92]. Accordingly, an automatic

objective newborn screening tool based on neonatal EEG that makes it feasible to continuously monitor infants in NICUs and other clinical situations constitutes the first motivation of this research.

B) Neonatal EEG source localization:

The low temporal resolution and high cost of functional brain assessment techniques such as fMRI has produced the opportunity for techniques based on EEG source localization (ESL) with a low cost and high temporal resolution to take their place. ESL has been employed to localize the sources of abnormalities, such as tumours and epilepsy in studies of physiological, psychological, pathological, and functional brain abnormalities in adults [93]. It has been also used in the presurgical evaluation of adult patients with refractory epilepsy to localize the epileptogenic area [25] and it is expected to be included in the clinical routine practices for patients suffering from focal epilepsy in near future [94]. The partial relationship between the anatomical and functional organization of human brain may reveal the basis for specific abnormalities such as autism, Williams syndrome and schizophrenia that are observed in certain developmental and neuropsychiatric disorders. There are indications of the early brain developmental roots of these later symptoms [95]. However, these observations have been performed only on adults and because of technical and anatomical constraints there is no report of applying ESL to neonatal EEG [25]. Consequently another motivation for this dissertation is to propose methodological development and validation of an ESL scheme for neonatal EEG to provide accurate neurological-functional information of the brain, especially in preterm infants.

1.5 Objective of the research

The principal objective of this study is to create a solution for neonatal EEG source localization using advanced signal processing techniques including time-frequency analysis and digital image processing algorithms. This will be realized in the form of a tool that can be utilized by neonatal brain researchers and in the advanced form, in clinical practices. Due to dissimilarities between adult and neonatal EEG, and the technical limitations relating to acquisition of relevant parameters of newborn head, applying adult ESL techniques for neonatal ESL problem has not been attempted. Consequently the final goal of this thesis is to fill this gap in the field of neonatal brain research and consists of several detailed objectives in the different stages of study as below:

Objective 1: Parameterize a neonatal head model by investigating the features of focal transients in neonatal EEG.

Objective 2: Create and validate a neonatal head model through solving the forward solution.

Objective 3: Choose appropriate adult source localization techniques for the case of cortical sources and apply them to the neonatal head model.

Objective 4: Enhance the selected method to adapt it for neonatal EEG source localization and validate it.

1.6 Proposed approach and methods

The proposed approach consists of 5 stages:

1- Generate an estimation of unknown parameters of the neonatal head including skull layer conductivity, appropriate source depth, the effect of fontanelles and the required number of EEG electrodes.

2- Implementation of the neonatal head model by using the estimated parameters and also segmentation of neonatal EEG and solving the Boundary Element Method for the mesh point constructed upon segmented MRI.

3- Choose an appropriate inverse solution for the neonatal ESL problem and implement it by means of statistical signal processing techniques and time-frequency signal processing techniques using the previously developed neonatal head model.

4- Define and calculate a performance metric and use it to evaluate and validate the proposed method by means of simulated realistic EEG and comparing the performance of localization to other methods.

5- Enhance the proposed method by creating an automatic ROI identification in the time-frequency plane owing to the significance of ROI in the final performance of the proposed neonatal ESL method.

1.7 Major Contributions of the Thesis

Contributions of the thesis are as follows

Objective 1: Several parameters involved in the calculation of inverse solution of the neonatal EEG have been calculated and presented in chapter 3 and 4. The acceptable range of the neonatal skull layer conductivity and the proper source depth in modelling neonatal head are presented in chapter 4. These parameters significantly affect the accuracy and the performance of the ESL and lack of accurate knowledge about them has been the main obstacle in the realization of neonatal ESL. The number of EEG electrodes needed to capture neonatal EEG in full spatial detail is calculated and presented in chapter 3. The spatial patterning of the neonatal EEG is the other essential issue in a genuine neonatal ESL methodology which calculates the sufficient number of EEG electrodes for recording neonatal EEG without losing information.

Objective 2: The effect of the fontanelles, the main difference in the geometry of the neonatal and adult skull, as another prerequisite for the neonatal ESL is investigated in chapter 2. While the histological similarity of the other layers between neonates and adults allow approximation of their conductivities across ages, neither direct nor indirect information is currently available about the conductivity of the cartilage layer and fontanelles. Implementation of parameters achieved in objective 1 and the result of investigation about the effect of the fontanelles, along with the segmentation of neonatal MRI, facilitated the realization of a realistic neonatal head model that is presented in chapter 4.

Objective 3: An inverse solution for the neonatal EEG source localization problem is proposed and validated in chapter 5. Choosing the appropriate localization approach for the neonatal EEG inverse problem is a challenging task because it requires the exact interpretation of prior knowledge about the elements of neonatal ESL including neonatal head model parameters and neonatal EEG. The dominant features of normal and abnormal neonatal EEG, focal transients, are

generated by focal sources and accordingly, methods based on a limited number of dipoles will better fit this purpose. A methodological approach is presented in chapter 5 to select and propose the appropriate neonatal ESL.

Objective 4: The proposed neonatal inverse solution, time-frequency multiple signal classification algorithm (TF-MUSIC), is enhanced through the automatic region of interest (ROI) identification that is explained in chapter 5. In addition, a new ESL performance metric that makes it possible to measure the effect of individual parameter in the final performance of an inverse solution has been introduced in chapter 5. It has been shown also in chapter 5 that the ROI plays the most fundamental role in the superiority of the TF-MUSIC algorithm over MUSIC or other methods. Consequently, the effective determination of ROI significantly affects the performance of a source localization technique such as the TF-MUSIC that uses the ROI. It has also been shown in chapter 5 that the choice of time-frequency distribution (TFD) kernel does not independently change the localization performance; though the effect of TFD kernel on ROI identification is noticeable.

1.8 Thesis Organization

The thesis comprises six chapters as below:

Chapter 1: provides a background of the research topic and a short review of different adult EEG inverse solutions. The motivations, aims and objectives of the research are then described. The last sections of this chapter explain the proposed approach and the methodology used and lists the major contributions of this thesis.

Chapter 2: describes the parameters of the neonatal head model. A brief theoretical background is presented which is followed by the explanation of the parameters of neonatal head model. The two techniques used in this chapter to acquire the neonatal head model parameter, i.e. spatial decay of amplitude in focal transients and spatial decay of linear correlation between scalp EEG signals are then explained.

Chapter 3: is dedicated to spatial patterning of neonatal scalp EEG. First the spatial power spectrum is described and then the linear array experiment is presented which is used to calculate the sufficient number of electrodes in a full recording of the neonatal EEG. The clinical implication of spatial patterning in EEG and the results relating to the analysis of linear array are the two last sections of this chapter.

Chapter 4: this is where the proper skull conductivity range in realistic neonatal head models is estimated. A short theoretical background at the beginning of the chapter is followed by the experimental methods for the estimation of neonatal conductivity and then procedures for generating the head model including the BEM and FEM, for calculating the theoretical values of the neonatal skull conductivity.

Chapter 5: suggests the neonatal EEG source localization, i.e. the enhanced TF-MUSIC. First a review of time-frequency analysis is presented and then the TF-MUSIC algorithm is discussed. A method of objective ROI identification which is used to enhance the TF-MUSIC algorithm is then

presented. The last section of this chapter is dedicated to the evaluation and validation of the proposed method for the neonatal ESL. The performance evaluation through introducing a new performance metric is explained in the last section. Then ROI and its significance in the performance of the method are described later.

Chapter 6: Conclusion and possible future direction in this study.

1.9 Author Publication List

[1] M. Odabaee, A. Tokariev, S. Layeghy, M. Mesbah, P. B. Colditz, C. Ramon, and S. Vanhatalo, "Neonatal EEG at scalp is focal and implies high skull conductivity in realistic neonatal head models," *Neuroimage*, vol. 96, pp. 73-80, 2014.

[2] M. Odabaee, W. J. Freeman, P. B. Colditz, C. Ramon, and S. Vanhatalo, "Spatial patterning of the neonatal EEG suggests a need for a high number of electrodes," *Neuroimage*, vol. 68, pp. 229-235, 2013.

[3] M. Odabaee, S. Layeghy, M. Mesbah, G. Azemi, B. Boashash, P. Colditz, *et al.*, "EEG amplitude and correlation spatial decay analysis for neonatal head modelling," in *Information Science, Signal Processing and their Applications (ISSPA), 2012 11th International Conference on*, 2012, pp. 882-887.

CHAPTER 2: PARAMETERS OF THE NEONATAL HEAD MODEL[1]

2.1 Introduction

The EEG is an important diagnosis tool for the evaluation of seizures and other disorders of the central nervous system (CNS). It has also been used in monitoring the progress of such diseases and for prognosis of long term developmental outcome [96]. There is a need to better understand the relation between brain structures and function in newborns which can be achieved using EEG source localization (ESL) techniques. This includes, as explained in the first chapter, techniques used to non-invasively investigate the brain functions for better understanding of development processes and pathologies such as seizures.

ESL is the procedure of mapping EEG to the brain regions responsible for its generation. The accuracy of such a technique is critically dependent on the quality of the head model [27, 97]. Head models are mathematical representations for the electromagnetic relationships between neural currents and the scalp potentials. They include parameters such as tissue conductivity, thickness and geometrical specifications of the different layers of the head. However, the precise parameters to model the neonatal head have not been accurately determined which has prohibited the development of specific neonatal source localization techniques. Instead adult source localization techniques have been applied to the neonatal EEG [25].

There are several differences between the neonatal and adult head which make it difficult to produce an accurate neonatal head model. A realistic head model needs to take into account the different macroscopic and microscopic structures of neonatal skull, which have an effect on tissue conductivities. The neonatal brain is surrounded by a set of cartilaginous cranial bones with sutures and fontanelles between them and because these tissues are soft and relatively wet they are a good conductor. However, adult skull bone is well ossified and relatively dry, so is a poor conductor [96-

[1] **This chapter is an extension of the following paper :** Maryam Odabaee, Siamak Layeghy, Mostefa Mesbah, Ghasem Azemi, Boualem Boashash, Paul B. Colditz, Sampsa Vanhatalo, "EEG amplitude and correlation spatial decay analysis for neonatal head modelling," in *Information Science, Signal Processing and their Applications (ISSPA), 2012 11th International Conference on*, 2012, pp. 882-887.

101].

The importance of conductivity's role in the solution of an inverse problem comes from the fact that EEG signals are produced by the ohmic current flow in the head rather than capacitive or inductive currents. This makes EEG signals highly sensitive to the value of conductivity and likewise the inverse solution [10]. While neonatal skull conductivity is known to be the most accountable layer for the significant dissimilarities in the behaviour of newborn scalp EEG and adult EEG, this difference has been avoided in the studies of human neonatal EEG source localization (nESL) [25, 102]. These studies have simply adopted conductivity values from prior adult literature; however the lack of empirical reference makes interpretation of those results difficult.

Therefore, the main challenge in designing a suitable neonatal head model is to find the tissue conductivity profile for different layers and most importantly the skull. However, direct measurement of the *in vivo* head tissue conductivities is not ethically feasible in newborns and there is a need for indirect measurements. The methodology developed in this chapter to investigate the influence of the fontanelles on the neonatal skull conductivity profile is the first step to address this issue. This indirect measurement method, which is based on the application of statistical analysis and digital signal processing techniques to the scalp EEGs, will be followed in the next chapters for measuring other *in vivo* parameters effective on a realistic neonatal head model and henceforth on EEG source analysis.

2.2 Theoretical background

Many EEG source localization techniques have been developed to identify the brain structures (i.e. current sources) that generate EEG signals [36]. One of the main prerequisites for the successful realization of these methods is a sufficiently accurate volume conductor model with appropriate tissue conductivity profiles [97]. In the adult EEG literature, concentric spherical shells with different conductivities have been commonly used to model the different tissue layers comprising the head [47, 103]. More realistic head models based on segmented MRIs [25, 104, 105] have also been developed

and used in conjunction with advanced computational methods such as Finite Element Methods (FEM) and Boundary Element Methods (BEM) [1, 13, 106] to achieve more accurate results.

In the context of neonatal EEG source localization, it has been recognized that the neonatal head cannot satisfactorily be represented by the adult models [25]. The adult skull is well ossified, relatively dry, and much more resistive to electric current flow than the underlying layer of CSF. Different values have been reported for the *in vivo* conductivity ratio of CSF to skull in the adult ranging from 20 - 200 [100] measured by temporarily removing part of skull during epilepsy surgery. This ratio is reported as about 15 [99] or 24 [97] by injecting small electric currents into the scalp and measuring the potentials at the other electrodes. Yet in [101] using finite element modelling of the layered structure of the human skull the ratio was estimated at 40 rather than the commonly used value of 80 [96, 101, 107]. One possible reason for the difference in values of skull conductivity could be due to the region of the skull examined or position of the skull used for estimating its conductivity [108].

In neonates, on the other hand, there are no dry ossified bones and the brain is surrounded by the future skull tissue and cartilage, which is soft and relatively wet and therefore a good conductor. Hence, the constituent elements of the neonatal skull contribute to its different conductivity index from the adult. The skull thickness is another important parameter in ESL as it directly affects the spatial flow of current in the head [109]. The thickness changes during human development with a sharp increase from birth to the end of the first year. While the infant skull thickness varies from 1 to 2 mm, it is 5 to 8 mm in the adult [110-112]. Accordingly, since the length of the path directly affects the resistivity against the electrical current, less of the passing flow of current is lost in the neonatal skull less of the passing flow of current is lost in the neonatal skull neonatal .

A major difference between the conductivity profile of the neonatal and adult skull is the fontanelles region for which there is no information available. While there are similarities between the other head tissues in terms of microscopic anatomy, fontanelles and cartilage do not have a comparable compartment in the adult head. This wide opening in the skull is a major difference in the head

geometry between the neonatal and adult head (see Figure 4). It is a section of the foetal and neonatal skull encompassing the gaps between the incompletely formed cranial bones where the cartilage will close later in development. Neither direct nor indirect information is currently available about the conductivity of the fontanelles (and cartilage layer). Though, the histological similarity of the other layers between neonates and adults allows approximation of their conductivities across ages. This information therefore is crucial in the construction of a practical neonatal head model. Hence, it is a prerequisite in each genuine nESL technique to address this singularity of the neonatal head model. Although direct investigation of the effect of the fontanelles is not feasible in neonates, it can be studied by the application of the electromagnetism theory in dielectric materials.

The technique employed here for this purpose is based on the spatial distribution of potential and potentials correlation over the scalp. It is shown that the spatial decay of both potential amplitudes and their correlations are an indirect measure of skull conductivity which are used to estimate the effect of fontanelles on skull conductivity. It uses the "lead field theory" which relates the scalp potentials generated by current sources in the brain / cortex and the externally generated currents over the scalp. The main idea here is to study the spatial correlation of potentials due to volume conduction of randomly spaced, uncorrelated radial cortical sources. The result of comparisons of these measures in different regions of skull are used to investigate the effect of fontanelles in neonatal head modelling [113].

2.2.1 Lead field theory

Transmission of the information in a nerve cell is accomplished by the exchange of ions across its membrane that causes a temporary variation in the potential along the axon which is called the action potential [93]. The rise time of action potentials are about 1 ms which probably includes the highest significant frequency component in bioelectric systems of the order of 1 KHz [114]. Although the neural activity is time varying, the variation rate and the frequency components are considered very slow compared to the electromagnetic wave propagation speed. In other words, the wavelength of the

potential signals is about 300 Km which make the points with small distances equivalent in terms of time variations, i.e. propagation delay. Consequently, the behaviour of all fields and currents can be explained by the quasi-static Maxwell equations which assume them as stationary at each instance of time [47]. In this condition the electric potential over the scalp, v can be described by the following equation [98]:

$$\nabla.(\sigma\nabla v) = \nabla.\boldsymbol{J_s} \tag{5}$$

in which σ is the tissue conductivity, J_s is the current density due to transmembrane ion exchanges in neurons, $\nabla.(\,)$ is the operator for the divergence or the flux density, and ∇v is the gradient vector of potential. For the case of I, a flow from a point-like current source to a current sink, the Eq. (5) can be stated as:

$$\nabla.(\sigma\nabla v) = -\mathrm{I}\delta(\mathbf{r}-\mathbf{r}_2) + \mathrm{I}\delta(\mathbf{r}-\mathbf{r}_1) \tag{6}$$

If a current dipole is used to model the current source, as it commonly is in the literature [1, 37, 41, 81, 98, 115], the potential difference between two scalp locations $\mathbf{r}_1$ and $\mathbf{r}_2$ caused by the dipole source at $\mathbf{r}$ can be stated as:

$$v(\mathbf{r}_2) - v(\mathbf{r}_1) = \mathbf{L}(\mathbf{r}_1, \mathbf{r}_2; \boldsymbol{r}).\mathbf{m}(\mathbf{r}) \tag{7}$$

in which $\mathbf{L}(\mathbf{r}_1, \mathbf{r}_2; \boldsymbol{r})$ is called the field vector for a particular electrode pair and individual dipole position, and $\mathbf{m}(\mathbf{r})$ is the dipole moment. The dipole moment $\mathbf{m}(\mathbf{r})$ is defined by the unit vector $\mathbf{r}$ in the direction from current sink to current source and its magnitude $m = \|\mathbf{m}(\mathbf{r})\| = I.d$ as the product of the current and the distance between two poles, i.e. current source and sink. In other words, the current dipole can be stated as [47]

$$\mathbf{m} = m\mathbf{r} = \mathrm{I}.\mathrm{d}\mathbf{r} \tag{8}$$

or in the Cartesian coordinate system

$$\mathbf{m} = \mathrm{m}_x\mathbf{x} + \mathrm{m}_y\mathbf{y} + \mathrm{m}_z\mathbf{z} \tag{9}$$

where m_x, m_y and m_z are called dipole component in the direction of x, y and z respectively. Practically the lead field is calculated by [98]

$$\mathbf{L}(\mathbf{r}_1, \mathbf{r}_2; \boldsymbol{r}) = \frac{\boldsymbol{J_i}(\boldsymbol{r})}{\sigma \boldsymbol{I_i}(\boldsymbol{r})} \tag{10}$$

in which $\boldsymbol{J_i}(\boldsymbol{r})$ is the density of induced current at $\boldsymbol{r}$ if current $\boldsymbol{I_i}(\boldsymbol{r})$ were injected between $\mathbf{r}_1$ and $\mathbf{r}_2$. This relation holds for arbitrary geometry and inhomogeneous conductivity volume conductors.

2.2.2 Theoretical spatial distribution of potential correlation over the scalp

In order to derive the analytical expressions for the spatial distribution of the correlation of scalp potentials, the human head is approximated by a model of four layer spherical shells depicted in Figure 1.

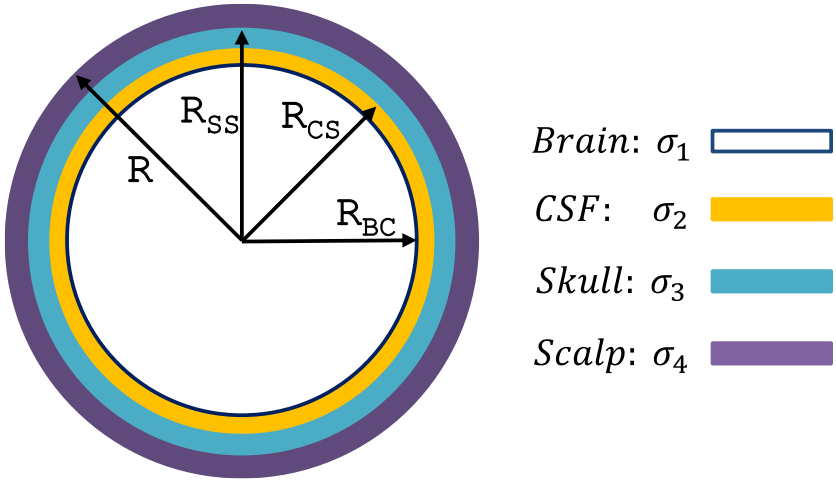

Figure 1 - The cross-section of the volume conductor model, including four spherical shells representing the brain, CSF, skull and scalp tissues. From the inner to outer layers the corresponding conductivity values are $\boldsymbol{\sigma_1, \sigma_2, \sigma_3, \sigma_4}$.

The boundaries between various tissues are located at R_{BC}, R_{CS}, and R_{SS} and R represents the radius of the head

The cortical currents are also modelled by a large number of randomly located radial dipoles. In this condition the potential at any scalp point $\boldsymbol{r}$ is the sum of the potentials generated by individual sources and accordingly can be described by [116]

$$V(\boldsymbol{r}) = \sum_{i=1}^{N} v_i(\boldsymbol{r}.\boldsymbol{r_i}) \tag{11}$$

in which $v_i(\boldsymbol{r}.\boldsymbol{r_i})$ is the potential at $\boldsymbol{r}$ due to a single dipole at location $\boldsymbol{r_i}$ which can be derived from Eq. (7) when the reference point,$v(\mathbf{r}_1)$, is located infinitely far from the head. For the case where the head is approximated by spherical shells it can be stated as [113]

$$v(\psi) = \frac{m}{4\pi\sigma_4 R^2} \sum_{n=1}^{\infty} c_n f^{n-1} P_n(cos(\psi)) \tag{12}$$

where m is the magnitude of dipole moment, σ_4 is the scalp conductivity, R is the outer radius of the head, P_n is the Legendre polynomial of degree n, ψ is the angular difference between source and measurement site, and c_n and f^{n-1} contain the model parameters as defined in [117] that include the radii and conductivities of the head layers depicted in Figure 2 for this model.

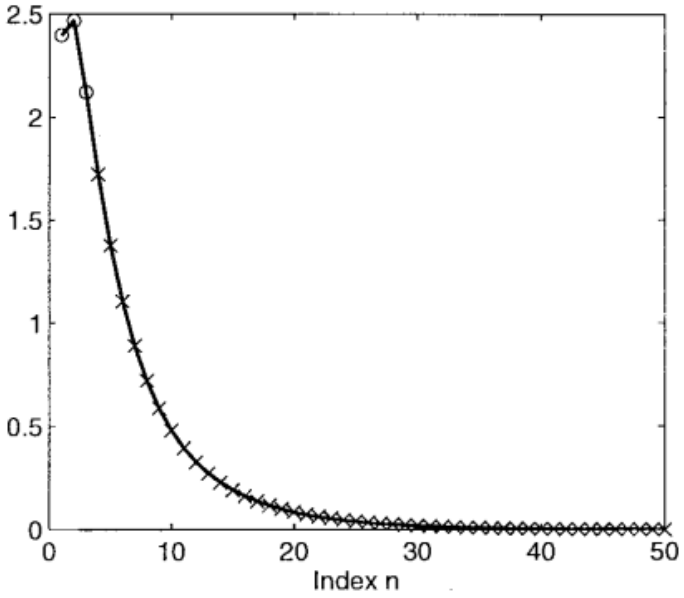

Figure 2 - The solid line indicates the values of $c_n\ f^{n-1}$ with respect to n and the fitted third-order polynomial is marked by the cross signs [33]

To calculate the spatial distribution of correlation of potentials over the scalp an infinite number of uncorrelated cortical dipoles model the continuous cortical source distribution. In this condition the

spatial correlation depends only on ψ, the angular difference between measurement sites and can be stated as a Legendre series of it [118]

$$\rho\big(cos(\psi)\big) = \sum_{n=1}^{\infty} \frac{(2n+1)}{2} \rho_n P_n(cos(\psi)) \tag{13}$$

where ρ_n are spatial power spectrum given for the employed model as stated in [113].

2.3 Features in neonatal EEG

The human skull is the most resistive tissue layer in the head and considered most responsible for the spatial blurring of the adult EEG [101, 113, 119]. In other words, the poor conductive adult human skull acts as a spatial low-pass filter for the passing potentials, which blurs its distribution at the scalp layer [120]. Theoretical potential decay on the scalp is inversely related to skull conductivity for a four spherical shells head model and variety of source arrangements [113]. These results are confirmed in the adult by applying a small amount of current into the head and calculating the conductivity of different layers [97]. In addition, similar results are achieved for the theoretical spatial decay of correlation of scalp potential and the skull conductivity [113].

These results indicate that the spatial decay of scalp potential amplitude and the spatial decay of correlation of scalp potentials can be viewed as an indirect product of skull conductivity. This work exploits spatial decay of neonatal EEG signal recorded from the scalp to study the effect of fontanelles in nESL. Spatial decay of the amplitude of focal transients in neonatal EEG are specifically investigated in this study as they have physiological interpretation and discriminate neonatal EEG from the adult. These salient features, which are common in normal and abnormal neonatal EEG, are assumed to be generated by focal sources [22-24, 78, 79].

These features are characterized by short and relatively sharp transients in the neonatal EEG [32]. Typical focal transients of neonatal EEG are depicted in Figure 3,Figure 5 and Figure 6. The time-

frequency representation of the selected focal transient in Figure 3 includes time varying spectral content. Time-frequency representation [76] of signals is an analysis tool which takes into account the non-stationarity of signals, i.e. the variation of spectral content of signal in time. This method is explained and briefly reviewed in Chapter 5 of this thesis. The spatial linear correlations between the EEG signals recorded from different parts of the neonates' scalps are investigated for the comparison with adult EEG datasets.

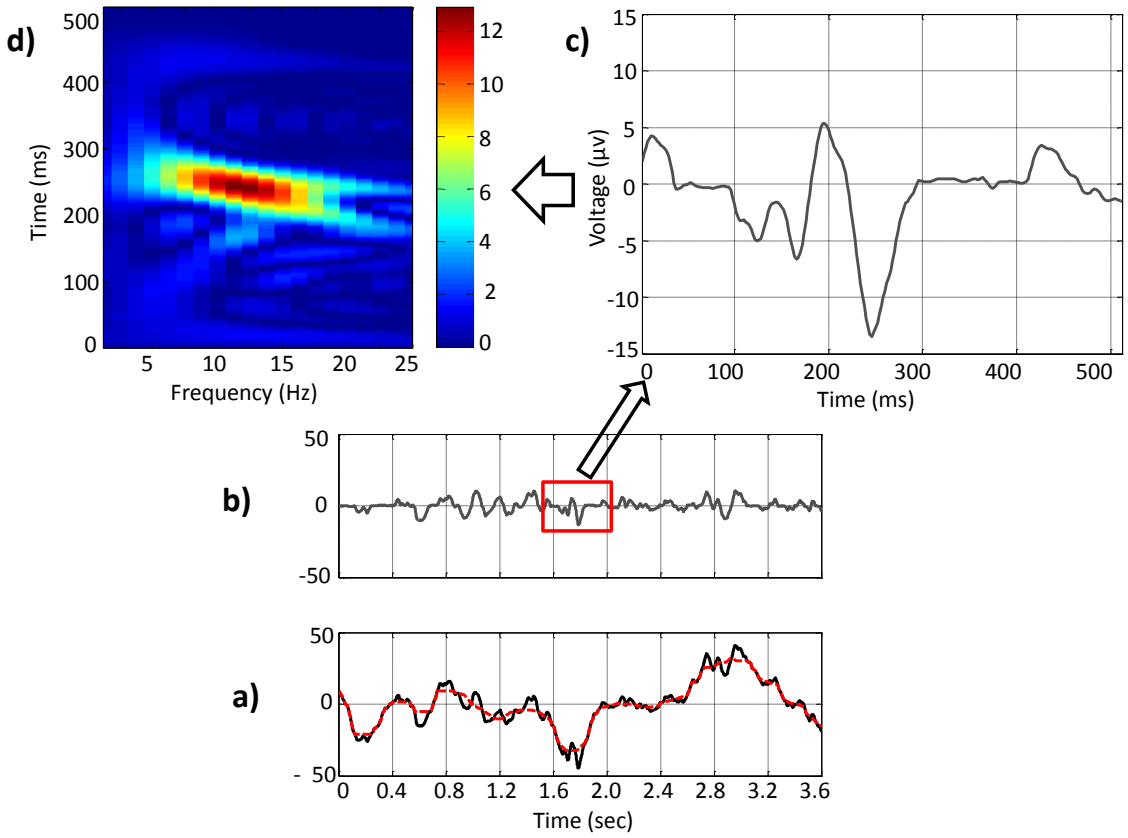

Figure 3 - An example of focal transients marked by a clinical expert. a) The raw neonatal EEG in black and its median in red. b) Neonatal EEG after removing its median. c) zoomed version of the selected part of (b) , and d) Time-Frequency Distribution (TFD) of the selected part by means of Doppler independent kernel with a hyperbolic cosine type window of length 100 sample (sampling frequency: 512).

2.4 EEG Signal acquisition

An adult and a neonatal EEG database were used for this study. The neonatal dataset included six 64-channels EEG recordings (Figure 5) from normal full term neonates with a sampling rate of 512Hz

and the adult dataset included one 256-channel EEG of normal adult with 1000Hz sampling frequency.

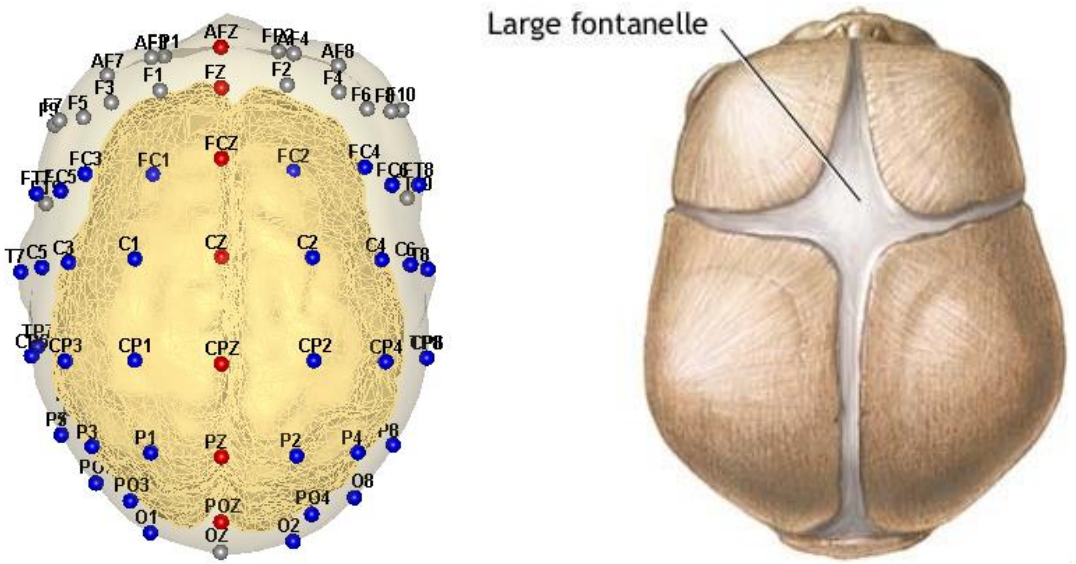

Figure 4 - Right - The location of fontanelles and sutures on the neonatal skull (picture from ADAM INC. website), Left - The three scalp regions of interest (Fontanel in red, Left & Right in dark blue; The Group "All" is all of them together).

Neonatal EEG data were recorded at the Department of Children's Clinical Neurophysiology at Helsinki University Hospital using a Cognitrace amplifier (ANT B.V., Enschede, The Netherlands, www.ant-neuro.com). Electrodes (sintered Ag/AgCl) were placed according to the international 10-10 standard using the Waveguard electrode cap (Waveguard, ANT-Neuro, Germany; www.ant-neuro.com; see also http://www.nemo-europe.com/en/educational-tools.php). Common average reference was used in the recording. Informed consent was obtained from the parents of the babies. Adult EEG recording was performed with a 256-channel EEG system (Geodesic Inc, www.egi.com) and was kindly provided to us courtesy of Dr. German Gomeq-Herrero from VU University of Amsterdam.

2.5 Method

Different signal processing techniques such as filtering and statistical analysis were used to prepare data and perform experiments to test the two head model hypothesis. In the first hypothesis fontanelles make significant effect on the skull conductivity and need to be treated accordingly. The second hypothesis assumes they are not effective on skull conductivity and no special treatment is required. Two signal processing approaches were utilized for investigating the spatial characteristics of neonatal scalp EEG. First, the spatial amplitude decay of focal transients, selected from three different scalp regions as shown in

Figure 4, were examined and compared. Based on their spatial distributions, the selected features were likely produced by a focal source within the brain. These features were defined as relatively sharp brain-borne potentials and were manually identified and marked from neonatal EEG by Dr. S. Vanhatalo, a clinical neurophysiologist. An example of these markings is depicted in Figure 5.

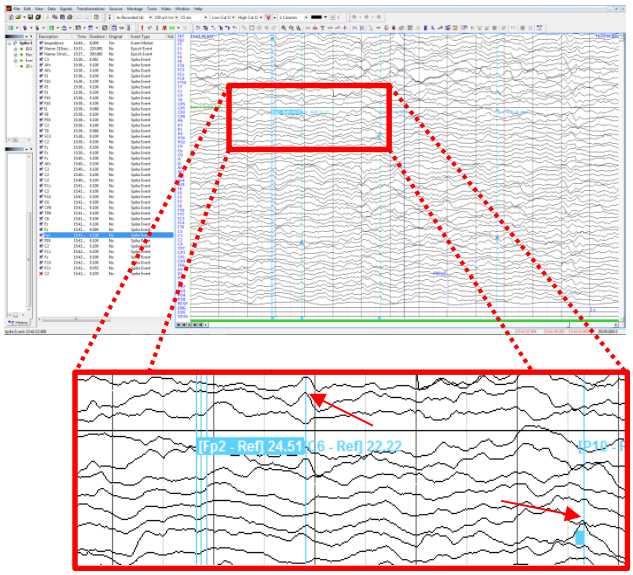

Figure 5 - A sample of multi-channel EEG signal with focal transients highlighted in blue (pointed by red arrows).

The absence of comparable, focal physiological EEG transients in adults precluded the comparison of results to neonatal scalp EEG and hence another technique was used for this comparison. The spatial decay of linear correlation function between EEG signals, selected from the same three areas,

was calculated. This approach has been previously applied to EEG signals in adults and older children whose fontanelles is partly closed, to estimate the skull conductivity [113]. This last approach therefore made it possible to directly compare EEG from neonates and adults.

2.5.1 Pre-processing

Preprocessing was designed to optimally extract the spectral properties of these neonatal EEG transient signals from the other, ongoing EEG activity. A digital low-pass Finite Impulse Response (FIR) filter with 30Hz cut-off was first applied to the EEG data to remove mains and other high frequency noise. In order to highlight and focus on the analysis of faster focal transients only, a nonlinear median filter was applied to remove low-frequency background drift. The window of 120 samples (~230ms) was selected based on the length of transient which was typically about half of this window. We then subtracted the median low-pass (MLP; 120 samples, ~230ms) filtered data from the original trace $w[n]$, which yielded an output $v[n]$ without the "ringing" typically seen with conventional high pass filters. This operation is expressed as:

$$v^{(k)}[n] = w^{(k)}[n] - median\{w^{(k)}[n]\} \quad (14)$$

For $120k \leq n \leq 120(k+1)$ where $k = 0,1, \dots, M$ refers to the k^{th} segment of the EEG signal, $M = \left[{}^{N}/_{M}\right]$, and N is the length of the original signal. A typical output of this procedure is depicted in Figure 6. Through filtering, the lower frequencies (0-0.25 Hz) are attenuated and the effects of higher frequencies (2.5-5 Hz), related to the faster focal transient, are highlighted.

2.5.2 Spatial decay of amplitude in focal transients

Spatial decay of EEG amplitude within four scalp regions, namely 'Fontanel', 'Left', 'Right' and 'All' region (see Figure 4) was investigated. Due to the lack of cartilage in the fontanelles area of the

newborn skull, this area was expected to have different volume conduction (conductivity) to the left and right regions. Since Left and Right regions are assumed equivalent in terms of conductivity, they are merged to constitute a single "Left & Right" region. The aim was to determine whether the amplitude decay of the focal transients in the fontanelles region is steeper (because of the higher conductivity of the region) than the other regions. First, a channel with the specified transient was selected as the reference channel in the selected region. Then, the decay in the amplitudes of other neighbouring channels (in that area) with respect to the reference area was calculated as a function of the distance between those channels.

2.5.3 Spatial decay of linear correlation between scalp EEG signals

Lack of focal EEG transients in adults precluded the direct comparison of neonatal and adult EEG. Hence, a complementary step was taken. The spatial decay of linear correlation of EEG signals was calculated for each of the four scalp regions and compared. The Pearson correlation was used to measure the strength of linear dependence between two channels. A higher value of the correlation between two channels indicates a higher similarity of the transients in two channels which naturally decreases as inter-electrode distance increases. To compare results from neonatal data with those from adults, a 256 channel EEG dataset of normal adult was used as the mean inter-electrode distances in neonatal 64ch and adult 256ch recordings are similar.

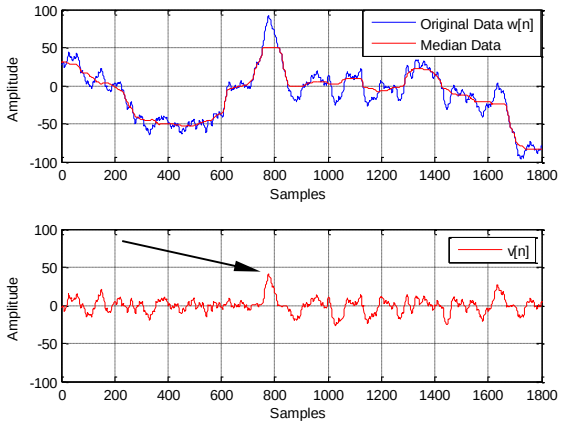

Figure 6 - (up) The original EEG signal (blue) and the output of MLP filterapplied on the original EEG (red), (Down) The EEG signal w[n] after subtracting the MLP filter output (The transient is pointed out by the arrow).

For the channels in a particular region, the correlation matrix $C_{L\times L}$ was calculated where L is the number of channels in the region (for example, $\mathrm{L} = 15$ for the left region). The entry c_{ij} of the correlation matrix, represents the Pearson correlation coefficient between 2-minute EEG recordings of channels i and j. If the EEG signals recorded from i^{th} and j^{th} channels are denoted as $v_i[n]$ and $v_j[n]$ respectively, where $n = 1,2, \dots, N$ with $N = 2 \times 60 \times 512 = 61440$ samples, then c_{ij} is given by:

$$c_{ij} = \frac{\sum_{n=0}^{N-1}(v_i[n] - \overline{v_i})\left(v_j[n] - \overline{v_j}\right)}{\sqrt{(\sum_{n=0}^{N-1}(v_i[n] - \overline{v_i})^2)\left(\sum_{n=0}^{N-1}(v_j[n] - \overline{v_j})^2\right)}} \tag{15}$$

2.6 Results

Results are represented separately for neonates and adults in the following sections respectively.

2.6.1 Expermintal results from neonatal EEG

The spatial decays of focal transients were investigated using two different approaches. In the first approach, the spatial decay analysis was constrained to the three spatial regions shown in Figure 4. The results obtained are shown in Figure 7-a (Fontanel Region) for a typical marked focal transient on data from channel FZ. In the second approach, the spatial decay was analysed using all 64 electrodes (Figure 7-b).

The behaviour of the amplitude decay vs. distance was approximated using first quadratic and cubic regressions. Since a linear behaviour could be seen over the first neighbouring electrodes (at least up to 5-6 cm), the linear regression was adopted for these variations. Figure 8 shows a typical sample of amplitude decay vs. inter-electrode distance. The slope of spatial decay was measured in different regions.

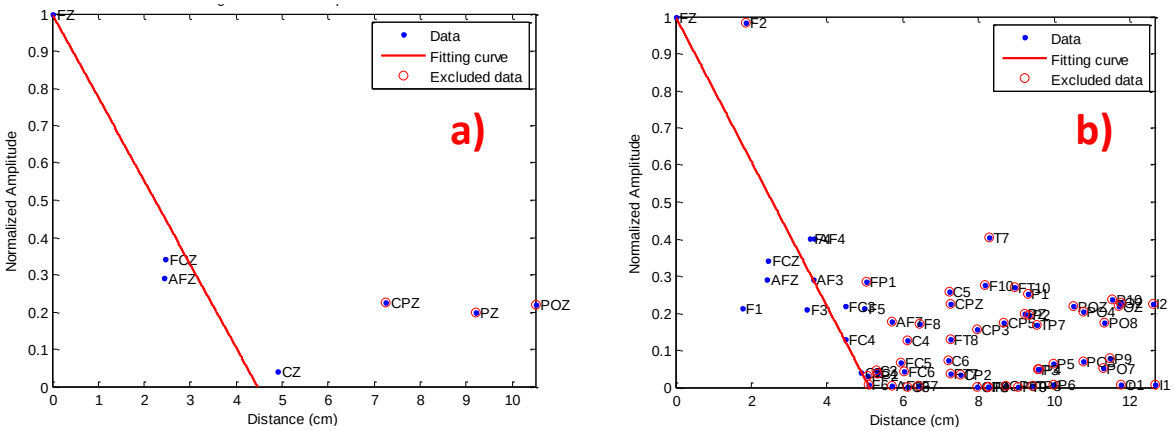

Figure 7 - a) typical spatial decay of amplitude within fontanelles, b) among all, calculated from the focal transient, peak amplitude at FZ channel.

Figure 8 depicts an example of spatial amplitude decay of a transient with the highest amplitude in the 'Right' region (electrode position ‘FC4’) with different regression lines (Cubic, Quadratic, and linear). A linear regression was fitted on the linear part of higher order curves by using electrodes with 2 or 3 inter-electrode distances from the reference electrode. It is clear from Figure 8 that electrodes located within 5 cm of the reference electrode exhibit a linear decay with spatial distance. This is confirmed by the statistical analysis of 40 plots of the different marked transients. The slopes of fitted linear functions were calculated for each region.

Figure 9 displays the boxplots of the calculated slopes for different regions, i.e. Left & Right, Fontanel and All.

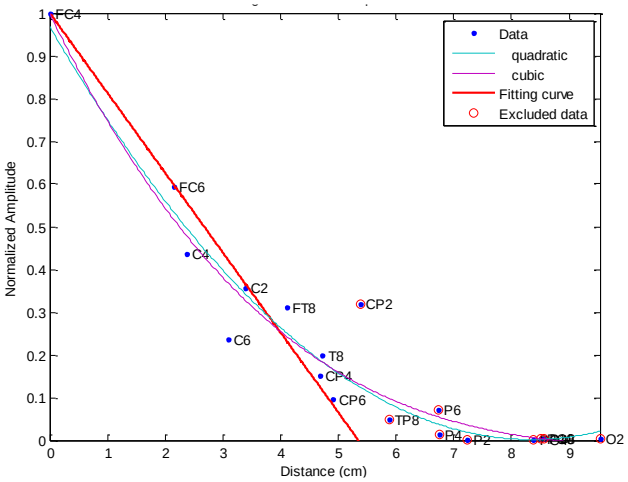

Figure 8 - Comparison of different regressions (Linear, Quadratic, and Cubic) demonstrates that they are comparable over the first 5 cm. (data is taken from spatial decay of amplitudes in over the 'Right' region).

2.6.2 Comparison of neonatal and adult EEG

In order to measure the statistical difference of the computed slopes pertaining to lines fitted using linear regression, the Analysis of Variance test (ANOVA) [121], was then applied. ANOVA is a statistical method which analyses differences between group means of different variables. The result of the ANOVA test returned the p-value of 0.55 which indicated no significant statistical difference exists between the amplitude decays in different regions of the scalp. These results suggest that neonatal head models can be considerably simplified as compared to prior suggestions that the fontanelles area needs special attention [25].

In order to study the EEG spatial decay, we plotted the correlation coefficient given in (15) as a function of the spatial distance taking one of the electrodes (or channels) as a reference. This is applied to the different scalp regions defined above for both newborn and adult EEG. To estimate the inter-electrode correlation vs. inter-electrode distance, we applied quadratic, cubic and linear regressions. (Figure 10) shows that correlation decays linearly over the closely spaced neighbours; hence a linear regression was applied. To compare the slopes between neonatal and adult EEG (Figure 10), the reference electrode was selected from the Fontanel region (on the central of the scalp, Cz for neonate, E90 for Adult).

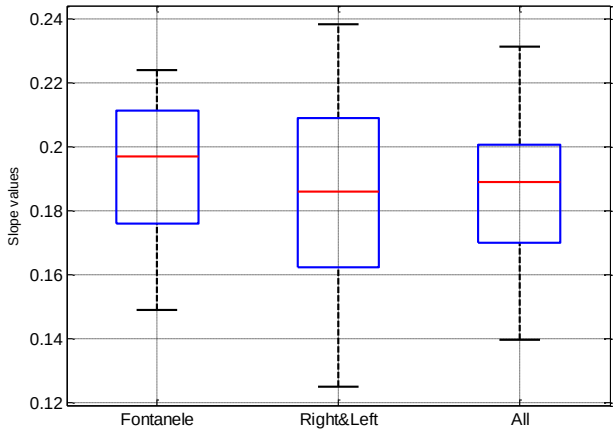

Figure 9 - Comparison of the values of slopes in three scalp region shows that there are no meaningful differences in the spatial decay of scalp EEG amplitudes.

The correlation analysis (Figure 10) showed the slope of the correlation decay is up to several times steeper in neonates than in adults. This magnitude of difference is not readily explained by the difference in head geometry (head radius and skull thickness) and, therefore calls for further experiments to define relevant conductivity estimates for neonatal skull tissue which will be considered in the two next chapters.

2.7 Conclusions

Two different methods were used to probe the spatial properties of neonatal EEG signals. These methods were established on theoretical background calculated for spherical volume conductor models. The results suggest that a neonatal head model can be constructed using complete tissue layers (i.e. ignoring the existence of the open fontanelles). A possible reason for this phenomenon can be related to the similarity of conductivity in neonatal skull and the fontanelles. The main findings were; i) there is no statistically significant difference between head areas covered by cartilage and fontanelles in terms of EEG amplitude spatial decay, ii) neonatal scalp EEG has significantly higher spatial density (information per unit distance which is a result of spatial decay) compared to adult

scalp EEG and iii) there is a clear difference between adults and neonates. These findings will affect the design of an appropriate head model for source localization of neonatal EEG.

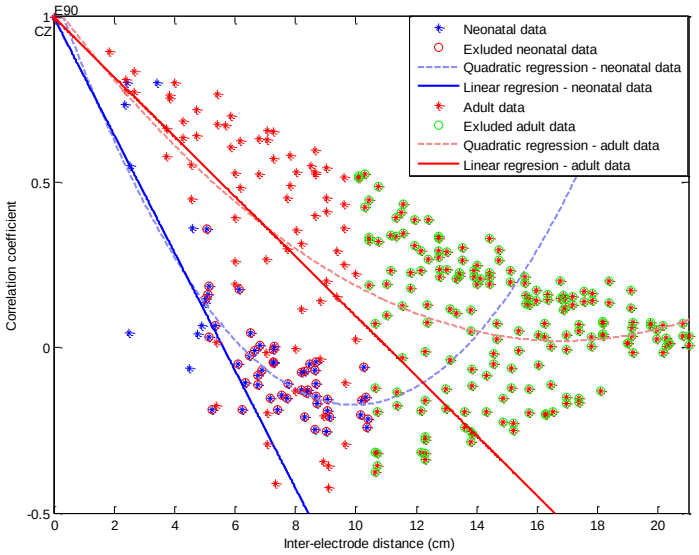

Figure 10 - The comparison of spatial decay of linear correlation between neonate and adult. Each point indicates the value of correlation between an EEG channel with the corresponding distance to the reference point (CZ in neonates and E90 in adult). Channel with a distance bigger than 5 cm (neonates) and 10 cm (adults) were excluded. Linear and Quadratic regression used to estimate the variation of spatial correlation. For the first 5 cm, the two regressions are similar and the slope of the correlation decay is up to several times steeper in neonates than in adults.

Further development will require accurate values of tissue conductivities for the newborn skull. The construction of a forward model suitable for the neonatal head, incorporating appropriate conductivity values that could replicate the spatial decay measured in our present work would also be required. This would achieve a solution to source localization in the neonate. Generation of a pertinent head model will enable us to study, for instance, the time-frequency characteristics of neonatal EEG in the source space. This issue is addressed in Chapter 5 of this thesis.

CHAPTER 3: SPATIAL PATTERNING OF THE NEONATAL EEG [2]

3.1 Introduction

Functional brain analysis is a key component in progress in diagnosis and prognosis of central nervous system pathologies in adults. Recent studies in infant neuroimaging have shown that the main functional network distributions are focused around brain regions responsible for perception-action tasks [17]. Activity patterns synchronize cortico-subcortical networks well before inputs on sensory regions of the brain are dominated by environmental influences [20]. These findings, along with other recent neuroimaging studies [16, 18] and in developmental neurobiology [19, 21] have made it clear that brain functions are already highly specialized early in development. Accordingly, functional brain analysis tools are of equal interest, necessity and importance in neonates as in adults.

EEG and EEG source localization techniques are among the most important tools and provide the best temporal resolution for mapping brain functions to anatomical sources in adults. However, the spatial resolution currently provided by conventional neonatal EEG recording, hardly suffices to distinguish brain lobes from each other. This lack of spatial resolution has severely hampered the functional assessment of neonatal brain activity [22]. Several studies have recently pursued the objective to devise a technique for fulfilling this shortcoming in neonatal EEG. Subsequently, better spatial resolution has been achieved using high density EEG (hdEEG) from the neonatal head in the laboratory environment [25, 122, 123], and in neonatal intensive care units [123, 124].

The theoretical benefits of increasing the number of recording electrodes are clear (examples can be seen in [113, 125]). EEG is the result of spatial sampling of a continuous potential field that can be measured over the entire scalp surface [126]. Variations of this potential field in time and space (regional differences) correspond to the changes in the generator currents (neural activity) in time and brain areas. In other words, EEG electrodes measure the potential only at a discrete set of electrode

[2] **This chapter is an extension of the following paper:** M. Odabaee, W. J. Freeman, P. B. Colditz, C. Ramon, and S. Vanhatalo, "Spatial patterning of the neonatal EEG suggests a need for a high number of electrodes," Neuroimage, vol. 68, pp. 229-235, 2013.

sites while for an accurate topographical map of scalp potential field, numerous measurement sites are required [122].

A useful analogy in this context is that the number of pixels in a digital picture must exceed a minimum that is necessary to form an image that is not blurry and distorted. Similarly, if the number of EEG electrodes is less than a limit which is determined by the amount of spatial changes / variations in the potential field, some spatial changes / variations cannot be seen. Practically this has been confirmed by recording cerebral activities previously not known, or difficult to localize, through improved spatial resolution obtained from a higher number of electrodes (e.g. [127, 128]).

The increase in spatial sampling has opened the pathway to genuine source localization of neonatal EEG [25, 102, 129], akin to what is routine with adult EEG. However, it is not clear how spatially compact neonatal EEG is. The richness in amplitude texture can be perceived as "spatial patterning" of the neonatal scalp EEG (hereafter referred to as "spatial patterning"). It has been measured in adults by estimating the spatial frequency content of scalp EEG [33, 34].

It would then be possible to estimate the errors related to the conventional under-sampling of EEG (also in [125]), once the spatial information content of neonatal EEG is known. It would also be necessary to define the number of EEG electrodes needed to record neonatal brain activity in full detail. A true realistic forward and inverse solution for neonatal EEG source localization can only be generated once this information is available. The spatial resolution of scalp EEG signals in adults is reduced by smearing due to the scalp and skull impedance, but this is of a lesser degree in neonates because these barriers are of lower impedance in infants ([102]). Consequently, the detailed spatial information should be more acquirable from the scalp EEG of neonates than adults [113, 125].

The effects of fontanelles in modelling of the neonatal skull were studied in the previous chapter. This Chapter investigates the second missing piece of information in neonatal EEG source localization (nESL), "spatial patterning" is investigated in this chapter. This requires two fundamental, complementary questions to be addressed: i) how complex is the EEG amplitude on the neonatal scalp? and ii) how large are the oscillatory bouts measured on the neonatal scalp? The answer

to these questions will subsequently determine the minimum number of required EEG electrodes and distance between electrodes to capture neonatal EEG in full detail. Finally, when neonatal skull conductivity is estimated in the next chapter, it represents the final step necessary to complete the missing parameters of the neonatal head model.

3.2 Materials and methods

3.2.1 Subjects and recordings

3.2.1.1 Subjects

EEG recordings were obtained from term healthy newborns. Two recordings were used for the linear array study and five recordings were used in the hdEEG recordings. EEG data was recorded in the Department of Children's Clinical Neurophysiology (Helsinki University Central Hospital) using a Cognitrace amplifier with sampling rate of 256 Hz or 512 Hz and an inbuilt average reference (ANT B.V., Enschede, The Netherlands, www.ant-neuro.com). Informed consent was obtained from the parents. This study was approved by the Ethics Committee of the Hospital for Children and Adolescents, Helsinki University Central Hospital.

3.2.1.2 Linear array recording

A linear electrode array was custom made by embedding 50 electrode pins (material Ag/AgCl; diameter 1mm; obtained from Biomed Product, USA) into a silicone strip with a 2.5mm interelectrode distance (Figure 11). The linear array was interfaced with the amplifier using a flat cable attached to a standard DB37 connector. Additional ground and reference electrodes were added as conventional cup electrodes (material Au), placed on the opposite side of the head. The scalp was cleaned and dried, and the array was lightly bound over either the parietal or occipitoparietal scalp or over the fontanelles (extending from about POz position along the midline to fontanelles).

3.2.1.3 hdEEG recording

64 channel hdEEG caps were used (Waveguard, ANT B.V., Enschede, The Netherlands, www.ant-neuro.com; see also [124]). A video clip showing an EEG recording of this kind is shown in the link www.nemo-europe.com/en/educational-tools.php.

3.2.2 Data analysis

Empirical methods were combined with simulations to study various aspects of the spatial texture of neonatal EEG. The study consisted of three complementary parts. In the first part a custom-fabricated linear array of electrodes (also available in [33, 130]) was used to obtain a theoretical estimate of the spatial information content / EEG patterning in selected scalp locations. A commercial high density (hdEEG, 64 channels) EEG cap was used in the second part in order to estimate the spatial extent of focal fluctuations of amplitudes, and to estimate the "practical" spatial EEG extent "patterning" from oscillatory events in the neonatal EEG [21, 22]. These events appear as short bursts of higher frequency activity, often nested [131] within slow waveforms and have multiple names related to their visual appearance (e.g. delta brush, Table 1 in [21] can be studied for further considerations). In the third part, a spherical head model was employed with neonatal dimensions to see i) whether our empirically measured spatial power spectral density (PSDx) can be reproduced by using a simple parametric model, and ii) how skull layer conductivity or source depth affect the PSDx. These will pilot the pathway to translate our results into future realistic head models.

3.2.2.1 Linear array experiment

A lack of gel coupling as used in conventional EEG recordings and the poor mechanical stability of the electrode-skin interface created a challenge for obtaining signal segments that were sufficiently clean enough artefacts. Epochs where there were more than 20 adjacent electrodes with sufficiently clean signal were selected. Altogether 54 seconds of such EEG from seven different time windows were identified (range 1.1-19 sec; mean length 7.7 sec). A representative epoch is shown in Figure

11). Epochs were exported in European Data Format (EDF) format for further analysis after bandpass filtering at 3-30 Hz to remove mains-related artefacts and trace instability due to mechanical movements.

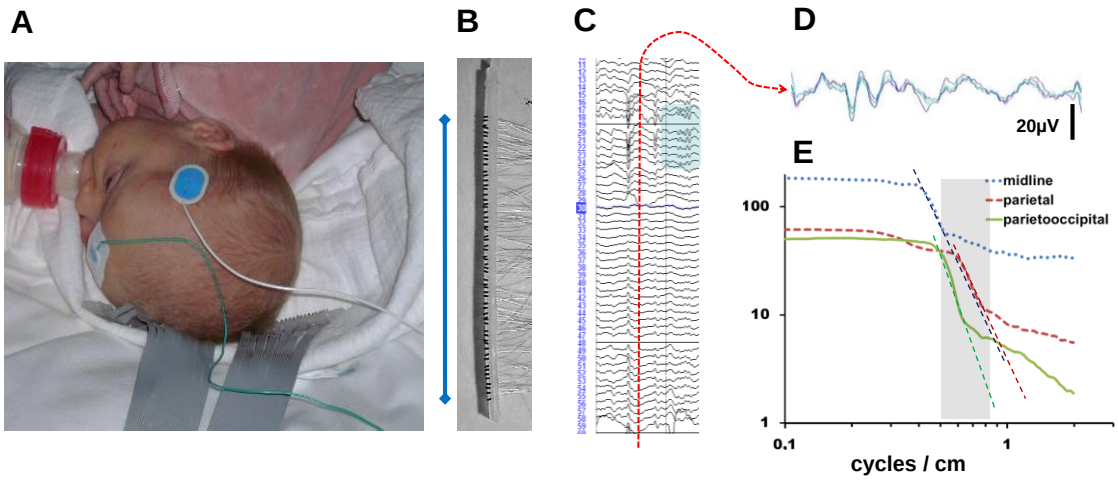

Figure 11 - Linear array experiment Linear array device, and the ground (green wire) and reference (blue) electrodes. The white cloth was used to wrap the array tightly against the baby's scalp, shown in the parieto-occipital position in this figure. B) The structure of the linear array device in more detail. Sensor pins (1mm thick) were placed at 2.5 mm intervals on a silicone bar. The blue vertical scale bar between photographs is 15cm. C) Example of a segment of raw data obtained from the linear array device. Note how a single transient or short oscillation (depicted with the shaded gray area) is limited to a part of the electrode array only. The stippled line shows the direction of sampling for the spatial frequency analysis. D) Examples of time series used for the analysis of spatial frequency. This time series consists of about 50 samples that were collected from a single time point over the linear array. E) Spatial spectra of linear array recordings from three different scalp locations. There is a clear roll-off of power at around 0.5-0.8 cycles/cm that is shown highlighted by the shaded area. Note the remarkably similar 1/f linear slope in the middle part between the PSDx traces from different brain areas. The PSDx traces are cut at 2c/cm, which is the spatial Nyquist frequency in these recordings with sampling of 4 electrodes/cm

Single missing traces (e.g. see Figure 11-C; traces #19 and #48) were interpolated using the nearest two neighboring channels, which introduces a spatial lowpass filter, and hence a small but unavoidable underestimation of the higher spatial frequencies. Then, PSDx were calculated from the vectors created from the signal values across the channels at each sampling instance (see Figure 11-

D; see also [33]). Due to the EEG sampling frequency of 256 Hz, 256 PSDx traces per second resulted. Then the median value of each spatial frequency bin was calculated from each EEG epoch. The use of the spatial frequency spectrum to estimate the optimal electrode density (i.e. spatial frequency) can be considered analogous to the common use of temporal frequency spectrum (PSDt) to estimate the required (temporal) sampling frequency of the EEG signal. The canonical form of the spatial spectrum is three segments: a flat low-frequency segment, a middle segment with rapid fall in power with increasing frequency, and a flat high-frequency segment resembling that of white noise (see [132]). Most of the desired information is contained in the middle segment between the two inflections. The first step is to define the point in the spectrum where it reaches the noise floor (termed the "upper inflection point") which gives the upper end of the frequency range that should ideally be captured.

The second step is to calculate the number of electrodes with the specified interelectrode spacing that are needed to sample the entire range of spatial frequency [33, 34]. The lower inflection point gives an estimate of the desired width of the array. According to the Nyquist theorem, at least two samples are required to capture each cycle at the highest frequency with preferably three samples required to ascertain the 'practical' Nyquist frequency. The width of the array must be great enough to encompass at least one cycle of the lowest spatial frequency. In the temporal domain, these would be cycles per second (or Hz) and recording duration in seconds, whilst in the spatial domain they are cycles per centimeter and dimensions of an array in cm. For instance, in the case of 1cycle/cm, one should have at least two electrodes in each centimeter (i.e. 5 mm interelectrode spacing) to sample adequately the given spatial pattern in EEG oscillation. The product of the sampling frequency in number of electrodes/cm times the width of the array in cm gives the number of electrodes and channels required.

Methodological considerations

It would have been ideal to record with headgear that has sensors positioned in 2D with the density used in our current linear array. Our pilot experiments with a prototype of such ultrahigh density 2D

array showed that, with the technology available to us now, it was not possible to manufacture a gentle enough 2D array for the neonatal scalp. This might be possible in the future, as very dense arrays with even 128ch for a preterm baby have been recently manufactured commercially (Dr. Philip Grieve, personal communication). Frontal locations were not used because the babies felt too uncomfortable after placing the array onto the forehead, which led to excessive frontal muscle activation and contamination of the EEG (cf. [33]).

3.2.2.2 hdEEG experiment

We visually identified focal oscillations from epochs within EEG background classified as trace alternant, the dominant pattern during quiet sleep in neonates [22, 131]. This state was selected to provide better signal to noise for the subsequent analysis that targeted the bouts of rapid oscillations typically associated with spontaneous activity transient (SAT) events (see also [131, 133]). The oscillation bouts were identified after applying bandpass filtering (for reading only) into three frequency bands: 1-5 Hz, 5-10 Hz and 12-18 Hz. The filtering during visual reading was based on Butterworth forward filter with slope of 24 dB per octave built into ASA software (Advanced Source Analysis (ASA) ANT Neuro, Colosseum 22, 7521 PT, Enschede, Netherlands, www.ant-neuro.com). These frequency bands were selected to roughly correspond to the individual oscillatory components in the neonatal EEG (cf. [133]). All data were exported to EDF format and filtered at 1-20 Hz by using Butterworth forward and backward filter (zero phase) with slope of 6 dB per octave built.

In the further quantitative analysis, all signals were filtered into three frequency bands with FIR linear phase bandpass filters: 1-5 Hz (slope 12 dB/Hz, phase response 180 degree/Hz), 5-10 Hz (slope 5 dB/Hz, phase response 52.5 degree/Hz), and 12-18 Hz (slope 1.5 dB/Hz, phase response 23 degree/Hz). The instantaneous amplitude was then obtained from these signals using the analytic associate of signal as:

$$Z_k[n] \triangleq S_k[n] + jH[S_k[n]] = a_k[n]e^{j\phi_k[n]} \quad (16)$$

in which $H[.]$ is the Hilbert transform operator and $a_k[n]$ is the instantaneous amplitude. Epochs annotated visually as oscillatory bouts were selected and signals ordered according to peak amplitude. The signal with the highest amplitude was taken as the index for the given epoch, and the instantaneous amplitude values in all other electrodes were plotted as a function of inter-electrode distance. This yields graphs of amplitude decay as shown in Figure 12-B.

Finally, linear regression lines were fitted over the amplitude values within the nearest 5 cm from the index signal (see Figure 12-B) in order to obtain the slopes of amplitude decays, and to compare the decays between frequency bands (Figure 12-C). The use of several frequency bands is reasoned by the previous studies in adults showing that the spatial extent of an oscillation is proportional to its temporal frequency [134]. In neonatal EEG, the highest frequency range (>10 Hz) is likely most relevant [131, 135].

3.2.2.3 Simulation experiment

A 4-layer spherical head model was constructed (Figure 13) to study the effects of source depth and tissue conductivities on the PSDx in scalp EEG. To this end, we defined model dimensions to closely mimic the neonatal head (Figure 13) with a circumference of 36cm. This lead to the choice of the following radii: R_1 = 4.9 cm representing brain; R_2 = 5.3 cm representing CSF; R_3 = 5.5 cm representing skull; R_4 = 5.7 cm representing scalp. The following conductivity values were used based on a recent study [102]: σ_1 = 3.3 mS/cm for brain; σ_2 = 17.9 mS/cm for CSF and σ_4 = 4.3 mS/cm for scalp. For the skull layer, we tested two conductivities, 2.0mS/cm and 0.22mS/cm, to mimic previously published estimates of neonatal and adult conductivities, respectively. To analyze the effect of the dipole depth on PSDx, the simulations were run for dipole depths of 0.85, 1.0 and 1.2 cm from the scalp surface.

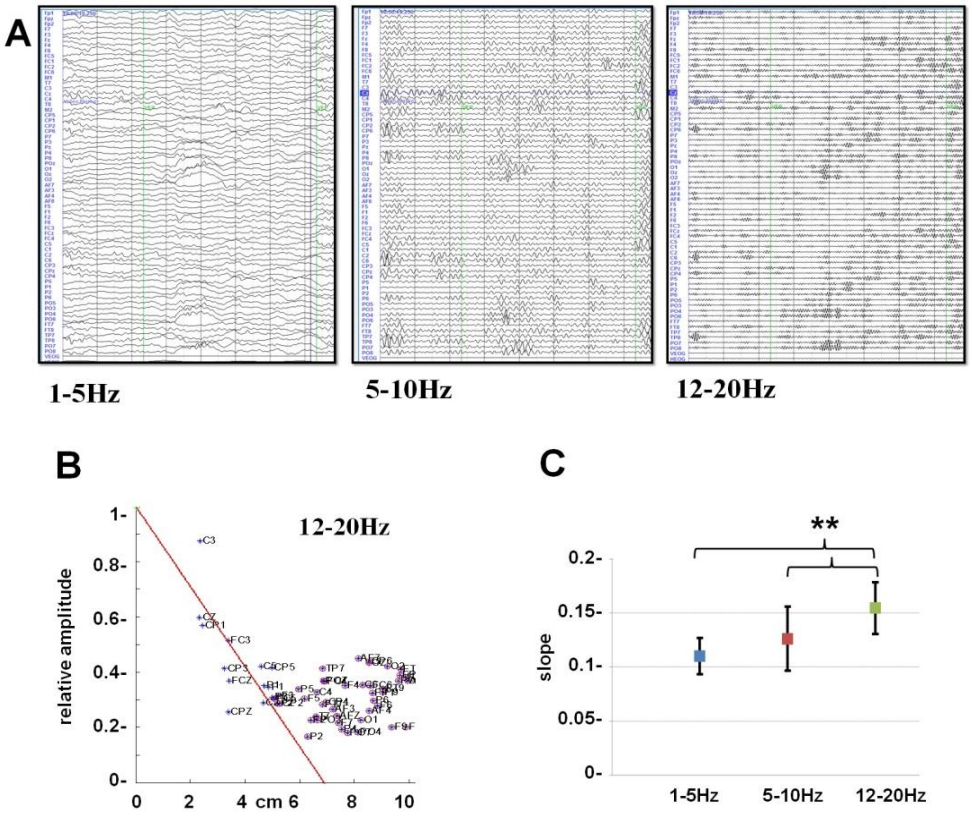

Figure 12 - Spatial decay of oscillation amplitudes, the hdEEG experiment A) Examples of a 64ch EEG tracing after band pass filtering for three different frequency bands . All frequency bands show spatially selective activation bouts, but comparison of the frequency bands shows clearly that the oscillatory bouts become patchier, i.e. more focal, as the frequency increases. B) Examples of analyses of the spatial decay of oscillation amplitudes at two frequency bands. The instantaneous amplitude of the given frequency band in each electrode is plotted as a function of distance from the electrode in the center of this oscillatory bout (i.e. the signal with the highest amplitude). Note how the amplitudes decay rapidly until they reach the "noise floor" at around 5cm from the peak. The slope of spatial amplitude decay is calculated from the signals that are within 5cm from the peak, as shown by the linear fitting in these graphs. C) Summary of the findings of slopes of spatial amplitude decay in different frequency bands. Note the increase in the slope, i.e. steeper decline of amplitudes, at higher frequency bands. Significant differences are shown with asterisks ($p<0.01$; Mann Whitney U-test).

In order to mimic our linear array device, we placed 50 electrodes with 2.5 mm spacing on the outer surface of the sphere simulating the scalp EEG points. The sources, point dipoles, were located on

radii at different depths from the scalp giving spacing between them slightly less than 3 mm. The linear separation between the dipoles was dependent on the depth of the dipole layer and the 3.0 mm separation between scalp potential points. Each dipole was oriented perpendicular to the tangent of the layer at its point. The dipole intensity was assigned by a random number generator giving a normal distribution with zero mean and unit standard deviation (SD).

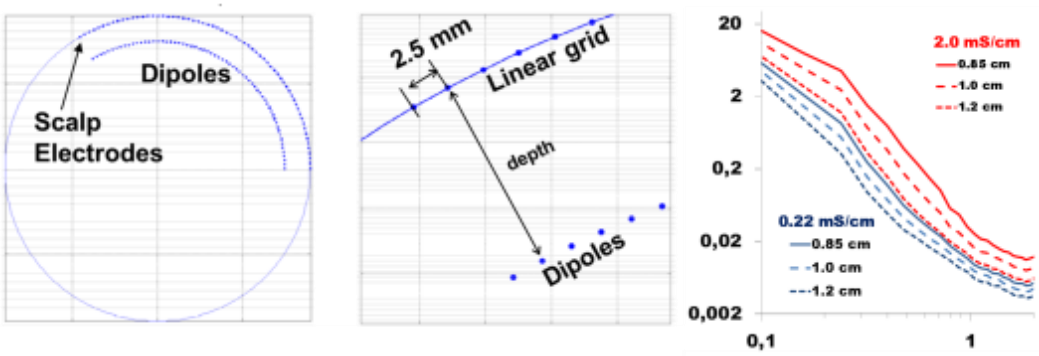

Figure 13 - Simulation experiment. Schematic drawing on the left shows the structure of our 4-layer spherical model (left) with neonatal dimensions (circumference ~36cm). The middle drawing demonstrates the placement of dipole sources on the cortex, as well as the 1-D linear array on the scalp. The graph on the right presents PSDx calculated as an average of 100 simulations in each trace. The upper three PSDx traces (red) represent situation where skull conductivity is set closer to the assumed neonatal value (2.0mS/cm) with varying depth of the source. The lower three PSDx traces (blue) represent situation with skull conductivity closer to the assumed adult skull bone conduction (0.22mS/cm). Note the strong dependency of PSDx, up to orders of magnitude, on both of these parameters.

The surface (scalp) potentials of the 4-layer head model were computed using the mathematical expressions described before by Sun [117] and using a Matlab 6.5 software package. The simulated scalp potentials were normalized to zero mean and unit SD by subtracting the mean of the spatial array of data and dividing by the SD. The spatial power spectral densities (PSDx) were computed using the 1-D FFT. The procedure was repeated 100 times with independent random intensity patterns of the dipoles, and the PSDx values were averaged.

3.3 Results

3.3.1 Linear array results

Inspection of the raw data from the linear array recordings showed that several EEG events, including single transients or short oscillations, were strictly confined to a few electrodes only. Figure 11-C shows an example where a rapid oscillation is evident in only about ten electrodes, which implies an extent of only 10 x 2.5 = 25mm on the scalp. The median PSDx calculated over the linear array electrodes shows that the PSDx of neonatal EEG follows the canonical form of the background EEG (cf. [33]) with a flat low-frequency plateau, middle nearly linear 1/f down-slope of log power vs. log frequency, as well as another plateau at a higher frequency range. The finding was qualitatively very similar between the two babies studied. Comparison of signals obtained from different scalp areas shows that the inflection point between the middle and higher frequency range is in all traces at around 0.5-0.8 cycles/cm (Figure 11-E), and the power law (1/f) –like linear slope in the middle part is similar in all three brain areas. The limited number of spatial points available in such real life recordings does not allow statistical testing of how strictly the neonatal scalp EEG follows a genuine power law distribution (cf. [136]), but the similarity between brain areas is notable.

There are, however, qualitative differences in the PSDx graphs between the slopes of the higher frequency segments: the signals measured from the parieto-occipital area (Figure 11-A) had steeper slopes than those measured from the parietal or midline areas. The exact anatomical match between the linear array positions and the underlying gyral and sulcal structures or inter-hemispheric fissures is unavailable. However, our observation suggests that the EEG information content extends to higher spatial frequencies over the cortical areas (parietal and parieto-occipital positions) as opposed to the scalp above the inter-hemispheric fissure (midline) (see Figure 11-E).

3.3.2 hdEEG results

Inspection of the raw data (Figure 12-A) shows that i) oscillations at all frequency bands cover only

part of the scalp, and ii) oscillations at higher frequencies tend to appear more "patchy" in the display that shows all electrodes. In other words, the higher frequencies appear to be spatially more limited. To assess the spatial extent of each individual oscillation, we looked at the spatial decay of oscillation amplitudes. The signal with maximal amplitude during the given oscillatory bout was taken as the index signal, and amplitudes of the neighboring electrodes were plotted as a function of distance. The amplitudes of focal oscillations decline to about half over the nearest 4-6 centimeters, and then the amplitudes reach the "noise floor" with no systematic further decline when moving away from the peak (see example in Figure 12-B). Using the linear regression line over the first 5cm from the index signal to see the slope of the amplitude decay showed that the highest frequencies had the steepest slopes (12-20 Hz: 0.15±0.02 (SEM); 5-10 Hz: 0.13±0.03; 1-5 Hz: 0.11±0.02, see Figure 12-C). The difference between the highest frequency and the lower frequencies was also statistically significant (Mann-Whittney U-test; $p<0.01$ for 12-20 Hz vs 5-10 Hz; $p<0.01$ for 12-20 Hz versus 1-5 Hz), however the difference between 1-5 Hz and 5-10 Hz frequency bands was not significant ($p=0.17$).

3.3.3 Simulation results

The averaged PSDx over the 100 PSDx from random dipole intensities is shown in Figure 13. Using the spherical model with neonatal dimensions (radii and tissue thicknesses) resulted in PSDx graphs with rapid decay between 0.1-1.0 c/cm, which is strikingly comparable to the PSDx computed from the linear array recordings (see Figure 11). Comparison of PSDx generated by using different scalp conductivities and source depths shows a clear effect of both parameters on the PSDx. Increasing the depth of the dipole layer from the highest position just below the highest gyri at about 8.5mm below the scalp towards cortical sites closer to the edges of gyri (up to 1.2 mm below the scalp) substantially decreased the power of PSDx at the spatial frequency range of 0.1 to 1.0 c/cm (note that the power in Figure 13 is shown in logarithmic scale).

This clear trend was seen using both values of skull layer conductivity. However, increasing skull conductivity near to values recently suggested for neonatal skull [102] lead to more than an order of

magnitude increase in PSDx at the spatial frequency range of 0.1 to 1.0 c/cm. A closer inspection of the PSDx from our simulation experiment suggests further that i) the slope within 0.1-1.0 c/cm range tends to be steeper with higher conductivity values, and ii) the higher conductivity is needed to create an apparent lower frequency inflection point at around 0.2 c/cm which is also seen in the real EEG from the linear array recordings (Figure 11- E).

3.4 Discussion

There is an increasing demand for source analysis of neonatal EEG, but currently there is inadequate knowledge about i) the spatial patterning of neonatal scalp EEG and hence ii) the number of electrodes needed to capture neonatal EEG in full spatial detail. This study addresses these issues by using a very high density (2.5mm interelectrode spacing) linear electrode array to assess the spatial power spectrum, by using a high density (64 electrodes) EEG cap to assess the spatial extent of the common oscillatory bouts in the neonatal EEG and by using a neonatal size spherical head model to assess the effects of source depth and skull conductivities on the spatial frequency spectrum.

The findings support the notion that the spatial patterning, the amount of unique information in neonatal scalp EEG, is much richer than has been commonly believed. Notably, the common perception has not been based on knowledge, but has emerged as a consequence of the way clinical routines were set by the early pioneers of neonatal EEG (reviewed in [22]). It is intriguing in this context, that the idea of rich spatial texture of this kind has been implicitly embedded in the conventional reporting and classification of neonatal EEG. It is well known that neonates may have focal sharp transients or epileptic discharges that only appear in one electrode (see e.g. [22, 78, 79]). If the spatial texture of neonatal EEG was smoothed (i.e., smeared) by volume conduction, such relatively high amplitude transients would be seen in many more electrodes. Our work is hence fully compatible with the implicit knowledge from prior descriptive literature on neonatal EEG, as well as with the prior theoretical analyses on EEG of older infants [113, 125].

Our observations from the linear array showed that the spatial characteristics of neonatal EEG follow

the canonical form of PSDx that is qualitatively similar to that previously published from comparable adult recordings [33]. The essential features of the PSDx for our present study were the inflection points at the lower and higher frequency ends of the middle part of the PDSx with a linear slope (in log-log coordinates). The middle segment delimits the frequency range with the maximal likelihood of finding information content with relevance to brain's electric activity. The inflection point on its right side yields the Nyquist frequency for spatial EEG sampling (see also [33]). The spatial frequency of this point (~0.5-0.8 c/cm) is equivalent to a wavelength of 1.25-2 cm.

Prior work analyzing PSDx from the adult scalp at a comparable temporal frequency range reported the corresponding spatial frequency to be ~0.2-0.4 c/cm, equivalent to a wavelength of 2.5-5cm [33, 34]. Because the spatial texture of EEG is spatially mostly noncyclic, it would be more robust to have the sample frequency 3–5 times higher than the frequency limit [137] which would yield interelectrode spacing of about 3-5mm in neonates and 5-8 mm in adults. Simulations with adult head model have even suggested need for interelectrode spacing as high as 3mm (see [138]). The inflection point on the left side (0.5 cycles/cm in Figure 11-E) indicates the minimum width of an array (2 cm) needed to capture a complete spatial pattern in the EEG in each temporal frequency band [130].

The hdEEG study showed that each oscillatory bout decayed to the level of the noise floor within about 4cm (higher frequencies; see Figure 12-B) around its peak location. In order to be detected, multiple electrodes within the given diameter of about 8cm are required. This would suggest that one needs to have electrodes spaced no more than 2-3 cm apart or conversely, that each electrode covers roughly about 3cm of scalp. These spatial considerations are even more important if source localization is an aim. To translate this to actual neonatal EEG recordings, we plotted examples of 3cm circles on the photographs of newborns with conventional neonatal EEG electrode positions and the hdEEG used in the present study (Figure 14).

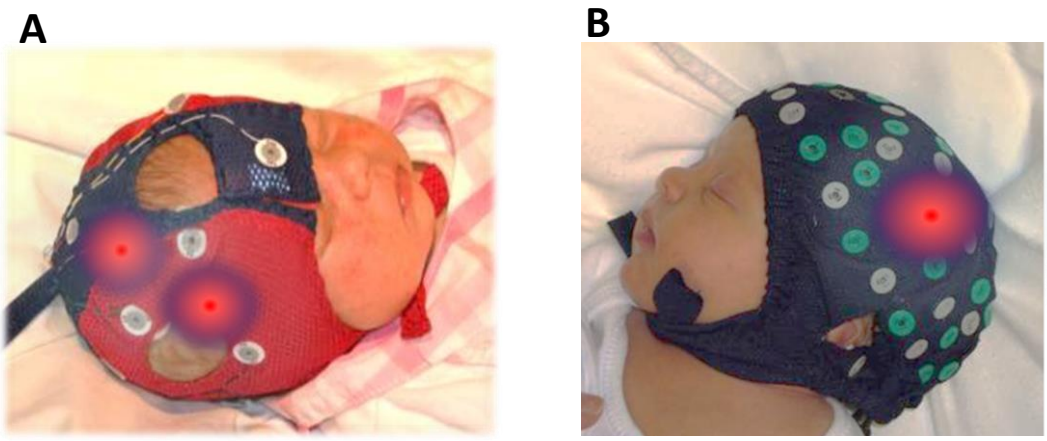

Figure 14 - Comparison of conventional and hdEEG recordings. A) the conventional "full array" neonatal EEG setting (10 electrodes) and B) the hdEEG setting (64 electrodes) used in the present study. The circles with graded colors plotted over the photograph have a diameter of about 4-5cm. They give a schematic representation of an oscillatory bout that declines to half of its amplitude within the circle, meaning that more than one electrode should be located within this area for its reliable detection. Note how the conventional neonatal EEG severely under-samples the scalp resulting in a high likelihood of missing oscillations of this kind.

The conventional electrode positioning, considered to be "the full neonatal array" [22] clearly ignore major parts of brain activity. In particular, electrode coverage of the parietal and centro-temporal areas, the areas with the most developmentally significant rapid oscillations, is so poor that even a majority of focal events may go undetected.

The difference in the estimates of the ideal interelectrode spacing between the linear array and hdEEG study is probably mostly related to the difference in the electrode contact area. The diameter of skin contact area in the hdEEG recordings (i.e. the diameter of the skin gel interface) is around 10-15mm, whereas it was only 1mm in our linear array. The scalp amplitudes within the skin-gel contact area are averaged, so each contact in the hdEEG is spatially averaging four to six consecutive linear array contacts. As a practical example, the local oscillatory bout seen in Figure 11-C (contacts 15-25) spans only 25mm, and so may be readily ignored by the spatial averaging inherent with the larger electrode

contacts.

These two ranges of ideal interelectrode estimates should be viewed in the practical context. The theoretical ideal obtained from the linear array recordings sets the upper limit to the density of scalp electrodes as 6-10mm spacing, but this raises practical challenges in devising appropriate and practical electrode caps. Approaches could include the use of dry electrodes [139], if their mechanical stability can be improved, or a modification of dense EMG arrays [140], if they can be developed to establish firm contact with the spherical-shaped baby scalp.

Our observation of the spatially highly varying patterns of neonatal scalp EEG suggests an opportunity for adjustment of the head model used in source localization paradigms. Recent studies have defined head model parameters for neonatal EEG source localization, most importantly tissue conductivities, by estimating the anatomical match between a known brain lesion and the inverse solution of a pathological EEG transient [25, 102]. This approach assumes that pathological EEG transients are generated within the lesion, which may not always be the case.

Our study on the spatial patterning of scalp EEG opens an alternative approach: as shown in our tentative forward model stimulation with spherical model, the head model parameters can be sought by modifying them in a forward solution so that the spatial patterning of the calculated lead field matrix resembles that of empirically observed scalp EEG. Our tentative experiment with a spherical model showed clearly how source depth will dramatically affect PSDx power. This observation implies that building a source analysis paradigm by using EEG from deep brain lesions as the anatomical reference (cf. [25, 102]) does likely present a significant bias when aiming to develop and validate source localization paradigms for cortical EEG activity. Moreover, our simulation experiments support the previous suggestions that skull conductivity does strongly affect PSDx. This highlights the urgent need to validate the range of physiologically relevant conductivity estimates to support realistic head models which is explained in next chapter of this thesis. Intriguingly in this context, electrical impedance tomography has been recently developed to a stage that it may offer an alternative paradigm for empirical estimation of *in vivo* tissue conductivities in humans [141, 142].

The clinical implications of our study must take into account the indication for each EEG study. Some applications such as long term brain monitoring, will likely not gain from higher spatial resolution. Recent advances in neonatal neuroimaging have clearly highlighted the clinical gain from increased spatial resolution in the anatomical domain. (e.g. [16-18]). The next obvious advance will be to define the functional correlate of any altered structure, and this can only be accomplished with improved spatial EEG information.

Finally, the observation of highly varying spatial patterning and power law-like (1/f) linear slope in the spatial spectrum is consistent with the idea that the development of infant cognition may be able to be studied by analysis of the formation of spatiotemporal patterns like cinematic frames [130] that in some respects resemble “neural avalanches” [143, 144]. Capturing these with novel dense array EEG devices, akin to what has been recently achieved with adult EEG [145-147], may open a novel window to capturing the details of emerging large scale brain processes, such as those related to perception and cognition [148].

CHAPTER 4: ESTIMATING SKULL CONDUCTIVITY IN REALISTIC NEONATAL HEAD MODELS[3]

4.1 Introduction

With the aim of solving the neonatal EEG source localization problem, some prerequisites were identified which must be fulfilled before proposing an inverse solution algorithm. The list of insufficiencies in realistic neonatal head models include the effect of fontanelles on the neonatal skull conductivity profile, the number of EEG electrodes required to support the spatial patterning of neonatal EEG, the appropriate dipole depth to model neural sources, and the neonatal skull conductivities. Each chapter of this dissertation has been dedicated to address one of these parameters which after completion will enable us to implement an inverse solution algorithm.

An empirical methodology was presented in chapter 2 to study the effect of the fontanelles in the neonatal skull conductivity profile. Then the spatial patterning of the neonatal EEG, i.e. the proper number of EEG electrodes to capture it in full spatial detail was studied in chapter 3 using the methodology presented in chapter 2. The main objective of this chapter is to estimate the two other remaining parameters of the neonatal head model; the skull conductivity which is considered the most significantly different element between neonatal and adult head models, and the appropriate dipole depth to model neural sources in the neonatal head models.

In order to address the question of the value for neonatal skull conductivity, empiric measures of spatial spreading in the neonatal EEG are combined with forward simulations using realistic neonatal head models. Accordingly two questions were answered: First, what is the extent of spatial correlations in the neonatal EEG signal? And second, by comparing this information to forward simulations with a realistic neonatal head model, what levels of skull conductivity could explain such spatial correlation in the neonatal scalp EEG?

Similarly to the previous chapter, the two empirical methods presented in chapter 2 i.e. the analysis

[3] **This chapter is an extension of the following paper:** Maryam Odabaee, Anton Tokariev, Siamak Layeghy, Mostefa Mesbah, Paul Colditz, Ceon Ramon and S. Vanhatalo, "Neonatal EEG at Scalp is Focal and Implies High Skull Conductivity in Realistic Neonatal Head Models," Neuroimage, vol. 96, pp. 73-80, 2014.

of spatial amplitude decay and the analysis of spatial correlation decay are used to empirically estimate neonatal skull conductivity. Then the finite element method (FEM) and boundary element method (BEM) techniques are used to generate realistic head models based on a manually segmented magnetic resonance image of a neonatal brain. Different skull conductivities (from 0.003 to 0.3 S/m) were implemented in these head models to calculate the spatial decays of scalp potentials produced by a single dipole in the cortex. Then the results of the spatial analysis in the simulations and real neonatal EEG were compared to estimate the appropriate range of neonatal skull conductivity.

The cortex-scalp distance is variable in different cortical regions, as explained in the first chapter, and because of insufficient knowledge of these variations in neonates and children it is necessary to determine the proper source depth before solving the inverse problem. In order to address this necessity, the generated head models were different in terms of the source depth chosen as were different skull conductivity values. Head models generated using FEM included radial sources in three different depths from the scalp surface placed in a parietal position. Each of these models were simulated using all three skull conductivity values. It has been shown in chapter xx that the spatial frequency of neonatal EEG also depends on the source depth. The produced models were used to study the relationship between different source depths and the spread of scalp EEG potentials.

4.2 Theoretical Background

It is now known that the conventional recording configuration using only 6-10 electrodes [22] hardly suffices to distinguish brain lobes from each other, and severely compromises spatial information content [35, 125, 149]. A better spatial parcellation has been recently attempted by devising various means to record high density EEG (hdEEG) from the neonatal head in the laboratory environment [25, 122, 150, 151], and in neonatal intensive care units [123, 152]. Increasing the number of recording electrodes leads to clear theoretical benefits, including recognition of cerebral activities that may, otherwise, go either unnoticed or unlocalized. Most importantly, a larger electrode number (i.e. increased spatial sampling), as explained in previous chapter, opens the possibility of genuine

source localization of neonatal EEG [25, 102, 153].

Previous studies have shown that neonatal / infant scalp EEG has a very high spatial content or spatial patterning [35, 125]. These works not only confirm that adding more electrodes adds non-redundant information, but also that spatial smearing of scalp EEG is substantially lower in neonates [35] than in adults [34, 103, 154]. This notion has far reaching implications: The salient low spatial smearing in the neonatal EEG means that the conductive pathways from the cortex (the generator) to the scalp electrode is not yet be ready in a manner Jan significantly different in babies compared to adults. An obvious difference is the head geometry where tissue layers are thinner in newborns. The shorter cortex-electrode distance is, by itself, unlikely to explain the observed differences in spatial smearing which in adults is commonly considered to arise from the poorly conductive skull layer.

Histological comparison of cranial tissues in infants and adults shows that the skull layer undergoes a significant development from the soft and relatively wet, un-ossified skull matrix [155] to a hard and relatively dry (ossified) skull bone in the adult. It is likely that this histological difference would lead to higher skull conductivity and hence less spatial smearing in neonates. It is not known; however, what skull conductivity values would be plausible in the neonatal EEG source localization. While electric impedance tomography has been developed to provide potential alternative paradigms for empirical estimation of *in vivo* tissue conductivities in humans [156, 157], there is no report of any direct experimental data on conductivity in live human neonatal skull. Skull conductivities have been studied in animal neonates [158], but those results cannot be used for the human because of the marked differences in the cranial histology in early development. Studies with EEG source localization of human neonatal EEG [25, 102] have avoided the issue by simply adopting conductivity values from the adult literature, however the lack of empirical reference makes interpretation of those results uncertain.

4.3 Methods and Materials

This study consists of two complementary parts, one empirical and the other based on simulations. The empirical part uses high density EEG (hdEEG) recordings to compare the spatial correlations in neonatal and adult EEG signals in order to estimate the spatial extent of focal transients in neonatal scalp EEG. The simulation part uses a realistic newborn head model to compute scalp potentials (forward solution) generated by discrete cortical dipoles mimicking cortical sources of focal transients in the real EEG. The simulations were computed for different skull conductivities to find the range of values of the conductivity of the skull capable of explaining the empiric observations.

4.3.1 Subjects and hdEEG recording

Four hdEEG recordings were acquired from four different newborns at term age in the Department of Children's Clinical Neurophysiology (Helsinki University Central Hospital) using a Full-band EEG [159] acquisition system with sampling rate of 256Hz or 512Hz (Cognitrace; ANT B.V., Enschede, The Netherlands, www.ant-neuro.com). A 64 channel hdEEG cap tailored for neonates (Waveguard, ANT B.V., Enschede, The Netherlands, www.ant-neuro.com; see also Stjerna et al., 2012) was used in this study. A video clip showing an EEG recording of this kind is available at www.nemo-europe.com/en/educational-tools.php. Informed consent was obtained from the parents prior to recordings. This study was approved by the Ethics Committee of the Hospital for Children and Adolescents, Helsinki University Central Hospital.

The four adult EEG recordings used in this study were kindly provided by Dr. German Gomeq-Herrero. They were recorded with a 256-channel EEG system (Geodesic Inc, www.egi.com) for unrelated studies in VU University of Amsterdam, The Netherlands.

4.3.2 Preprocessing and electrode grouping

4.3.2.1 Preprocessing

The data were first inspected visually using the ASA review software (Advanced Source Analysis (ASA) ANT Neuro, Colosseum 22, 7521 PT, Enschede, Netherlands, www.ant-neuro.com). Artifact-free epochs were selected irrespective of the sleep state. Data were then filtered with a 30Hz lowpass FIR filter prior to exporting it into European Data Format (EDF). All data were processed using common average reference (CAR). Further analysis was performed in the MATLAB (MathWorks, Natick, Massachusetts, U.S.A) environment using customized scripts described below.

4.3.2.2 Electrode grouping

The initial analysis assessed whether decays in EEG spatial correlation and / or EEG amplitudes depend on the scalp area. This is particularly relevant in neonates where fontanelles, a wider skull opening in the midline, is often claimed, without supporting evidence, to distort the scalp EEG potentials. To investigate this, spatial decays among three groups of electrodes were compared (see Figure 15 C): Group 1 electrodes included those located above the confluent layers of skull over central-parietal-temporal-occipital regions. Group 2 constituted the midline electrodes that always stand above or at the edges of the fontanelles. Group 3 electrodes were those in the frontal region where the skull layer is mostly closed, but the frontalles EEG phenomena are separated from other brain areas in the neonates [22]. When performing a within group analysis, amplitude / correlations were only computed among electrodes that belonged to the same group (e.g. group 2 decay did only reflect decay of amplitude / correlation along the midline). Finally, all electrodes together were also grouped and spatial decays were computed in all directions irrespective of its initial grouping.

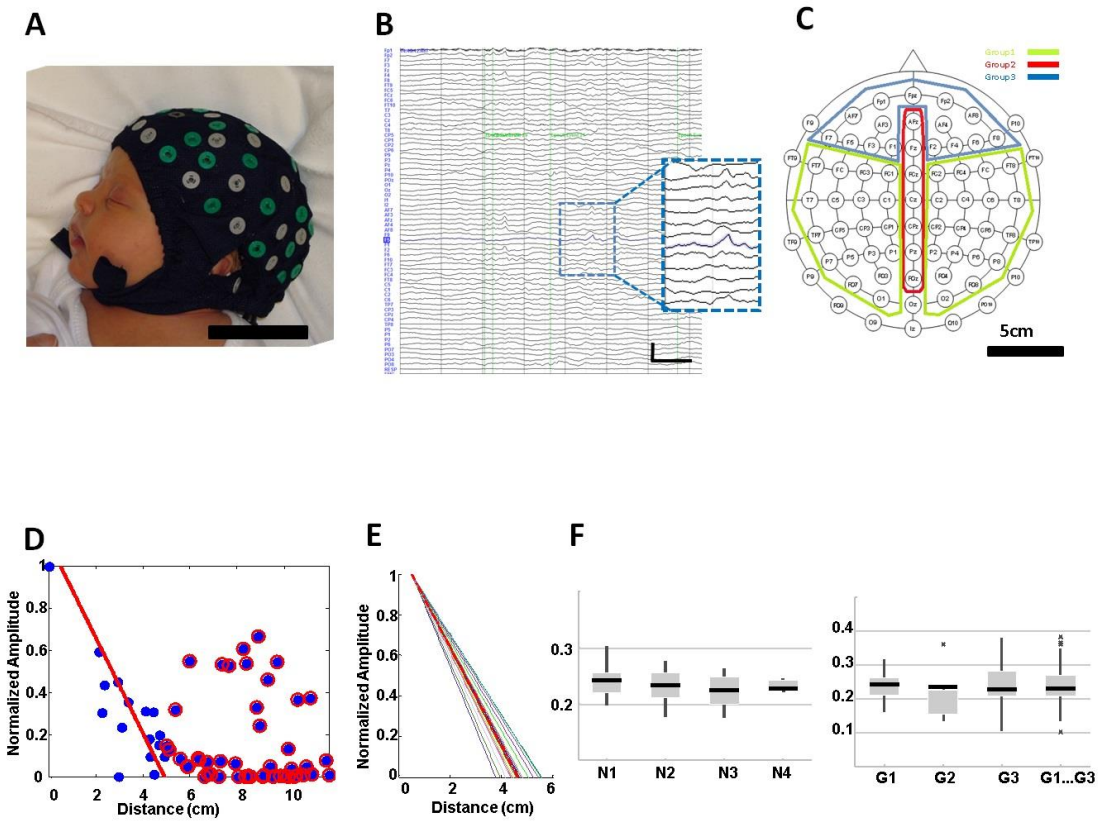

Figure 15 - Experimental setup and results of amplitude decay. A) An example of a 64 channel (hdEEG) recording in a term neonate. B) A seven second epoch of 64 channel EEG data with inset highlighting an example of focal transient in F5 electrode. C) The grouping of electrodes used for initial analysis of spatial amplitude and correlation decays (Group 1: Centro parietal areas, Group 2: midline above the fontanelles, and Group 3: frontal areas). D) Example of an amplitude decay result from an individual transient. The red line shows the linear fit over electrode amplitudes within 5 cm from the given index electrode. The circled electrodes (>5cm) are excluded from the linear fit. E) An example of all transients in one baby (thin black lines individual transients; red line the average). F) Summary of results from each baby (N1-N4; left graph) and from each electrode group (G1-G3, as well as all together G1-3), respectively.

4.3.3 Analysis of spatial amplitude decay

Focal transients, as explained in chapter 2, are a common and salient occurrence in both normal and abnormal neonatal EEG [22, 79, 160]. They are characterized by a short and relatively sharp

appearance and focal spatial distribution that is consistent with an underlying cortical origin. In this study, focal transients were marked by a board certified EEGer (S.V.) using the ASA review software and further analysis was performed using MATLAB. The electrode with the highest amplitude peak at the marked location was chosen as the reference electrode, and all potential values from other electrodes were plotted as a function of distance from this reference electrode. The reference electrode in this context is the electrode that was plotted at location zero in the spatial decay graphs (Figure 15 and Figure 16), and is not to be confused with the recording reference which in this study was grand average. This procedure was repeated for all focal transients, 110 in total (group 1 n= 38; group 2 n=21; group 3 n=51). Finally, a linear regression was computed over the nearest 5 cm (for newborns) or 10 cm (for adults) from the index electrode. Electrodes whose amplitudes were found to be >90% of the reference value were excluded from further analysis in order to mitigate the effects of noise and other artifacts.

4.3.4 Analysis of spatial correlation decay

Spatial decay of linear correlations between electrodes were computed using 2 minute long scalp EEG segments to see how rapidly these correlations decay as a function of distance from the reference electrode. This decay was taken as a measure of spatial smearing of scalp EEG. This approach, however, cannot distinguish between signal spread due to conductive tissue layers and multiple local sources from that generated by a large cortical source. However, results from previous studies strongly favor the interpretation that the relative differences between neonates and adults are mainly attributed to spatial smearing via volume conduction [35, 113, 161] .

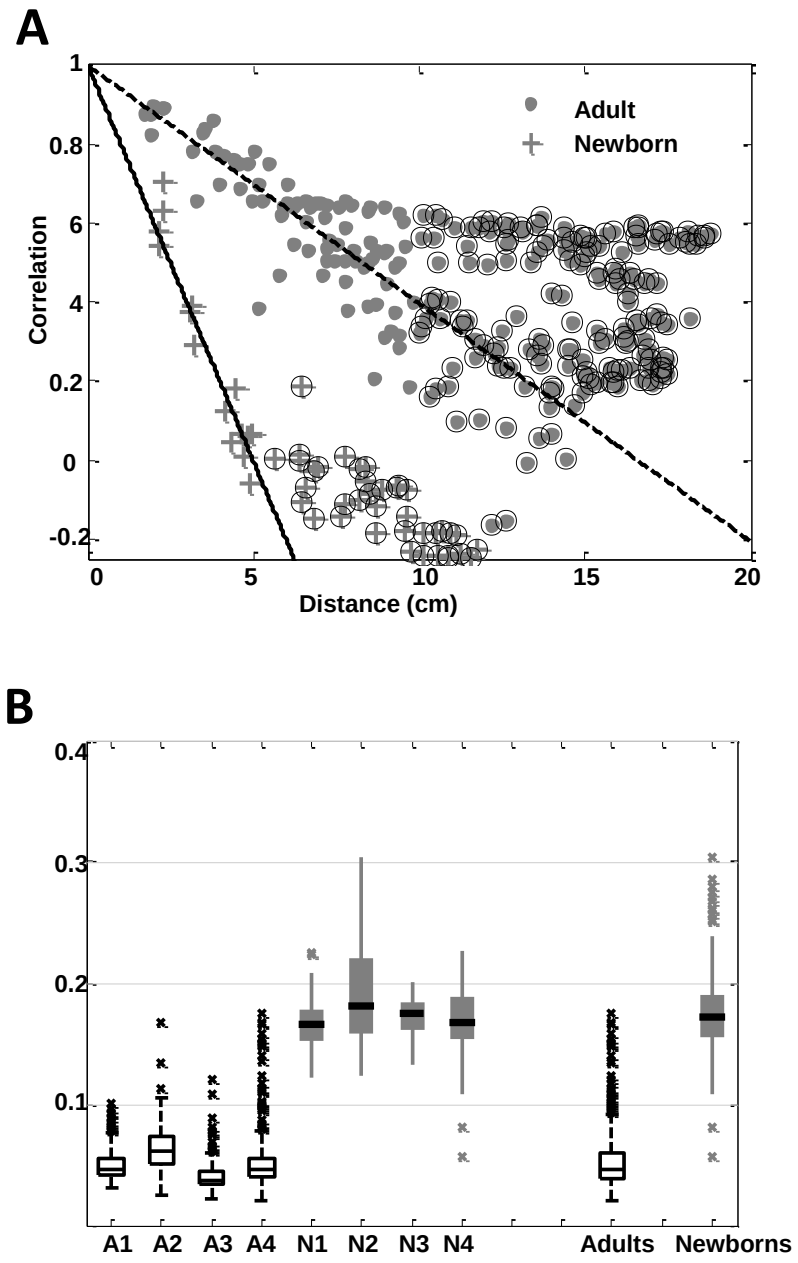

Figure 16 - Spatial correlation of amplitudes in neonates and adults. A) linear correlations between electrodes in a neonate (crosses) and in an adult (dots). Note the very steep decline of correlations in the neonate compared to adult. In the neonate, the background level (about zero) is reached near 5cm from the index electrode while in the adult the background level (about 0.4) is reached only at 10cm from the index electrode. Circled symbols are excluded from the linear fitting because of the distance. B) Spatial decays in linear correlations in all subjects. The decay slopes are comparable within groups (adults (A1-A4) and neonates (N1-N4) but are significantly different between groups ($p < 0.0001$).

It is known that temporal frequencies correlate inversely with the size of cortical generator [154]. In order to limit the analysis to cortical activities that likely encompass relatively small cortical areas, slow events were removed from the EEG as described in chapter 2. A median filter was applied using a window length of 120 samples (~230 ms in data sampled at 512Hz), which was seen to cover about half of focal transients analysed elsewhere in this work. Then the median low pass filtered data was subtracted from the original trace [162]. The advantage of this approach compared to conventional low pass filtering, is that it removes the low frequencies without introducing the typical "filter ringing" that would confound any subsequent analysis based on instant amplitudes.

Next, linear (Pearson) correlation was computed between the 2min (61440 samples) EEG segments from every electrode pair, and correlation coefficient was plotted as a function of distance between the electrodes. With the intention of assessing the general nature of the spatial decay, quadratic, cubic and linear functions were fitted to the different plots. It was found that the inter-electrode correlation decays can be adequately approximated by a linear function over closely spaced neighbors (see Figure 15 D), hence a linear approximation was adopted. Finally, the slope of the linear regression of these linear approximations was computed as a measure of the scalp EEG spatial decay.

4.3.5 Statistics

As most data was non-normally distributed (see Figure 16 B), nonparametric tests were used in all analyses. Comparison between individuals and groups was performed using analysis of variance with Kruskall-Wallis test. Any significant findings were followed by *post hoc* pairwise comparison with non-parametric Mann Whittney U test, which was also used for all pairwise group comparisons. Statistical significance was considered if $p<0.01$ was observed.

4.3.6 Head model generation

A T1 magnetic resonance image (MRI) was acquired with a Philips 3T scanner in Helsinki University Central Hospital from a full-term healthy baby. Each slice was 240x256 pixels with a pixel resolution of 1x1mm, and slice thickness of 0.9mm. From the full image stack, 176 slices covering the cranium were segmented manually into 5 compartments (scalp, skull, CSF, brain, eyes) by a clinician using FSL software [163]. The same segmented image stack was used for generation of both head models as described below.

4.3.6.1 Finite element method (FEM)

A 3-D FEM head model was generated using custom made scripts [164] from the segmented image stack where voxel resolution was 1×1×1mm. The electrical conductivities of various tissues were obtained from the literature as detailed below. For a given dipole position, flux and potential distributions were computed using an adaptive FEM solver [164]. The scalp potentials were extracted for further analysis. For a typical FEM run, voxel sizes varied from 1x1x1 to 16x16x16 pixels. A detailed image of a FEM run voxels is shown in Figure 17 where voxels near the dipole are of 1x1x1 pixel size, while voxels further away have varying size. The size of voxels was automatically adjusted in the FEM solver based on a preset L2 norm error limit on the normal and tangential fluxes at the voxel faces.

4.3.6.2 Boundary Element Method (BEM) head model

To generate the BEM-based head model, Brainstorm software [165] was used along with the previously segmented MRIs to construct 3D surfaces of the scalp, outer skull, inner skull and brain (Figure 17 A). To reduce the computational load, the raw 3D surfaces were down-sampled to sparser grids: scalp, inner skull and outer skull to 2562 vertices (5120 faces) and brain surface to 4322 vertices (8640 faces). The brain surface (that corresponds to be outermost cortical surface) was used as a source space (with a distance between sources are about 3 mm). The forward operator for this three-

shell model was computed using Symmetric Boundary Element Method in the OpenMEEG software [166].

4.3.7 Tissue conductivities

The purpose of this work was to define a plausible range of conductivities in the neonatal skull, which is the only conductive layer that undergoes substantial developmental change with respect to its histological and hence conductive properties. The conductivities were adopted for other tissue compartments (brain 0.33 S/m, CSF 1.79 S/m, scalp 0.33 S/m) directly from the prior literature [25, 164, 167]. The forward solutions were then computed with three different skull conductivities that ranged from the very poorly conductive estimate of adult skull to a high conduction similar to scalp (i.e. 0.0033 S/m, 0.033 S/m, and 0.33 S/m). It would be histologically acceptable to assume that the soft and well vascularized neonatal skull tissue [155, 168] has conduction properties comparable to scalp.

4.3.8 Forward solutions and their analysis

Forward solutions (scalp potentials in each scalp points, n=90649; see Figure 17 D) with FEM were computed for radial sources placed in a parietal position at three different depths (8mm, 13mm and 16mm) from the scalp surface, and the procedure was repeated for all three skull conductivity values (i.e. total of nine runs). Source depth was varied because the cortex-scalp distance is variable as shown in the present analysis (Figure 17 C) and the prior study of Beauchamp et al [169]. It has also been shown previously that spatial frequency of neonatal EEG depends on the source depth [35]. The source space in BEM is at the brain surface, so locations near the FEM source (parietal) were sought that were at depths of about 10-13 mm from the scalp surface.

The highest (peak) value of scalp potentials was defined, and then all other scalp potential values were plotted as a function of distance from the peak value (Figure 17 E). As the amplitude decay was found to be linear, in line with the empiric data, a linear regression line was fitted over the nearest 5

centimeters from the peak. The slope of this line was used to generate the graph that compares conductivities and source depths (Figure 17 F) as well as to finally compare these results to be empirical findings presented above.

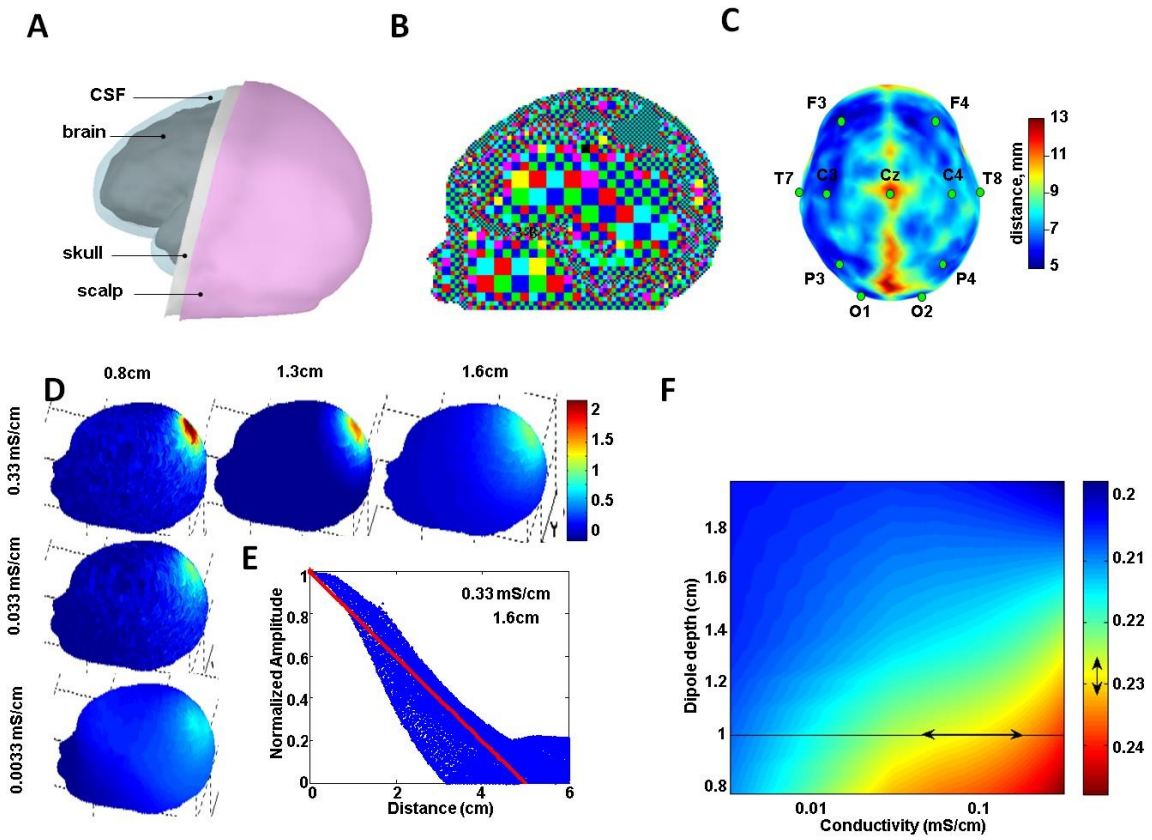

Figure 17 - Forward simulation using realistic head models. A) Segmentation of the neonatal MRI that was used for constructing both FEM and BEM. B) The adaptive FEM model generated from the segmentation shown in A. C) Topography of scalp-cortex distances in the segmented head model as computed from the BEM surfaces. D) Comparison of the effects of skull conductivity (0.33 to 0.0033 S/m) and source depth (from 8mm to 16mm) on the scalp distribution of EEG potentials. Note how the scalp potential becomes smaller and spatially flatter when the conductivity becomes higher or the source becomes deeper. E) An example of the spatial decay of scalp potential. Each blue point represents a scalp point in the head model (FEM). The linear fit used to obtain slopes is calculated for the first 5cm. F) Summary of all simulation results combining skull conductivity (X axis), source depth (Y axis) and the slope of spatial potential decay (Z axis). This combination plot can be used to suggest the skull conductivity that fits empirical observations of potential decay: First, the analysis of scalp-cortex distances (E) suggests that a relevant depth of the cortical sources could be around 10mm. Second, analysis of real EEG (Figure 15 D-F) suggests that the slope of amplitude decays is around 0.23. These will limit yield the suggested range of skull conductivities that is at around 0.06-0.2 S/m.

4.4 Results

4.4.1 Spatial amplitude decay

Inspection of the raw hdEEG data (Figure 15 B) shows that transients in the neonatal EEG often cover only a few electrodes, and that they can, hence, be assumed to have been generated by a focal cortical generator. All signal amplitudes at the given peak times were then plotted as a function of inter-electrode distance (Figure 15 D). Such graphs demonstrate clearly that the amplitudes decay rapidly within the first few centimeters before becoming scattered further away due to the presence of unrelated ongoing activity in other cortical areas. The slope of the linear fit was thus taken as a proxy of spatial amplitude decay. The slope values within each subject (example shown in Figure 15 E) were found to be notably consistent. The slope values in different newborns showed no significant difference ($p=0.52$; Figure 15 F). Moreover, comparison between electrode groups showed no significant differences between midline region (fontanelles) and other brain regions covered with newborn skull tissue ($p=0.21$ for comparison between groups). Taken together, these indicate that spatial decay of scalp amplitudes is consistent across scalp areas as well as between individuals.

4.4.2 Spatial correlation decay

Plotting the linear correlations between electrodes as a function of inter-electrode distance in the neonatal EEG showed a clear decay to near zero within about the first five centimeters (an example subject is shown in Figure 16 A).

Inspection of a similar analysis in the adult (256 channel) hdEEG recordings showed that the slope of spatial decay in the adults is strikingly flatter, and the levels of correlation tend to be more scattered throughout the scalp (i.e. at all distances). After inspecting a larger number of individual graphs (an example is shown in Figure 16 A), it was concluded that the adult EEG data exhibits a relatively linear slope up to about 10 cm from the reference electrode. Hence, the linear regression fit in the adult data was performed for the nearest 10 cm from the index electrode. The regression slopes were found to be consistent and without significant differences within the groups of neonates and adults

(Figure 16 B). However, the slopes were generally about three times steeper in the neonates compared to adults (mean slope in adults 0.052; mean slope in neonates 0.17), and the difference between age groups was highly significant ($p < 1e-5$).

4.4.3 Forward model simulations

Spatial decay of scalp EEG was next estimated from the realistic shape neonatal head model where the EEG source was placed at varying depths in the parietal cortex. The distribution of scalp potentials has a clear peak above the source consistent with the radial source orientation. Comparison of different skull conductivities showed, as expected, that the scalp potential becomes progressively smoother towards the lower conductivity. Indeed, with the skull conductivity adopted from the adult literature (0.0033 S/m), the scalp potential distribution from a single focal cortical source extended over half of the head which is different from the empirical results observed in the neonatal EEG signals.

Similar analysis using the BEM model (Figure 18) showed that the plots of spatial amplitude decay have considerably less scatter, which is likely due to reduced noise in the relatively simple forward solution of BEM. As shown in Figure 18, the results between FEM and BEM models were generally comparable. Consistent with the results from prior studies using the 4-layer spherical neonatal head model as explained in the previous chapter, a clear relationship between different source depths and the spread of scalp EEG potentials was found. The most superficial source (at 8mm depth) produced a highly focal potential distribution, which became considerably broader as the source was placed deeper at 13mm or 16mm.

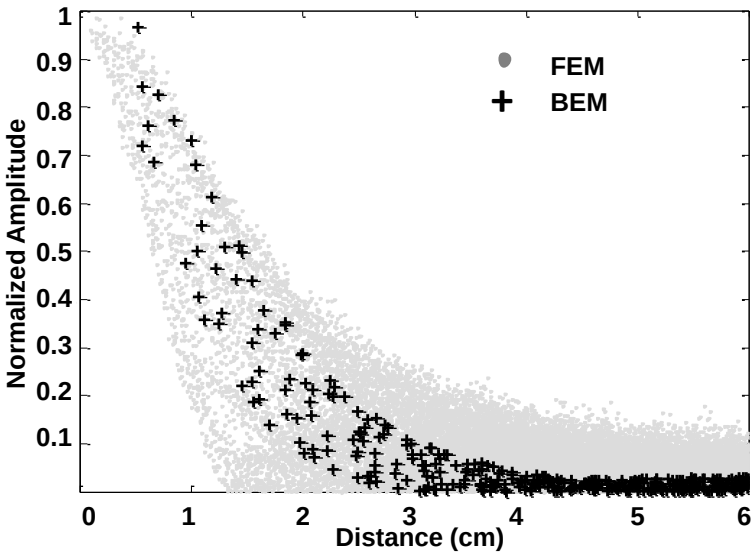

Figure 18 - Comparison of FEM and BEM models. This graph has superimposed plots of spatial decays of scalp amplitudes from FEM (gray) and BEM (black) forward simulations. The overall rate of spatial decay is notably similar, though there is more scatter in the FEM model. In these plots, conductivity was set to 0.33 S/m, and the dipole depths were 8mm and 13mm in FEM and BEM, respectively.

4.4.4 Comparison of empirical and simulation results

The simulations yielded a two dimensional relationship of spatial decays (Figure 17 F) of scalp EEG potentials as a function of the skull conductivity and the source depth. In order to determine empirically the range of plausible conductivity values associated with neonatal skull, there is first a need to define an anatomically reasonable source depth. For that purpose, skull-cortex distances were computed (Figure 17 C) that, together with a recent study [169] suggest that the surface of cortex is at around 6-10mm from the scalp. Second, the range of empirical regression slope values (around 0.23) that resulted from the analysis of neonatal EEG (Figure 15) to limit the focus in the z axis. After limiting the focus in depth and slope (x and y, respectively), the graph will return the range of y values, the skull conductivity, that here is within the range of about 0.06-0.2 S/m.

4.5 Discussion

These findings support the notion that the EEG recorded from the newborn scalp is very focal in nature, and that this is in part the result of the high conductivity of the skull tissue. The EEG activity generated by a focal source was found to decay within a few centimeters at the scalp, on average, three times faster than in the adult EEG. Simulations using a realistic neonatal head model indicate that neonatal skull conductivity is close to that of soft tissues, and hence orders of magnitude higher than conventionally assumed for the adult skull. These results are fully consistent with recent empiric [151] and simulation findings [113], and our findings of spatial correlation in the adult EEG data compare well with prior similar analyses on adults [161]. Notably, this work also validates recent suggestions [35, 102] to use higher skull conductivity values for the neonatal skull.

The observed steep spatial decay of amplitudes is consistent with the results reported in the previous chapter for the high spatial complexity in the neonatal EEG. Moreover, it implicitly explains why there is no significant difference between electrodes in the midline and other scalp areas. This is in apparent conflict with the common assumption of EEG distortion by fontanelles in neonates; however such thinking results from ignorance of the particular developmental histology of the neonatal skull tissue and its conductivity value. It has been clearly established [168] that neonatal skull bone is not ossified at birth, that the skull tissue undergoes a membranous type ossification during early life, and that the histological structure of skull remains trabecular [170, 171] for a longer time, hence providing tissue pathways with high electric conductivity until the skull becomes fully ossified later in life. Our conclusion of very high neonatal skull conductivity, indeed comparable to other soft tissues, is fully compatible with these anatomical considerations.

There are three factors that cannot be directly controlled, but they may potentially confound our empirical analysis. Their bias is, however, likely to lead to a conservative estimate of skull conductivity, because they tend to make the slopes of spatial decay flatter. First, the hdEEG only includes 64 channels which results in inter-electrode distance of about 20-30mm. Such spatial sampling implies that the amplitudes and linear correlations would have already decayed within the

nearest few electrodes. The linear regression slopes were computed from the nearest few electrodes in each case.

Second, an unrelated brain activity across cortical areas may unavoidably bias estimates of spatial decays (of both transient amplitudes and inter-electrode correlations) towards flatter slopes. Third, it is obvious that the cortical generators are not point sources, but that they have an unknown spatial extent. The true spatial decay related to signal smearing in the conductive tissues should be analyzed from the edge of the putative cortical generator area, if such was known. It is also possible that distant cortical sites have high signal correlations due to their genuine synchrony [133, 148, 172-174], which would lead to a flatter spatial decay of correlations due to physiological rather than volume conduction effects.

Source localization in neonatal EEG has recently generated considerable interest due to rapid progress in developmental neuroscience and computational methods as explained in the first chapter [25, 167]. The recent introduction of hdEEG recording methods [25, 122, 150, 152]; has been the crucial technical advance opening the way for improvements in source localization approaches. It is intriguing in this context, that the result of neonatal EEG analysis are indirectly challenging the view based on adult EEG, that source localization or source space signal analysis [174, 175] would be superior to signal space (i.e. raw scalp EEG data) analysis. The high spatial specificity of neonatal EEG shown here [35, 113] implies relatively little cross talk between scalp EEG channels. Hence, the typically used low numbers of scalp electrodes, ranging from the conventional eight [22] to about 20-30 electrodes [173], can be considered to yield relatively non-redundant signals. However, anatomical localization of EEG signal sources is still required for the process of combining EEG and functional MRI studies that became accessible once they were reported to be safe in neonates [176].

While conventional neonatal EEG recordings are spatially too under-sampled to genuinely gain from source localization, it is possible to add further spatial localizing information using the following advances: First, the number of electrodes from the presently used 64 channels should be increased, and the anatomical positioning of electrodes in each recording session should be considerably

improved from the presently used anatomical landmarks [177]. These challenges are already solved and the methods exist for their clinical implementation [178]. Second, the head model used for source localization needs to be computed for each individual recording session because of the substantial variability in head geometries between neonates, as well as within the same infant (due to development) between different recording sessions. Third, the EEG activity in neonates arises from different underlying mechanisms where much of the early activity is, indeed, orchestrated by immature thalamo-cortical or subplate-cortex networks. Details of the networks involved in early EEG generation are only known from experimental animal models, which have been shown in the spatially coordinated spontaneous activity transients that are distinct from those giving rise to traditional EEG oscillations of older subjects [19, 179-183], which are not compatible with the *a priori* assumptions that underlie the adult source reconstruction paradigms. All these issues pose significant technical, physiological, ethical, and logistic challenges in attempts to push the limits of spatial source localization of neonatal brain activity.

CHAPTER 5: LOCALIZATION OF NEONATAL EEG USING AN ENHANCED TIME-FREQUENCY MUSIC APPROACH

5.1 Introduction

This chapter proposes, evaluates and validates an accurate source localization technique for the neonatal EEG (nEEG) based on time-frequency analysis. A requirement of such a method is that it should have the capacity to accurately localize normal EEG patterns such as focal fluctuations of amplitude as a common feature of nEEG. Solving the EEG source localization (ESL) problem requires an accurate model of the newborn head. To have such a model, an accurate knowledge of the electrical conductivities and thicknesses of the different head layers (CSF, Skull and scalp) is required. Currently, no accurate value of these parameters exists and, as a consequence, I proposed in previous chapters to indirectly obtain these parameters. Therefore, values of these parameters, along with the appropriate number of electrodes and the dipole's depth, were indirectly estimated using the approach proposed in chapters 3 and 4 (see also [32, 35]). These values were used as a basis to develop a realistic head model which, in conjunction with the time-frequency multiple signal classification (TF-MUSIC) algorithm, was used to solve the EEG inverse problem.

Unlike previously reported studies [71, 72], in the proposed TF-MUSIC-based ESL method, the regions of interest (ROIs) for nEEG in the time-frequency plane are identified automatically, rather than manually. Since manual ROI identification is subjective, and hence the result of EEG source localization can be changed based on the competency of the user, it is preferred to be avoided in the possible applications. More importantly, determining the ROI in the time-frequency plane requires knowledge and expertise not present in clinical practices. Consequently, the important advantage of automatic ROI identification is that it makes it possible TF-MUSIC algorithm can be used even where no knowledge of Time frequency conversion of EEG signals is available. In this new approach, time-frequency representations of nEEG signals are interpreted as images that are processed to identify the ROIs automatically. A new performance metric was introduced to objectively evaluate the

performance of the proposed method using realistic simulated EEG data (EEG simulations generated using a realistic head model). It was also evaluated by comparing to other previously proposed source localization techniques. The proposed method was also evaluated using real EEG data such as Visually Evoked Potentials (VEP) with known cortical representations. The next section contains the theoretical background used to develop the TF-MUSIC source localization algorithm including time-frequency analysis, forward and inverse problems.

5.2 Theoretical Background

5.2.1 Time-frequency analysis: a brief review

Time-frequency signal analysis is an advanced harmonic analysis technique [184] introduced to analyse nonstationary signals, or signals whose frequency content varies with time. The widely used Fourier analysis, regarded as a major achievement in Physics and Mathematics [185], fails to provide information on incident time of spectral components [186, 187]. This is because the Fourier representation transform is defined as a weighted average of the time-domain signal [188]. This is mathematically expressed as:

$$X(f) = \int_{-\infty}^{\infty} x(t) e^{-2\pi f t} dt \tag{17}$$

where $X(f)$ stands for the Fourier transform. This representation is appropriate when the signal $x(t)$ is stationary. However, when the signal is nonstationary, as in the case of EEG [93], the Fourier transform does no longer lead to an accurate representation of the signal [188].

In the case of a signal with slowly time-varying spectra, a possible strategy to overcome the limitation of the Fourier transform, is to use the windowed Fourier transform for the time periods in which the signal is stationary [189]. This approach, called short time Fourier transform (STFT), was the earliest proposed linear time-frequency representation / distribution (TFD) [186, 187]. The name “linear”

comes from the fact that the transform is a linear function of the time domain signal. However, many natural and man-made signals have spectral content that varies quickly with time. As a consequence, no appropriate window exists that achieves a good time-frequency resolution trade-off while satisfying the stationary condition [186, 190]. It is therefore necessary to use other more advanced techniques to overcome this problem. A possible solution would be to use higher (than linear) order time-frequency representations. One of the most widely used classes of higher order time-frequency representations is the quadratic class discussed below.

5.2.1.1 Linear time-frequency distributions

One of the main properties of this category of TFDs is linearity. If the signal $x(t)$ under analysis is a linear combination of components $x_i(t)$, its TFD is a linear combination of the components' TFDs.

$$x(t) = \sum_i a_i x_i(t) \;\Rightarrow\; TFD\{x(t)\} = \sum_i a_i \, TFD\{x_i(t)\} \tag{18}$$

Two important members of the linear class of TFDs are the STFT and wavelet transforms (WT). STFT of the continuous time signal $x(t)$ at time t is essentially the Fourier transform of the signal multiplied by a finite length analysis window $w^H(\upsilon - t)$ centred at the time t. In other words,

$$STFT_x^w(t,f) = \int_{-\infty}^{+\infty} [x(\tau) w^H(\tau - t)] e^{-j2\pi f\tau} d\tau \tag{19}$$

where $-^{\boldsymbol{H}}$ denotes the conjugate transpose [191]. The STFT strongly depends on the choice of analysis window. It can also be expressed in terms of the spectra of the signal and the analysis window as

$$STFT_x^w(t,f) = e^{-j2\pi ft} \int_{-\infty}^{+\infty} [X(\upsilon) W^H(\upsilon - f)] e^{j2\pi f\upsilon} d\upsilon \tag{20}$$

where X and W stand for the Fourier transform of $x(t)$ and $w(t)$ respectively. This formulation

indicates that the STFT can be derived by passing the signal through a bandpass filter with the centre frequency f. This makes it possible to implement the STFT using a filter bank.

Wavelet transform is the other widely used linear TFD which has found numerous applications in different areas of engineering. Although WT is mostly known as a time-scale transformation, it can be shown to be a time-frequency representation through a simple manipulation:

$$WT_x^w(t,f) = \sqrt{|f/f_0|}\int_{-\infty}^{+\infty} x(\tau)w^H\left[\frac{f}{f_0}(\tau - t)\right]d\tau \tag{21}$$

in which $w(t)$, a real or complex bandpass function with the central frequency f_0 centred on $t = 0$, serves as the analysis wavelet [187]. The relationship between scale a and frequency f is given by $a = f_0/f$.

5.2.1.2 Quadratic time-frequency distributions

Although a linear relationship between a signal and its TFD is a desirable property in many situations, it is not the case when one uses the TFD to represent the signal's energy distribution in time and frequency. In this case, the quadratic representation is more suitable. However, because of the uncertainty principle

$$\Delta t \Delta f \geq \frac{1}{4\pi} \tag{22}$$

which relates to the average analysis window Δt to the average analysis bandwidth Δf , it is not possible to analyse the signal with desirable accuracy in both time and frequency domains. In other words, the uncertainty principle limits the ability of any quadratic TFD to have a high resolution in time and frequency simultaneously. Nonetheless, it does not put any limit on marginal properties which states instantaneous power and energy spectrum; hence an ideal TFD is expected to comply with these marginal properties [187] as

$$\rho_{xx}(t,f) = QTFD\{x(t)\}$$

$$\int_{-\infty}^{+\infty} \rho_{xx}(t,f)\, df = |x(t)|^2 \tag{23}$$

$$\int_{-\infty}^{+\infty} \rho_{xx}(t,f)\, dt = |X(f)|^2 \tag{24}$$

There are a number of quadratic TFDs that satisfy both marginals. Among those is the well-known Wigner distribution [190]. The Wigner distribution of signal $x(t)$ is defined as

$$W_{xx}(t,f) = \int_{-\infty}^{+\infty} x\left(t + {}^{\tau}/_{2}\right) x^{H}\left(t - {}^{\tau}/_{2}\right) e^{-j2\pi f\tau} d\tau \tag{25}$$

or equivalently by

$$W_{xx}(t,f) = \int_{-\infty}^{+\infty} X\left(f + {}^{\upsilon}/_{2}\right) X^{H}\left(f - {}^{\upsilon}/_{2}\right) e^{j2\pi f\upsilon} d\upsilon \tag{26}$$

Due to the Hermitian symmetry [192] of the Fourier transform for real-valued signals; that is

$$x(t) \in \mathbb{R} \Rightarrow X(-f) = X^{*}(f) \tag{27}$$

the spectral representation for negative frequencies does not convey any extra information. This means that ignoring the signal's spectrum associated with the negative frequencies, when calculating the Wigner distribution, will not lead to any loss of information. To the contrary, doing this allows for a reduction in computational cost and sampling rate without introducing aliasing [193]. This is achieved by replacing the real-valued signal $x(t)$ by its analytic associate $z(t)$ in equation (25) [188]. The analytic signal $z(t)$ is obtained by:

$$z(t) = x(t) + j\mathcal{H}\{x(t)\} \tag{28}$$

where the $\mathcal{H}\{x(t)\}$ stands for the Hilbert transform of the signal $x(t)$ and is defined as

$$\mathcal{H}\{x(t)\} = \mathcal{F}^{-1}\{-jsgn(f)\mathcal{F}\{x(t)\}\} \tag{29}$$

$\mathcal{F}$ and $\mathcal{F}^{-1}$ stand for the Fourier and the inverse Fourier transforms respectively [194]. Using the analytical signal leads to a new TFD, known as the Wigner-Ville distribution [195] (WVD),defined as:

$$WVD_{xx}(t,f) = \int_{-\infty}^{+\infty} z\left(t + {}^{\tau}/_{2}\right) z^{H}\left(t - {}^{\tau}/_{2}\right) e^{-j2\pi f\tau} d\tau \tag{30}$$

The many desirable mathematical properties of the WVD make it one of the most important and widely used member of the quadratic TFD class. The other members can be obtained by simply smoothing or filtering the WVD. The general form of the quadratic class of TFDs can be expressed as:

$$\rho_{xx}(t,f) = \int_{-\infty}^{+\infty} \int_{-\infty}^{+\infty} G(t-u,\tau) z\left(u + {}^{\tau}/_{2}\right) z^{H}\left(u - {}^{\tau}/_{2}\right) e^{-j2\pi f\tau} du d\tau \tag{31}$$

in which $G(t)$ is the smoothing function, also known as the kernel [188]. A comprehensive review of the quadratic time-frequency distributions can be found in [187-191, 196-198].

5.2.2 Forward problem

Solving the forward EEG problem is part of the method proposed for neonatal ESL in this chapter. In order to solve the inverse EEG problem, that is to find the brain current sources responsible for generating the EEG measured at the scalp, it is necessary to have a model of the head. In the case of the TF-MUSIC algorithm, this translates to having access to the Lead Field Matrix (LFM). The LFM is obtained by solving the forward problem that is to find the potentials generated by current sources within the brain.

5.2.2.1 Lead field matrix

As mentioned above, the EEG Forward problem describes the task of computing the scalp potentials generated by hypothetical dipoles, or more generally from current distributions, inside the brain [36].

Because most of the EEG energy resides in the 0.1 to 100 Hz frequency band [1], the forward model can be described using the quasi-static version of Maxwell's equations [47, 80]. Under this condition, the static electric field $\mathbf{E}$ can be expressed as [47]

$$\mathbf{E} = -\nabla \mathbf{V} \tag{32}$$

where $\mathbf{V}$ is the vector potential and ∇ represents the gradient. This can be combined with the other Maxwell equation [47] which relates divergence of the current density $\boldsymbol{J}$ to current source distribution $\boldsymbol{S}$

$$\begin{aligned} \nabla \cdot \boldsymbol{J} &= \boldsymbol{S} \\ \boldsymbol{J} &= \sigma \mathbf{E} \end{aligned} \tag{33}$$

where $\nabla \cdot (\ )$ represents divergence and σ is the electrical conductivity of the volume. This combination will result in the following equation, Poisson's equation, which gives the potentials $\mathbf{V}$ at any position in a volume conductor due to current source distribution:

$$\nabla \cdot \big(\sigma(\nabla \mathbf{V})\big) = -\boldsymbol{S} \tag{34}$$

The electrical conductivities of the different head tissues along with the geometry of the volume representing the head are the major factors that determine the accuracy of the forward solution. Due to the linearity of Maxwell's equations, the solution of the above differential equation, i.e., the measured potentials at each scalp site, is assumed to be a superposition of potentials generated by all point sources (dipoles) within the brain [10], expressed by:

$$\boldsymbol{V} = \boldsymbol{LS} \tag{35}$$

in which $\boldsymbol{L}$ is the LFM that indicates gain from each source to measurement positions. The EEG signal in this case can be stated as the linear combination of these potentials and the additive noise $\boldsymbol{N}$ collected by EEG electrodes

$$\boldsymbol{X} = \boldsymbol{V} + \boldsymbol{N} \tag{36}$$

The corresponding sampled multichannel (M channels) discrete-time EEG can be denoted as

$$\boldsymbol{X}[n] = \left[x_1[n], x_2[n], \cdots, x_M[n]\right]^T \in \mathbb{R}^{M\times 1} \tag{37}$$

in which $x_i[n]$ is the scalp EEG measured by the i^{th} channel and the discrete time source spatio-temporal variations for a set of P sources will be

$$\boldsymbol{S}[n] = \left[s_1[n], s_2[n], \cdots, s_p[n]\right]^T \in \mathbb{R}^{P\times 1} \tag{38}$$

Hence, the source signals and the measured EEG at each time instance n are related by a set of linear equations

$$\boldsymbol{X}[n] = \boldsymbol{L}\,\boldsymbol{S}[n] + \boldsymbol{N}[n]; \tag{39}$$
$$\boldsymbol{L} = \boldsymbol{\Lambda\Phi}$$

where $\boldsymbol{X}[n]$ (M × 1) is the multichannel EEG vector, $\boldsymbol{S}[n]$ ($P \times 1$) is the source vector, $\boldsymbol{N}[n]$ (M × 1) is the measurement noise vector, and $\boldsymbol{L}(M \times P)$ is the LFM which contains the location ($\boldsymbol{\Lambda}$) and orientation ($\boldsymbol{\Phi}$) information of the dipoles [36, 69, 73]. The LFM includes one column corresponding to each dipole (source) which states the gain values from that source to each measurement location (M rows) on the scalp. The orientations of the dipolar sources, representing the neural currents, are assumed to be normal to the cortex surface and fixed during a specified time period. The non-normal dipole orientations are implemented by means of three orthogonal dipoles within the same location. There are two commonly used numeric methods for solving the forward model and obtaining the LFM: the Boundary Element Method (BEM) [199] and the Finite Element Method (FEM) [200]. BEM calculates the potentials at the boundaries of a volume induced by a current source. Although it is restricted to isotropic conductivities, it is widely used because of its low computational cost [47].

FEM, contrary to BEM, solves the equations in the differential form for each single 3D segment of the volume. It has been shown, when piecewise constant conductivity is assumed (instead of a spatially varying anisotropic conductivity model), both methods perform similarly in terms of the accuracy of the inverse problem solution [10].

5.2.2.2 The neonatal head model

In order to solve the forward problem for a specific subject, parameters such as the geometry of the head, conductivity of the tissues forming the head and electrodes locations need to be known [32]. Then the head volume is divided into very small regions and the electrostatic equations are solved for hypothetical sources in these regions.

If spherical geometry with homogenous conductivity is used for approximating the head, analytical solutions of the forward problem can be obtained. However, spherical models that can reasonably approximate the upper regions of the head do not lead to satisfactory results in terms of the overall source localization accuracy. To remedy this problem, realistically shaped models are used to represent the whole head [10, 48]. These models are generated by incorporating anatomical information obtained from medical imaging modalities such as MRI.

There are several major differences between neonatal and adult heads, as explained in Chapter 2. In addition to the volume, the physical attributes of different tissues composing the head account for most of the dissimilarities. While the fontanelles comprise an important geometric distinction between the two heads, the skull conductivity is the most import source of the difference. The important role played by the conductivity in the solution of the inverse problem comes from the fact that EEG signals are predominantly produced by ohmic current flow in the head, rather than by capacitive or inductive currents [10].

5.2.3 Inverse problem

The EEG inverse problem is the problem of using the scalp potentials and the LFM to estimate the location, orientation, and strength of the different brain current sources or dipoles, i.e., solving Eq. (39) for $\boldsymbol{S}[n]$ given $\boldsymbol{X}[n]$ and $\boldsymbol{L}$. Although many methods were proposed for solving the inverse problem in the case of adults, no method currently exists for the case of the newborn [151]. The accuracy of the ESL technique critically depends on the quality of the head model [27]. The lack of an accurate newborn head model has been the major obstacle for solving the EEG source localization in neonates.

5.2.3.1 Selecting an inverse solution for the neonatal EEG source localization

This choice of an inverse solution method determines how data are interpreted and what approximations are involved [10]. Based on previous studies on adult ESL, the methods based on equivalent current dipole (ECD) give the most accurate results for somatosensory evoked potentials [43], seizures [44], and interictal spikes [45, 46], that is, when the EEG activities are highly localized. Imaging methods (distributed sources), on the other hand, are better fitted for EEG activities that involve large areas of the brain. Since imaging methods do not require prior knowledge of the number of sources, they are preferred for applications where it is not possible to predict the number of active regions such as in cognitive experiments [10].

The exact number of dipoles, as a key prerequisite in the ECD approaches, should be estimated beforehand. Several techniques have been proposed to address this issue by means of other imaging modalities or from physiological understanding of the brain [201, 202]. An alternative approach is to use temporal information (a given period of EEG data) to identify the appropriate number of dipoles [69]. This approach led to a number of methods known as scanning methods. In these methods, the search for equivalent current dipoles is performed by scanning a 3D grid or mesh that involves the whole brain or the cortical surface [1]. These methods can localize cortical sources with a high resolution, similar to ECD approaches, without requiring *a prior* knowledge of the exact number of

sources (in the price of extra computational load).

The MUSIC [68] approach and its derivatives such as Sequential-MUSIC (S-MUSIC) [203], ImprovEd Sequential MUSIC (IES-MUSIC) [204], Recursive MUSIC (R-MUSIC) [70] and Recursively Applied and Projected MUSIC (RAP-MUSIC) [42] are among the best scanning methods. The MUSIC approach uses the singular value decomposition of the spatio-temporal EEG signals to find the signal subspace. In this method a metric, which is an estimator of the contribution of each putative dipole location to the data, is derived [38] to find the dipolar topographies that project to the estimated signal subspace. The best performing putative source locations are taken as source [69]. Therefore, MUSIC takes advantage of ECD approaches without their constraint of prior knowledge of source number [13].

The candidate inverse solution in this study is selected to meet two major requirements. Firstly, the method should localize focal fluctuations generated by focal sources as a common feature of nEEG [22, 78, 79] (see Figure 19 for typical local fluctuations in the amplitude of nEEG). The prospective method should also be able to localize sources of event related potentials (ERP) or VEP which are used in the neonatal EEG studies. This requirement is better satisfied by approaches that use a small number of dipoles to model the current sources, e.g., both the ECD and the scanning methods.

Recordings of nEEG with 64 channels display many EEG events that seem to be distinct events (as explained in Chapter 3). The potential method, as a second condition, should be able to discriminate between the different EEG events seen in dense array EEG recordings in terms of their sources. These events are generated by sources that create signatures / features which can be recognized in the time-frequency domain. It is possible to use features of the signal in both time and frequency domains in order to identify a region in the time-frequency plane which includes the desired events. Then the inverse solution can be obtained for that particular segment of signal. TF-MUSIC from the scanning methods, when used with adult MEG signals, was shown to satisfy the second requirement [73, 74] as well as the first condition.

There are also other factors that are important when selecting the method that solves the inverse EEG

problem. But these are application dependent. For example when source localization is combined with the brain connectivity analysis tool, the method must be able to localize multiple sources simultaneously. This feature is present in MUSIC-based methods [14, 37]. The TF-MUSIC algorithm has been successfully applied to localize focal brain activities, proving the capability of the method to separate events in the time-frequency plane and matches to the multiple simultaneous source localization requirement. Therefore, it is the appropriate candidate for the present neonatal EEG source localization problem.

5.2.3.2 The advantage of the TF-MUSIC as an inverse solution

TF-MUSIC is different from MUSIC in that the signal and noise subspaces are extracted (through singular value decomposition) from the spatial time frequency (STFD) of the multichannel signal rather than the signal as is the case with MUSIC (the STFD is explained in the method section). In fact, the source analysis is only applied to a given region in the time-frequency plane (STFD). This makes it possible to localize neural sources with a signature in the corresponding region of the time-frequency plane [72, 205]. The key advantage of time frequency analysis in this application is its capability to enhance signal- to- noise ratio (SNR) by spreading the noise over all areas of the time-frequency plane whilst concentrating the signal around its instantaneous frequencies (this is explained in details in the method section) [206].

5.3 Materials

5.3.1 Functional and anatomical datasets

Different functional and anatomical datasets along with several realistic simulated EEG datasets have been utilized in various parts of this study. The real-life functional and anatomical datasets were kindly provided by Dr. Sampsa Vanhatalo[4]. Four neonatal high-density EEG recordings were

[4] Department of Clinical Neurophysiology, Children's Hospital, Helsinki University Hospital, PO Box 280, FIN-00029 HUS, Finland

obtained from four different infants using 64-channel hdEEG caps for neonates (Waveguard, ANT B.V., Enschede, The Netherlands, www.ant-neuro.com) in the Department of Children's Clinical Neurophysiology (Helsinki University Central Hospital) by means of a full-band EEG [207] acquisition system with a sampling rate of 512 Hz (Cognitrace; ANT B.V., Enschede, The Netherlands, www.ant-neuro.com). A T1-MRI of a full-term healthy infant (one of those four for whom neonatal EEG was recorded) was acquired using a Philips 3T scanner in Helsinki University Central Hospital. Each slice was 240 × 256 pixels with a pixel resolution of 1 × 1 mm, and slice thickness of 0.9 mm.

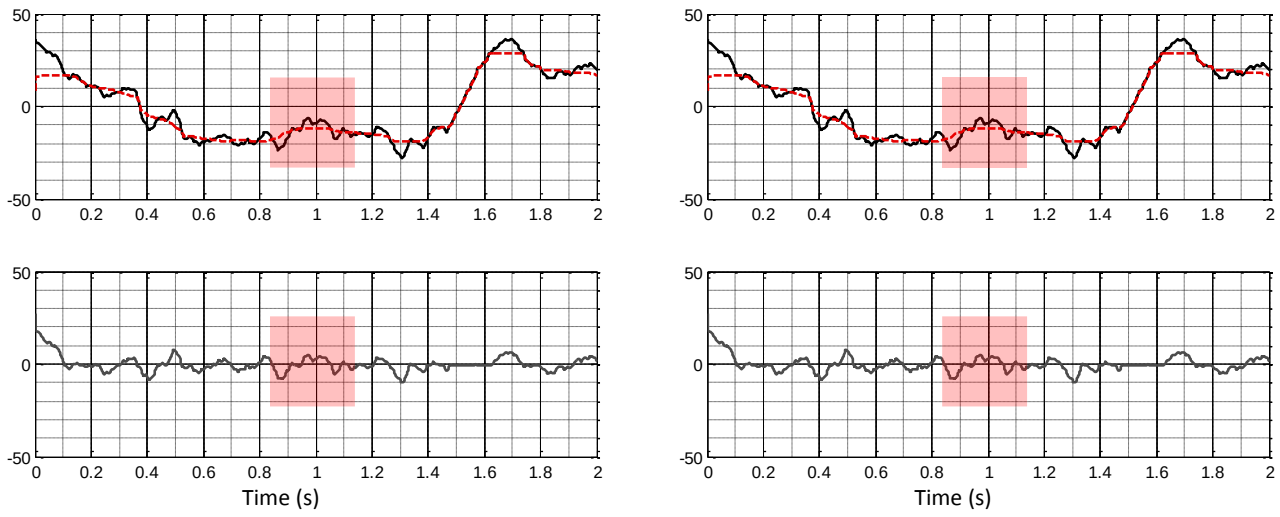

Figure 19 - Two examples of focal transients marked by a children's neurophysiologist shown by pink squares. Up) The raw nEEG in black and its median in red. Down) nEEG after removing its median. Removing the median of data highlights the focal transient as explained in Chapter 2 and [151].

5.3.2 Realistic simulated EEG

Realistic simulated EEGs are those simulated EEGs which have been generated using a realistic model of volume conduction [208]. The head model generation is explained in later sections. The head model parameters utilized in this simulation, as was shown in previous chapters, closely approximate real neonatal head parameters [32]. Several methods have been introduced to estimate

proper EEG source time series. Time series used in this simulation were adopted from [72]. They result in realistic simulated EEG generated by three sources over various locations of cortex

$$W_j[n] = k_j \times e^{\left[\frac{-(n-\xi_j)^2}{2\rho_j^2}\right]} \times cos\left(2\pi(\alpha_j n^2 + \beta_j n + \varepsilon_j)\right) \text{ j=1,2,3} \tag{40}$$

A range of values of the parameters $\{\alpha, \beta, \rho, \xi, k, \varepsilon\}$ were used in different simulations (parameters represent different time and frequency characteristics such as phase shift, frequency shift etc.) to generate different spacing in time and frequency or the strength and weakness of sources. These source signals were employed in the forward model to generate the scalp potentials. White Gaussian noise was then added to the resultant potential signals to yield a synthetic EEG with different SNR values (values of SNR from 0 dB to -15 dB were selected to measure the performance). Figure 20 illustrates a typical simulated multichannel EEG, along with the averaged TFD over all channels.

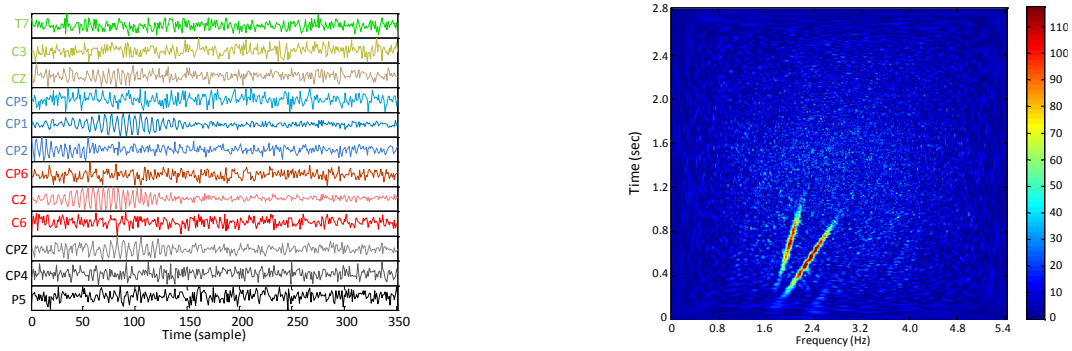

Figure 20 - Left) Selected channels from simulated EEG generated with 3 sources and SNR=-8 dB Right) The averaged time frequency distribution of all EEG channels using Extended Modified B Distribution kernel with typical kernel parameters α = 0.1 and β = 0.3 (explained in section 5.4.3) .

5.4 Methods

The method used to implement the TF-MUSIC algorithm with automatic ROI identification is illustrated in Figure 21. First the forward model, that constitutes an input to the TF-MUSIC algorithm, is detailed. Then the other input, starting from nEEG dataset, passing through the pre-processing stage and finally time frequency analyses are described.

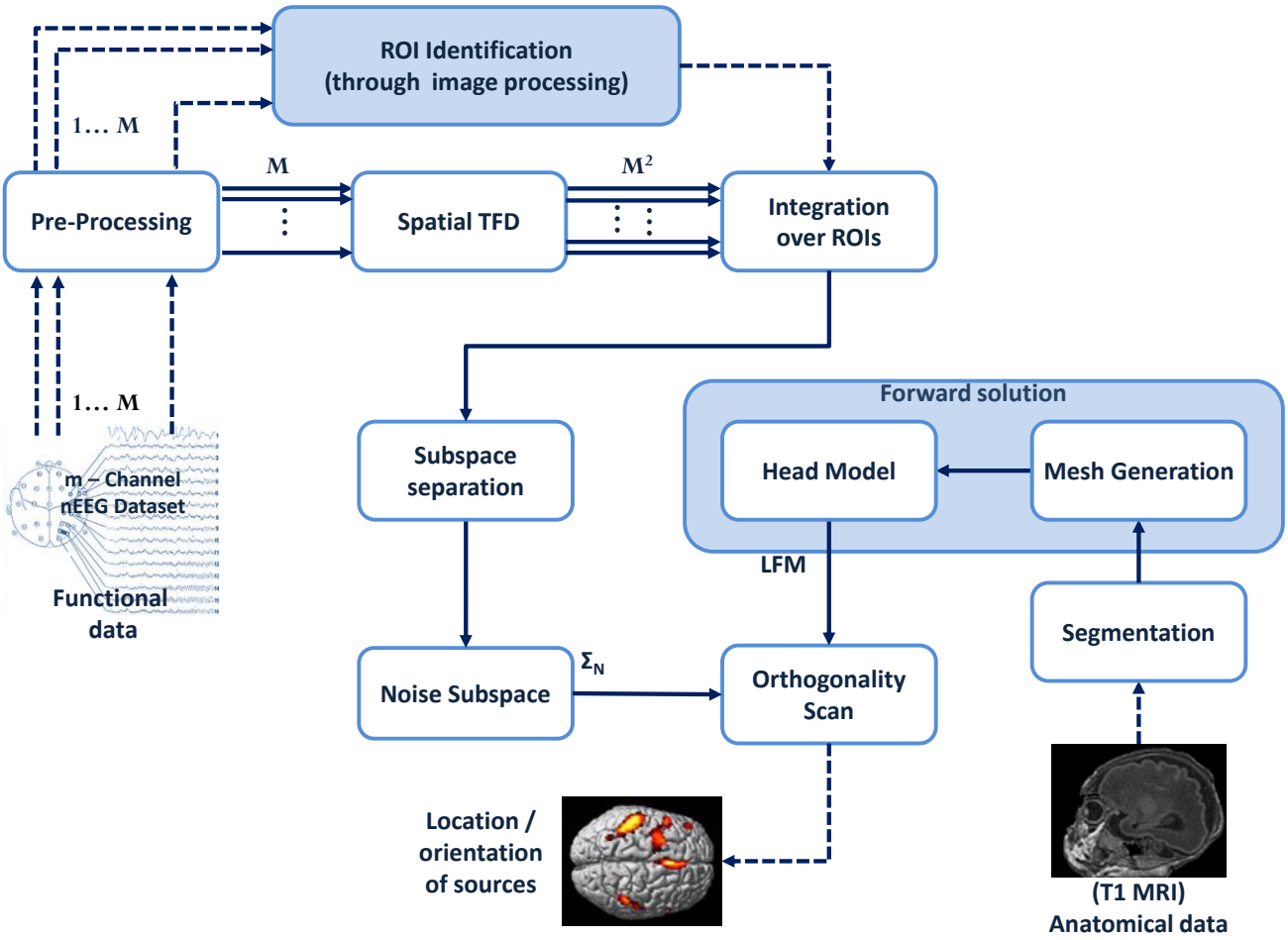

Figure 21 - The implementation of TF-MUSIC algorithm with automatic ROI identification. The inputs include anatomical (right input) and functional (left input) data. The identification of ROIs in the time-frequency plane is implemented by means of the object definition in image processing techniques.

5.4.1 Implementation of the forward model

Implementation of forward problem solution starts with segmenting MRI of the neonatal head. Neonatal magnetic resonance images have much lower white / grey matter contrast compared to adults (see Figure 22 for comparison). For this reason, none of the existing automatic segmentation software tools currently used for adult brain MRI segmentation could be successfully applied to segment the neonatal MRI. Therefore 176 slices covering the cranium from the full image stack were manually segmented into 5 compartments (scalp, skull, CSF, brain, eyes) using the FSL software (Analysis Group, FMRIB, Oxford, UK, http://www.fmrib.ox.ac.uk/research/analysis-group) [163]. The fontanelles gap in the skull was manually closed, as it was shown in Chapter 2 that it is not significantly different, in terms of electrical conductivity, from other skull regions [151].

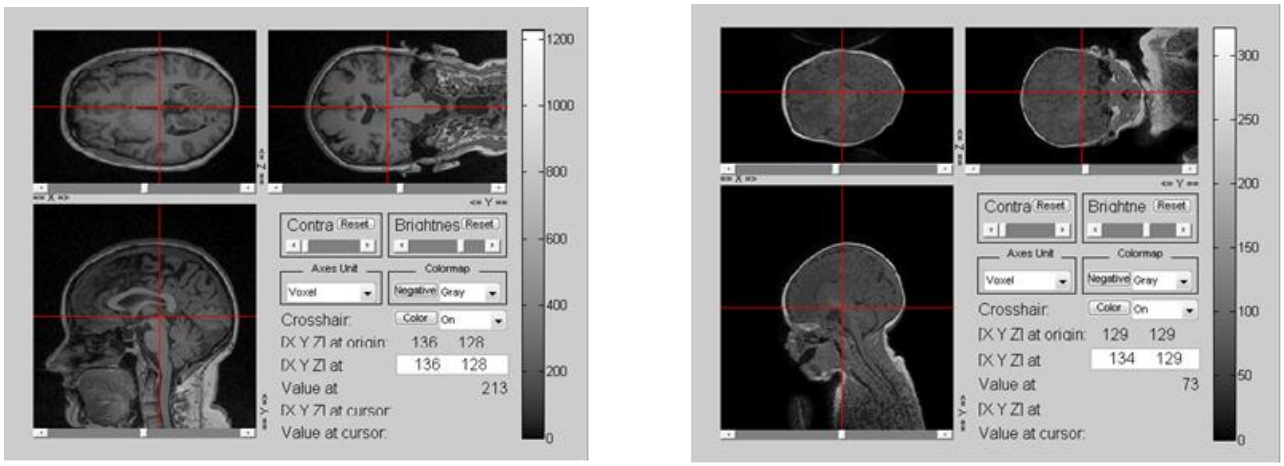

Figure 22 - Comparison of adult (top panel) and neonatal (bottom panel)
(Images generated using Tools for NIfTI and ANALYZE image by Shen, J.)

Brainstorm software [165, 209] was then used to construct a 3D mesh that fit the different layers of the newborn's head. A sample mesh is illustrated in Figure 23.

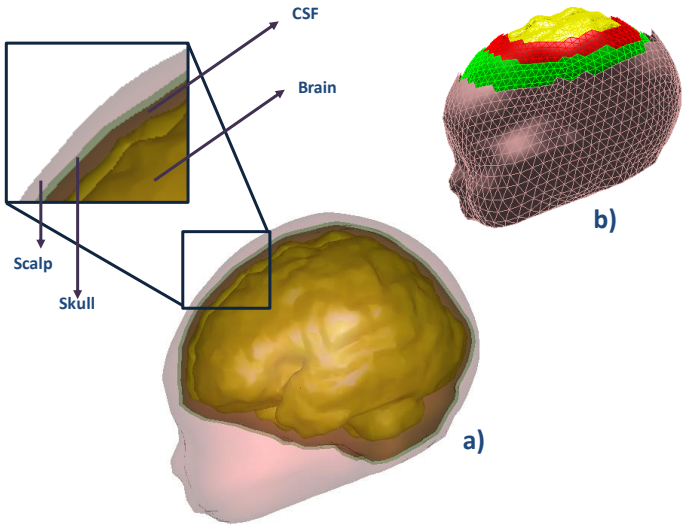

Figure 23 - a) Neonatal head tissues and b) their border surfacesconstructed through 3D meshes including Brain (yellow), the inner-skull (red) and outer-skull (green) and the scalp (dark pink)

Utilising this software, the 3D surfaces of the brain are built inner-skull, outer-skull and scalp, to designate the brain, CSF, skull and scalp tissues' borders (see Figure 23). The initially generated meshes were composed of 49010 vertices (98016 faces) for the brain, 49366 vertices (98728 faces) for the inner-skull surface, 105902 vertices (212356 faces) for the outer-skull surface and 64612 vertices (129220 faces) for the scalp. A down sampling stage (reduction of the number of vertices) was undertaken to reduce the computational load. The final mesh comprised 6001 vertices (11998 faces) for the brain and 1922 vertices (3840 faces) for each of the inner-skull, outer-skull and scalp surfaces (see Figure 24).

It was shown in Chapter 4 that the depth of the dipole representing the cortical source is usually around 10 mm. Consequently, the outermost cortical surface was selected for the distribution of hypothetical dipoles, i.e., the source space. Each node of cortex mesh hosted a dipole normal to the local cortex as depicted in Figure 25. The average distance between each node and its nearest neighbour was about 1.5 mm. Because of the anatomical arrangement of the nerve cells that give rise to the scalp potentials [1], only normal orientation for the cortical dipoles was considered.

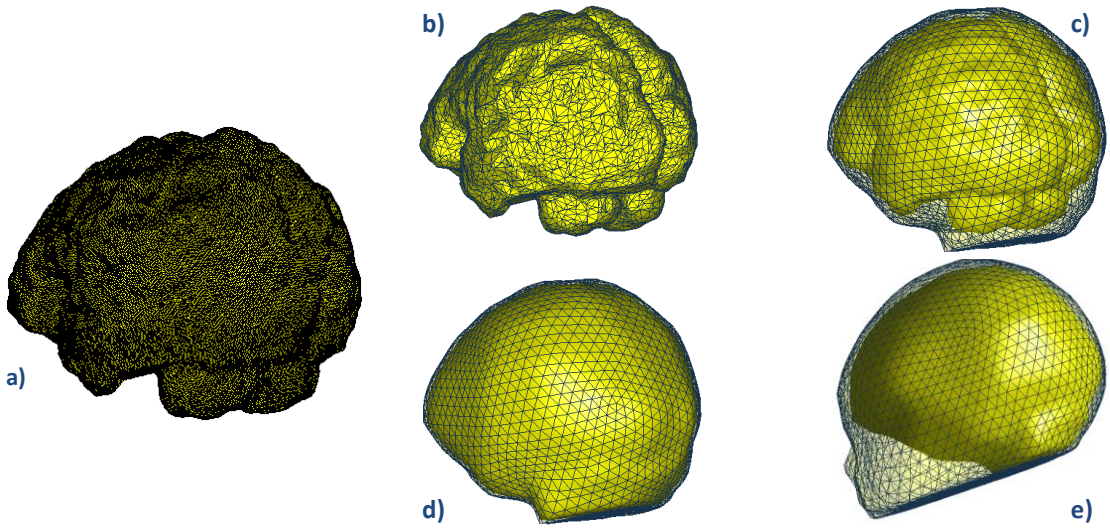

Figure 24 - a) The original surface mesh constructed for the brain(Composed of 49010 vertices) and down sampled surface meshes for Brain, inner-skull, outer-skull and Scalp. a) Brain: 6001 vertices (11998 faces) b) inner-skull: 1922 vertices (3840 faces) c) outer-skull: 1922 vertices (3840 faces) d) Scalp: 1922 vertices (3840 faces)

In order to capture the full spatial information content of nEEG signal, as indicated in Chapter 3, a 64-channels electrode position was selected for the calculation of the LFM.

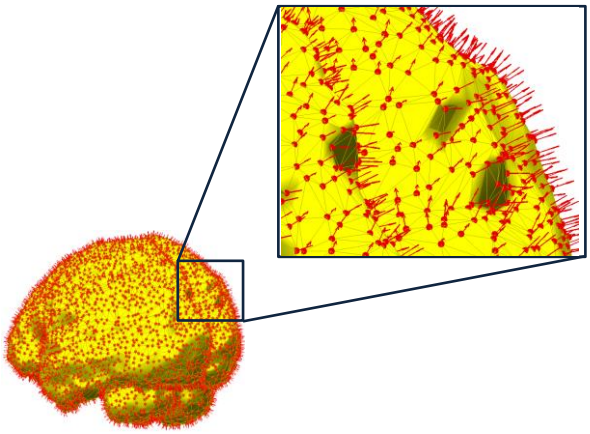

Figure 25 - The source space distributed on the cortical surface. The average distance between each nearest pair of sources is about 1.5 mm. The arrows indicate the direction of hypothetical dipoles which are normal to the local cortical surface

The last step was to find the boundary conditions in Eq. (34), i.e., assign conductivity values for the pair of volumes in two sides of each boundary, and solve Eq. (34). The estimated range of the neonatal skull conductivity value was shown in Chapter 4 to be around 0.06–0.2 S/m. A value of 0.1 S/m was selected for the neonatal skull conductivity and for brain and scalp conductivities, (0.33 S/m) and (0.33 S/m) were used respectively. Adopting adult conductivity values for neonatal tissues other than skull is acceptable as skull is the only layer where conductivity substantially changes during development [32].

Since it was not possible to estimate the exact spatial distribution of the conductivity (it could only be estimated in the layer level), applying FEM would not produce a better result than BEM; which is computationally more efficient. OpenMEEG forward solver software [210] was used to calculate the forward solution through BEM. Finally the forward solution (the gain matrix or LFM) was generated which included all the gain values from 6001 individual sources to each of 64 electrode positions on the scalp and the resulting lead field matrix was of the dimension 64×6001 .

5.4.2 EEG Pre-processing

Pre-processing is often the first step in processing EEG data as depicted in the left side of Figure 21. It includes selection of artefact free epochs and filtering. The ASA review software (ANT B.V. Enschede, The Netherlands www.ant-neuro.com) was used to visually inspect each dataset to select artefact free epochs. A 30 Hz low-pass Finite Impulse Response (FIR) filter was then used to remove mains artefact and higher frequencies. All subsequent analysis was performed in the MATLAB (MathWorks, Natick, Massachusetts, U.S.A) using customized scripts and open source toolboxes as explained.

5.4.3 Computing the EEG Inverse solution: The TF-MUSIC algorithm with automated ROI identification

The computed LFM and pre-processed EEG were used by the algorithm to compute EEG the inverse solution as indicated in Figure 21. As mentioned, TF-MUSIC belongs to the spatio-temporal approach of ESL which uses temporal information to estimate signal subspace over spatial domain. Therefore, it uses the expansion of TFD to spatial domain, i.e., spatial time-frequency distribution (STFD) of signal for this purpose. This is depicted in the left path, where the multi-channel EEG data is processed by the STFD block after the preprocessing stage. Since all the analysis was performed in the MATLAB using sampled discrete-time EEG signals, only discrete TF-MUSIC formulation is explained. The discrete form STFD of multi-channel EEG signals $\boldsymbol{X}[n]$ using a quadratic TFD is defined as [188]

$$\boldsymbol{\rho}_{\mathbf{xx}}[n,k] = 2 \underset{m \to k}{\mathrm{DFT}} \left\{ G[n,m] \underset{n}{*} (\boldsymbol{Z}_x[n+m] \boldsymbol{Z}_x^H[n-m]) \right\} \tag{41}$$

where $\boldsymbol{Z}_x[n]$ is the analytic associate of $\boldsymbol{X}[n]$, $\left[\boldsymbol{\rho}_{\mathbf{xx}}[n,k]\right]_{ij} = \rho_{\mathrm{x}_i\mathrm{x}_j}[n,k]$, for $i,j = 1,\dots,M$, $\underset{n}{*}$ indicates convolution in n, and $-^{\boldsymbol{H}}$ denotes the conjugate transpose. The diagonal elements of $\boldsymbol{\rho_{XX}}$ are auto-TFDs of $\boldsymbol{X}[n]$ channels while its off-diagonal terms are the inter-channel cross-TFDs of $\boldsymbol{X}[n]$. The term $G[n,m]$ is the discrete time-lag kernel associated with a specific quadratic TFD. Several TFDs were used in the context of nESL. Among those are the Wigner-Ville distribution (WVD) [191, 197, 198], the Spectrogram (SPEC) [188], the modified B-distribution (MB) [188], the Pseudo Wigner-Ville (PWVD) [187], the Choi-Williams distribution (CW) [188], and the extended modified B-distribution (EMBD) [211]. Table 1 lists the time-lag kernels of these TFDs along with the typical parameters used in the implementations performed in this study.

Table 1 - Discrete time-lag kernels and the kernels' parameters of the TFDs used in this study

TFD	**time-lag Kernel**	**Typical Kernel Parameter(s)**
Spectrogram	$w[n+m]w[n-m]$	$w = Hamming({}^{N}/_{4})$
Wigner-Ville	$\delta[n]$	-
Modified B	$\frac{\cosh^{-2\beta}[\mathrm{n}]}{\sum_n \cosh^{-2\beta}[\mathrm{n}]}$	$\beta = 0.01$
Pseudo Wigner-Ville	$\frac{\cosh^{-2\beta}[\mathrm{m}]}{\sum_m \cosh^{-2\beta}[\mathrm{m}]}$	$\beta = 0.01$
Choi-Williams	$\frac{\sqrt{\pi\sigma}}{2\lvert m\rvert}\exp\left[\frac{-\pi^2\sigma n^2}{4m^2}\right] ** \left[sinc[n]sinc[m]\right]$	$\sigma = 11$
Extended Modified B	$\frac{\cosh^{-2\alpha}[\mathrm{n}]}{\sum_n \cosh^{-2\alpha}[\mathrm{n}]}\frac{\cosh^{-2\beta}[\mathrm{m}]}{\sum_m \cosh^{-2\beta}[\mathrm{m}]}$	$\alpha = 0.1, \beta = 0.3$
$**$ indicates the convolution in time and lag domains n is the discrete time, m is the discrete lag and N is the length of the signal		

Applying the STFD transform on Eq. (39) results in:

$$\boldsymbol{\rho}_{\mathbf{xx}}[n,k] = (\boldsymbol{\Lambda\Phi})\boldsymbol{\rho}_{\mathbf{SS}}[n,k](\boldsymbol{\Phi}^{\mathrm{T}}\boldsymbol{\Lambda}^{T}) + (\boldsymbol{\Lambda\Phi})\boldsymbol{\rho}_{\mathbf{SN}}[n,k] + (\boldsymbol{\Phi}^{\mathrm{T}}\boldsymbol{\Lambda}^{T})\boldsymbol{\rho}_{\mathbf{NS}}[n,k] + \boldsymbol{\rho}_{\mathbf{NN}}[n,k] \quad (42)$$

After calculating the STFD, the ROIs are identified. The ROI in a TFD is a portion of plane which contains the signal's most powerful components. Since object detection and identification is a well-established technique in the image processing and there are currently well developed methods that can accurately identify objects in the images, ROIs are defined and determined in this study based on the concept of object in image (Eq. (44)). The procedure for identifying ROIs using image processing techniques is depicted in Figure 26. Since time-frequency distribution of a M-channels discrete-time EEG will result in M time-frequency distributions, extracting characteristic of the signal of interest requires a further process to generate single representation instead of the M time-frequency distributions. A possible solution, as used in [72], is to calculate the singular value decomposition of the M-channels discrete-time EEG and generate the time-frequency distributions of the significantly large singular values of temporal singular vectors. However, there are other methods that can be used

for this purpose. The method used in this study includes averaging of the M time-frequency distributions over channels. In this method first, auto TFDs of all channels are separately calculated then they are averaged over the channel to form a single averaged TFD:

$$\rho_{\mathrm{av}}[n,k] = \frac{1}{\mathrm{M}}\sum_{i=1}^{M}\rho_{x_i}[n,k] \tag{43}$$

in which $\rho_{x_i}[n,k]$ is the TFD of i^{th} channel and $\rho_{\mathrm{av}}[n,k]$ is the averaged TFD. The averaged TFD is then converted to a binary image using thresholding. Initially, the threshold was set to 50% of the maximum of $\rho_{x_i}[n,k]$ (the data was assumed artefact free, while in the case of data with artefact the median may result in faster convergence). In the next step, objects, connected portions of the image that can be interpreted as a single unit, are processed in the binary image. Then all connected components (objects) that include fewer pixels than a threshold (created mostly by noise) are removed. Next, disjointed areas of a single object are connected through morphological operations. In this manner, the borders of objects are determined, objects are dilated and the interior gaps of the object are filled. In the last step the number of connected objects is found. The number of objects is compared to the number of ROIs determined beforehand. If they match, the area of each ROI establishes the output of the algorithm. Otherwise, the value of the threshold is varied according to the number of objects. If it is greater than the number of ROIs, the threshold value increases, so fewer objects are identified and vice versa. The loop is repeated until the number of objects and ROIs are equal. A ROI of the focal transients of true nEEG that are identified using this method is depicted in Figure 27.

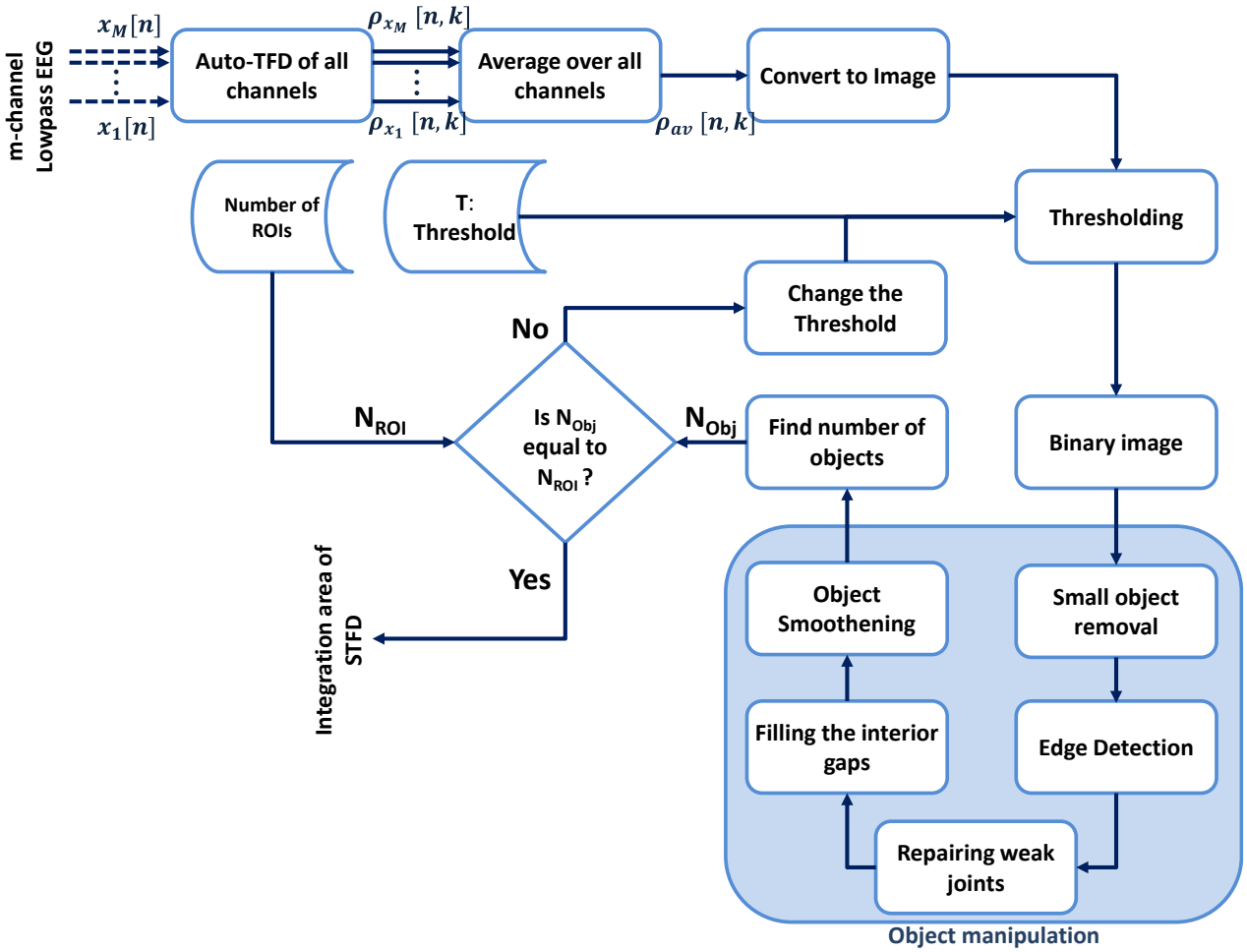

Figure 26 - Identifying ROIs in the TFD of the lowpass filtered EEG by means of image processing techniques.

The ζ identified ROIs $\boldsymbol{\Omega}$, which are based on ζ objects $\boldsymbol{\Theta}$ determined through steps explained above, are used to specify the integration area of STFD's (for each ROI) as:

$$\begin{aligned} \Omega = \{(n,k)/n, k \in [\Theta]\}, i = 1,2,\dots,\zeta \\ N_\Omega = N(\Omega) = area\{\Theta\} \end{aligned} \tag{44}$$

$$\boldsymbol{\Gamma}_{XX} = \frac{1}{N_\Omega}\sum_{\Omega} \boldsymbol{\rho}_{\mathbf{xx}}[n,k] \tag{45}$$

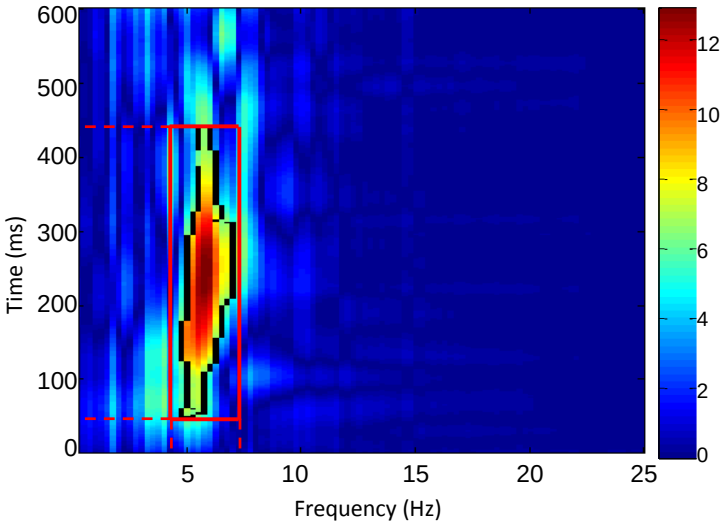

Figure 27 - The border of the automatically identified ROI of a focal transient in newborn EEG is shown in black. The red rectangle indicates the ROI limits in time and frequency.

$$\mathbf{\Gamma}_{SS} = \frac{1}{N_\Omega}\sum_{\Omega}\boldsymbol{\rho}_{\mathbf{SS}}[n,k] \tag{46}$$

$$\mathbf{\Gamma}_{NS} = \frac{1}{N_\Omega}\sum_{\Omega}\boldsymbol{\rho}_{\mathbf{NS}}[n,k] \approx \langle\boldsymbol{\rho}_{\mathbf{NS}}[n,k]\rangle = \mathbf{0} \tag{47}$$

$$\mathbf{\Gamma}_{SN} = \frac{1}{N_\Omega}\sum_{\Omega}\boldsymbol{\rho}_{\mathbf{SN}}[n,k] \approx \langle\boldsymbol{\rho}_{\mathbf{SN}}[n,k]\rangle = \mathbf{0} \tag{48}$$

$$\mathbf{\Gamma}_{NN} = \frac{1}{N_\Omega}\sum_{\Omega}\boldsymbol{\rho}_{\mathbf{NN}}[n,k] = \sigma_{NN}^2\,\boldsymbol{I} \tag{49}$$

in which $\langle\ \ \rangle$ indicates the ensemble average, and by assuming ergodic property for noise, the ensemble average is approximated with the average over ROI, and σ_{NN}^2 is the noise power density in the identified region. Hence the Eq. (39) will convert to

$$\mathbf{\Gamma}_{XX} = (\mathbf{\Lambda\Phi})\mathbf{\Gamma}_{\mathbf{SS}}(\mathbf{\Phi}^{\mathrm{T}}\mathbf{\Lambda}^{T}) + \sigma_{NN}^2\,\boldsymbol{I}, \qquad \text{or} \qquad \mathbf{\Gamma}_{XX} = \mathbf{L}\mathbf{\Gamma}_{\mathbf{SS}}\mathbf{L}^{\mathrm{T}} + \sigma_{NN}^2\,\boldsymbol{I} \tag{50}$$

which states the relationship between source and measurement covariance matrices in the time-frequency domain. Derivation of Eq. (50) and its final solution, i.e., the TF-MUSIC dipole fitting metric, is carried out using the following realistic assumptions:

- Dipole sources do not change their orientation (normal to the cortex)
- The noise generated by the EEG electrodes' hardware is the only noise source so
  - The noise is white and Gaussian (Eq. (49))
  - Noise and signal are not correlated in the time and frequencies limited by the ROIs (Eq. (47) and Eq.(48))

If ROI includes θ sources and $\mathbf{\Sigma}$ is the matrix of eigenvectors of $\mathbf{\Gamma_{XX}}$, then it can be stated in terms of $\mathbf{\Sigma}_S$ and $\mathbf{\Sigma}_N$ that their column span is equal to the signal and noise subspace respectively

$$\mathbf{\Sigma} = [\mathbf{\Sigma}_S, \mathbf{\Sigma}_N] = [[\boldsymbol{u}_1, \dots, \boldsymbol{u}_\theta], [\boldsymbol{u}_{\theta+1}, \dots, \boldsymbol{u}_M]] \tag{51}$$

where $\boldsymbol{u}_i, i = 1, \dots, \theta$ and $\boldsymbol{u}_j, j = \theta + 1, \dots, \mathrm{M}$ are signal and noise level eigenvectors respectively [72]. In order to drive the final TF-MUSIC metric, Eq. (50) is rearranged as

$$(\mathbf{\Gamma_{XX}} - \sigma_{NN}^2 \boldsymbol{I}) = \mathbf{L}\mathbf{\Gamma_{SS}}\mathbf{L}^{\mathrm{T}} \tag{52}$$

which by multiplying its both sides with a noise level eigenvector will result in:

$$(\mathbf{\Gamma_{XX}} - \sigma_{NN}^2 \boldsymbol{I})\boldsymbol{u}_j = \mathbf{L}\mathbf{\Gamma_{SS}}\mathbf{L}^{\mathrm{T}}\boldsymbol{u}_j, \qquad j = \theta + 1, \dots, \mathrm{M} \tag{53}$$

Since $\boldsymbol{u}_j, \boldsymbol{j} = \theta + \mathbf{1}, \dots, \mathrm{M}$ is a noise level eigenvector of $\mathbf{\Gamma_{XX}}$, left side of the above equation is zero and hence

$$\mathbf{L}\mathbf{\Gamma_{SS}}\mathbf{L}^{\mathrm{T}}\boldsymbol{u}_j = \mathbf{0}, \qquad j = \theta + 1, \dots, \mathrm{M} \tag{54}$$

which indicates

$$\mathbf{L}^{\mathrm{T}}\boldsymbol{u}_j = \mathbf{0}, \qquad j = \theta + 1, \dots, \mathrm{M} \tag{55}$$

This equation indicates that the orthogonality of LFM and noise level eigenvectors can be checked to estimate the source locations [72]. Therefore, the dipole fitting metric / localizing function can be derived as a measure of orthogonality between noise subspace and the LFM:

$$\boldsymbol{J}(\boldsymbol{x},\boldsymbol{y},\boldsymbol{z}) = \frac{1}{\lambda_{min}\left\{\boldsymbol{L}(x,y,z)^T \times \boldsymbol{\Sigma}_N \times \boldsymbol{\Sigma}_N{}^T \times \boldsymbol{L}(x,y,z), \boldsymbol{L}(x,y,z)^T \times \boldsymbol{L}(x,y,z)\right\}} \quad (56)$$

$$(\boldsymbol{x},\boldsymbol{y},\boldsymbol{z}) = \left\{(x_i, y_j, z_k) \in LFM/i,j,k = 1,2,\dots,G\right\}$$

where $\lambda_{\min}$ is the minimum generalized eigenvalue of the matrix pair in the bracket [72] and G is the number of grid points modelling the brain (these are the grid or mesh points that were generated in the forward model where the LFM was calculated and depicted in Figure 25). Calculating this function / metric for each ROI over all grid points (source space) will result in a map with a peak at or near the location of the corresponding source. When the number of ROIs is greater than one, the metric $\boldsymbol{J}$ is calculated as a function of source space for each ROI separately and a distinct TF-MUSIC metric map is depicted for each of them. A sample TF-MUSIC metric map for the case of 3 sources is depicted in Figure 28 along with the metric of the MUSIC for the same dataset in which the 3 sources are simultaneously identified as the 3 first values of the metric. Each map consists of the value of TF-MUSIC (MUSIC) metric in each grid location. All the STFDs in our implementation were calculated using "a computationally efficient implementation of quadratic TFDs" as presented in [212, 213].

5.4.4 Performance metric and evaluation

Throughout this and subsequent sections, TF-MUSIC refers to the algorithm with automatic ROI identification, unless otherwise stated. In this section, first a performance metric is derived for measuring the accuracy of the implemented source localization technique, and next the validation methodology is explained.

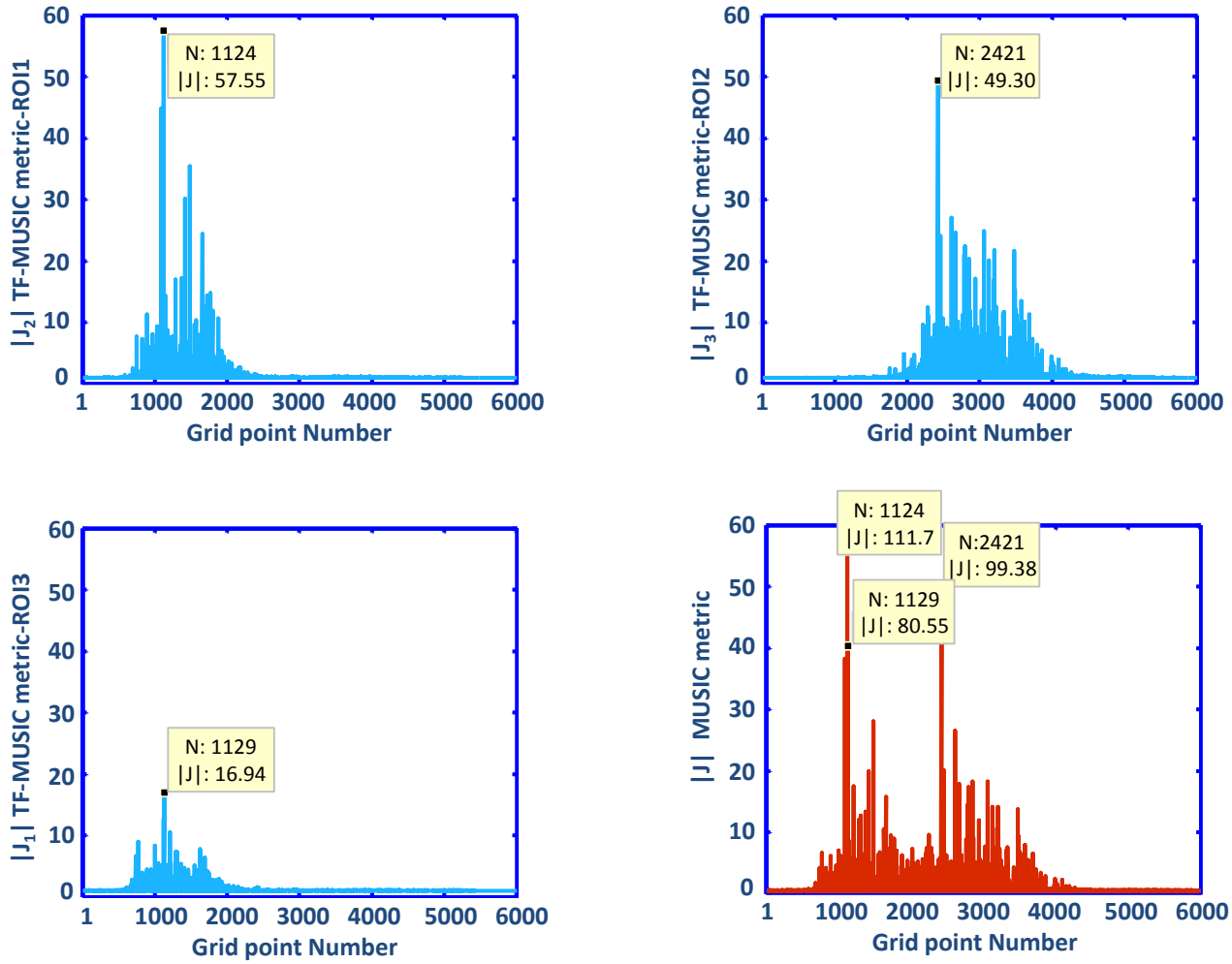

Figure 28 - The TF-MUSIC and MUSIC metrics for a simulated EEG using 3 sources. Blue maps belong to the TF-MUSIC where each source is identified in a separate peak of TF-MUSIC metric calculated in ROI1, ROI2, and ROI3 (happening in grid points N1=1129, N2=1124 and N3=2421 respectively). The red map is the output of the MUSIC algorithm for the same data in which sources are identified as the 3 first peaks of the MUSIC metric (the same grid points, N1, N2, and N3).

5.4.4.1 Performance metric

There is no current performance metric for the evaluation of MUSIC and TF-MUSIC algorithms. The most common ESL error parameter is the dipole localization error which is only applicable if there is a knowledge of the original sources [36, 214, 215]. Dipole localization error is calculated for the simulated EEGs where a dipole (original source) is used to generate EEG, then by applying the ESL algorithm, dipole location / orientation (source) is estimated. The error is then defined as the Euclidian distance between the original and estimated dipole locations. I, here, introduce a new performance

metric which considers the dipole localization error and two other effective factors. Since there is no accurate knowledge of the original sources in the real life EEGs, this performance metric is only applicable on simulated EEG datasets where positions of original sources are known. It consists of three effective parameters in the EEG source localization accuracy:

- **Distance**: Distance or dipole localization error is the most trivial parameter in determining the ESL error. As mentioned, it is calculated as the Euclidian distance between the estimated and original source locations. For the MUSIC and TF-MUSIC algorithm, the locations of the maximums of the MUSIC and TF-MUSIC metrics (Eq. (56)) are defined as the location of the estimated sources (see Figure 28 for an example). Hence the distance between the location of each maximum of metric and its corresponding original source (which give rise to the signal in corresponding ROI) is defined as the distance error which can be calculated through Eq.(59).
- **Current intensity in the location of the original sources**: This is another effective parameter in the accuracy of EEG source localization. If the source distribution is estimated accurately by an ESL algorithm, the maximum of the current intensity will happen in the location of the original source. Hence, the ratio of current intensity in the location of original source to the maximum current intensity is a measure of EEG source localization accuracy. As mentioned, in MUSIC and TF-MUSIC algorithms, the output is the metric (Eq. (56)) and the location of its maximum is defined as the location of estimated source. If source localization is done without error, the maximum of metric should happen in the location of the original source. Consequently the ratio of metric magnitude in the location of original source to metrics' maximum is a measure of EEG source localization accuracy.
- **Presence of other sources**: This is another parameter effective in the ESL accuracy which takes into account the similarity between estimated and original current distributions. As mentioned, magnitude of the current intensity in the location of original source is an effective parameter in ESL accuracy. Therefore, the number of locations (in the source space) with a

current intensity magnitude greater than its magnitude in the location of the original source indicates how similar the estimated and original current distributions are. This parameter indicates how many stronger sources than the original source are estimated by an algorithm. If two algorithms estimate the same current intensity in the location of the original source, the one which estimates more locations in the source space with greater current intensity magnitudes includes bigger error. Again for MUSIC and TF-MUSIC, in which output is the metric stated in Eq. (56), these calculations are performed using the metric's magnitude rather than current intensity magnitude. Hence, the number of source space locations (grid or mesh points) in which magnitude of metric is greater than its magnitude in the location of original source indicates how different the current distribution is estimated by the algorithm. In this manner, the order or "Rank" of the metric's magnitude in the original source location contributes to the performance metric.

These parameters are contributed in a single ESL performance metric through below empirical formulation (Eq. (57)). Different combinations of the above parameters through sum or product were possible along with various weighting functions and coefficients. A scenario was designed to choose the best combination (sum or product), weighting functions and coefficients. In this scenario, simulated EEGs of different SNRs were generated by N_{Orig} original sources, according to the previously explained method, and the source space (the brain) was modelled using a grid of N_{Grid} points. Both MUSIC and TF-MUSIC algorithms were applied on the simulated EEGs and the corresponding modelled source space. Then parameters of sources estimated by the algorithms were compared to the original sources through these performance metrics. The value of performance metric was supposed to vary from 0 to 1 where 0 indicates the maximum localization error and 1 indicates errorless localization (estimating the source in the location of the original source). In order to introduce the high localization errors (performance = 0) EEGs of very low SNRs were generated (less than -15dB) which are much lower than normal EEG SNRs. It was supposed that the localization of each source equivalently affects the performance and the final performance was calculated as the

average of localization performances of all sources. The final selected formulation and weighting coefficients are explained in the equations (57) to (60) as

$$P_{tfm} = \frac{1}{N_{Orig}} \times \sum_{k=1}^{N_{Orig}} w_1 \times \left(1 - \frac{Dist_{max(k)}(k)}{max(Dist(k))}\right) + w_2 \times \frac{\left|J_{Orig(k)}(k)\right|}{max(|J(k)|)} + w_3 \times \left(1 - \frac{Rank_{Orig(k)}(k) - 1}{N_{Grid}}\right) \quad (57)$$

in which Dist (k) is the distance to the k^{th} original source from each point of the grid

$$Dist(k) = \sqrt{\left(x - x_{Orig(k)}\right)^2 + \left(y - y_{Orig(k)}\right)^2 + \left(z - z_{Orig(k)}\right)^2} \quad (58)$$

so

$$Dist_{max(k)}(k) = \sqrt{\left(x_{max(k)} - x_{Orig(k)}\right)^2 + \left(y_{max(k)} - y_{Orig(k)}\right)^2 + \left(z_{max(k)} - z_{Orig(k)}\right)^2} \quad (59)$$

is the Euclidian distance from k^{th} original source to the point where the maximum of the localizing function (metric) in the k^{th} region of interest occurs. The other remaining terms are

N_{Grid}: Number of grid points (6001 in our generated source space)

N_{Orig}: Number of original sources (3 in the case of our simulated EEGs)

J(k): The TF-MUSIC metric (localization function) as per Eq. (56) for the k^{th} ROI, and hence

$J_{Orig(k)}(k)$ is the value of the metric in the location of the k^{th} original source (corresponding to the k^{th} ROI)

Rank(k) : The order of grid points based on the value of the TF-MUSIC metric in the k^{th} ROI so, $Rank_{Orig(k)}(k)$ indicates the order of the k^{th} original source in the k^{th} ROI.

The final selected Weighting functions:

$$W_1 = \mathrm{a}_1 * \mathrm{e}^{\left\lfloor b_1 - \frac{\mathrm{Dist}_{\max(k)}(k)}{\max(\mathrm{Dist(k)})} \right\rfloor}$$

$$W_2 = \mathrm{a}_2 * e^{\left\lfloor \frac{\left|\mathrm{J}_{\mathrm{Orig(k)}}(k)\right|}{\max(|\mathrm{J(k)}|)} - b_2 \right\rfloor} \tag{60}$$

$$W_3 = \mathrm{a}_3 * e^{\left\lfloor \frac{b_3 - Rank_{Orig(k)}(k)}{N_{Grid}} \right\rfloor}$$

$$\mathrm{a}_1 = 0.6, \mathrm{a}_2 = 0.35\,, \mathrm{a}_3 = 0.05, \mathrm{b}_1 = 0.2, \mathrm{b}_2 = 0.6, \mathrm{b}_3 = 50$$

in which $\lfloor x \rfloor$ indicates floor of x (the largest integer not greater than x). Each weighting function consists of two parts. The coefficients $\mathrm{a_i}, i = 1,2,3, \sum_i \mathrm{a_i} = 1$ indicate the importance of each term in relation to the others and the exponential part is selected to guarantee high values are not assigned when the estimated source locations are at a far distance from the original sources or the estimated and original source distributions are very different. For instance, when the estimated and original source are in a distance equal to half a maximum distance in the brain, the performance of the part relating to distance in Eq. (57) without weighting function W_1 i.e.

$$\left(1 - \frac{\mathrm{Dist}_{\max(k)}(k)}{\max(\mathrm{Dist(k)})}\right)$$

will be 0.5 which means the overall performance metric of this source is greater than 0.5. However, the exponential part of the weighting function W_1 i.e.

$$\mathrm{e}^{\left\lfloor b_1 - \frac{\mathrm{Dist}_{\max(k)}(k)}{\max(\mathrm{Dist(k)})} \right\rfloor}$$

modifies the value of this part (the part relating to distance) to 0.22 which looks more reasonable for such a large localization error.

5.4.4.2 Validation of the proposed ESL methodology

There is no established gold standard in ESL for the validation of different localization methods or for comparing their relative merits. The main difficulty is finding the true location of the sources in the case of real life data. Consequently, in most cases inverse solutions are validated and evaluated through simulated datasets. In this technique, as explained in previous sections, first the head model (LFM) is calculated in the forward procedure. Then, one or more current dipoles are located in the grid points (the source space as explained earlier) to generate potential on the scalp. Next, the corresponding potentials due to these dipolar sources are computed over the scalp. Finally, white Gaussian noises (WGN) with different variances are added to the simulated potentials to generate realistic simulated EEG with various SNRs and the localization error is calculated for each signal.

ESL Performance measurement using variation of the SNR is a common methodology in this field that has been utilized in many previous studies [215-220]. However, selecting a range for the variance or standard deviation of noise is not immediately obvious. This is mainly because of the widespread practice of averaging experimental data, EEG sensor's patterns and models and also other experimental parameters in collecting EEG that can affect the noise level in the measurement data [215]. In [215] they used a dipole of intensity 10 nA-m located in the most exterior layer of the cortex (near CSF) which gave rise to potential over scalp with roughly 4 μV peak in nearest EEG electrode. They added WGN with a standard deviation of 0.4 μV but they did not provide more information about the average signal power that can be compared to noise power. In [220] they applied a ratio of noise standard deviation to the signal's standard deviation equal to 0.5 (equivalent to SNR = 6dB) in their simulations for the outer most cortical sources. A value of 3 (equivalent to SNR ≈ -10 dB) as the noise standard deviation to the signal's standard deviation ratio was also used in their simulations to model deeper sources in the brain.

The first validation objective in this study was to investigate the potential of the proposed method to reconstruct the generators of realistic simulated EEG and to measure the accuracy of the method through the simulated signals. Therefore, a series of realistic simulated EEGs were generated as

explained above with SNRs ranging from 0 dB to -15 dB, and the performance of the TF-MUSIC and MUSIC algorithms were calculated for each signal. The proposed performance metric, as mentioned, not only could measure the dipole localization error (distance parameter) but it also enabled the measurement of similarity between the reconstructed and original source distributions taking into account the two other parameters outlined above.

Although realistic simulated EEG may be used for initial validation, it is unable to model the complex distributions and interactions of active sources in the brain. There are assumptions within each ESL method to estimate the source distribution; real EEG scenarios are necessary to evaluate the validity of these assumptions. In fact, the main reason for creating a new ESL is to apply it to actual EEG data to solve a specific real physiological inverse problem. Thus a complementary part of the evaluation procedure in this study is the assessment using real data such as VEP where the dominant sources are almost known (cortical representations are known).

5.5 Results and discussions

5.5.1 Validation and comparison datasets

Both simulated and actual EEG datasets were used for the evaluation of the method applied through realistic neonatal head model. Realistic simulated EEG was discussed in section 5.3.2. Nine different sets of parameters of 3 sources, along with the realistic head model produced in the forward model, were used to generate realistic simulated EEGs. The locations of sources were in the outer most layer of the cortex, the same as depicted in Figure 29. These simulated datasets were utilized in different parts of the evaluation procedure. It is clear these choices of source parameters are not the only possibility and there are many other sets of parameters that can be used to generate realistic simulated EEGs. Hence, the performance measurement and the evaluation procedure in this study only indicate the capacity of the proposed method.

The neonatal VEP EEG was the only available real neonatal EEG dataset that was used to evaluate

the method. It was provided by Dr. Sampsa Vanhatalo[5]. This full-term newborn EEG recording with 21 channels was obtained from EEG archives of the Department of Children's Clinical Neurophysiology (Helsinki University Central Hospital, Finland). Visual stimulus of 1 Hz was used to evoke EEG during sleep. The EEG was recorded in a rate of 256 Hz using a NicoOne EEG amplifier (Cardinal Healthcare, USA) and EEG caps (sintered Ag/AgCl electrodes; Waveguard, ANT-Neuro, Germany) with electrodes positioned according to the international 10-20 standard.

The comparison between the proposed method and other current ESL techniques was performed only using realistic simulated EEGs which included exact source locations.

5.5.2 Validation results

Results of applying the proposed method on the simulated nEEGs indicate that it is possible to localize 3 different simultaneous sources precisely using TF-MUSIC algorithm implemented using a typical TFD kernel in the low noise conditions (for instance at SNR = -5 dB) (see Figure 29 and Figure 30). As mentioned, a value of 6dB or more [220] is normally used for modelling the SNR in the simulated EEGs for an outer most cortical layer source. However, in order to model deeper sources, this value is modified and smaller SNRs are used. Consequently, the SNR variation can reasonably approximate a range of cortical and deeper sources and so the performance of the ESL algorithm can be estimated for these sources.

[5] Department of Clinical Neurophysiology, Children's Hospital, Helsinki University Hospital, PO Box 280, FIN-00029 HUS, Finland

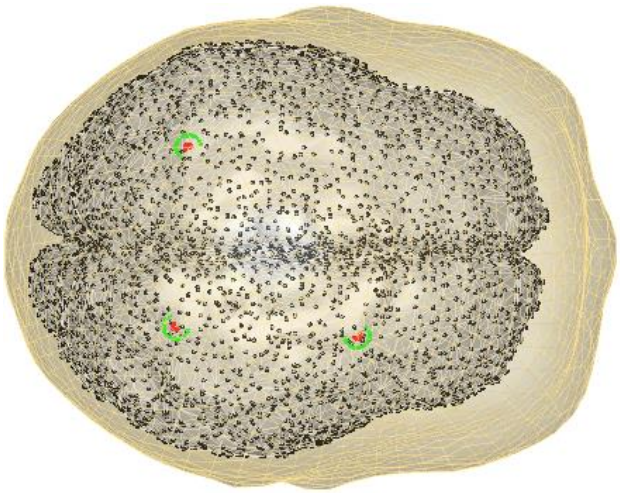

Figure 29 - Typical source reconstruction by TF-MUSIC for realistic simulated neonatal EEG in SNR = -5 dB (radial dipole orientation). The red spheres indicate the location of original sources and the green circles are source locations calculated by the TF-MUSIC algorithm (implemented using EMBD kernel with typical parameter as mentioned in Table1)

Although the above illustration depicts the capacity of the method for optimization and enhancement, a single implementation of algorithm cannot explain the overall performance and merit of the algorithm. In order to create a better illustration of the algorithm's performance it is preferred to generate a range of signals, implement the algorithm using various kernels, and calculate performance for each one. The performance value in each SNR is then the average of all performance values in the same SNR.

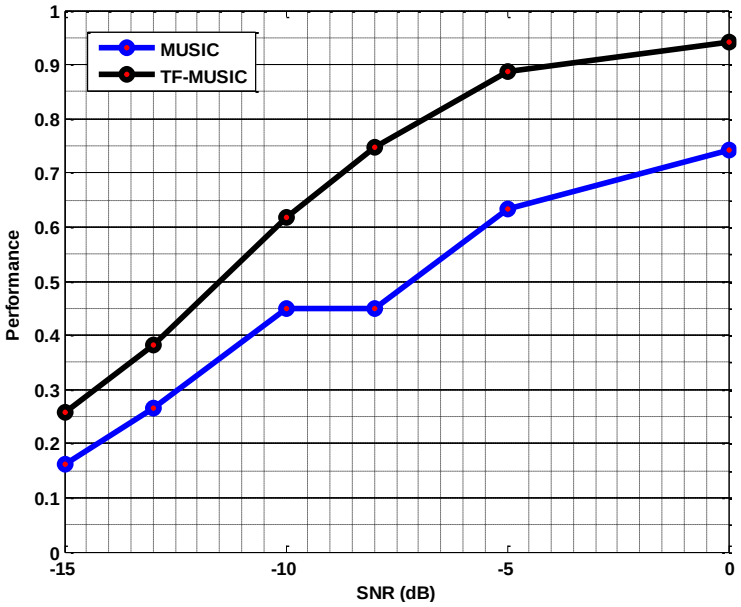

Figure 30 - The performance of the TF-MUSIC algorithm averaged over different kernels (TF-MUSIC was implemented using the 6 kernels listed in Table 1 and the performance was calculated for each one and then their average was calculated) compared to the MUSIC algorithm

Therefore, the performance of the TF-MUSIC algorithm for SNR values from 0 dB to -15 dB was calculated through averaging over various kernels and depicted in Figure 30. In these SNR values, 9 different sets of parameters (as mentioned earlier) were applied to generate 9 different realistic simulated EEGs. In this way, 9 EEG datasets with various spacing between their signatures in the time-frequency plane were produced in the same SNR value. Figure 31 depicts two samples from such EEG datasets. Each generated signal was analysed using all kernels listed in Table 1. In this way the TF-MUSIC algorithm was implemented using 6 kernels and applied to each of the 9 signals and the performance was calculated. In this manner for the TF-MUSIC algorithm 54 performance values were generated in each single SNR in Figure 30 and the corresponding performance was calculated as the average of these 54 performances. A similar procedure took place for the MUSIC algorithm in which the 9 generated signals were analysed by the MUSIC algorithm and performance was calculated for each one. Hence, the value of performance for the MUSIC was averaged over 9 values. As seen in Figure 30, the performance of the TF-MUSIC algorithm in SNR equal to -5 dB is about

0.9 (90%) which is almost 25% better than the MUSIC algorithm. According to the performance metric formulation, the 90% performance value for a 3-sources scenario is equivalent to localizing two sources in their original locations and localizing the third source with error. The performance of the MUSIC algorithm in the same SNR is about 65% that can be interpreted (based on performance metric formulation) as error-less localization of one source and localizing two sources with error.

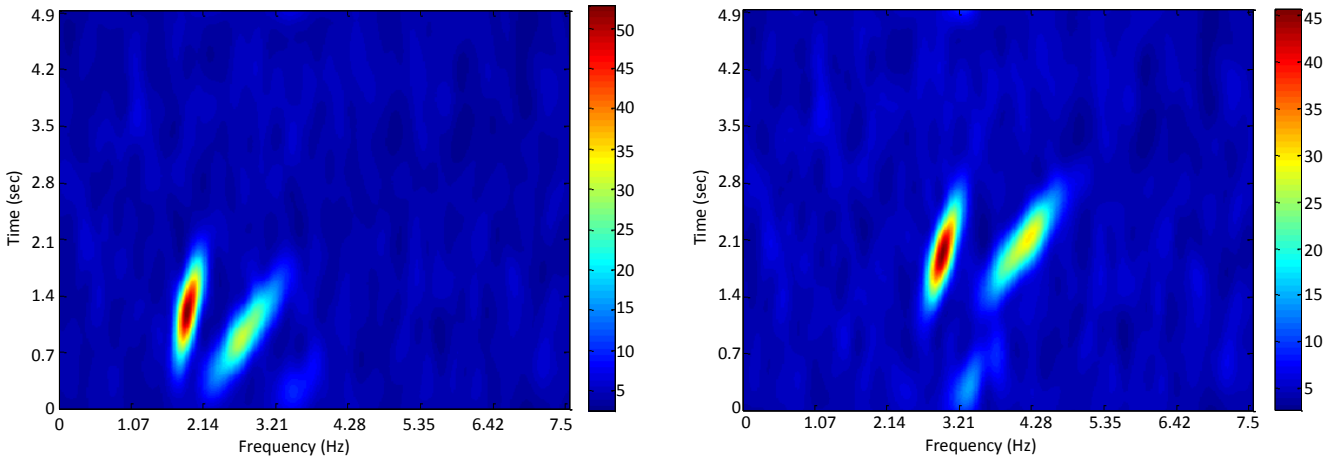

$\alpha = [-18 \;\; 55 \;\; 51.25], \beta = [-35 \;\; 75 \;\; 43.75]$
$\rho = [\,0.1 \;\; 0.2 \;\; 0.1], \xi = [0.25 \;\; -0.2 \;\; 0.2]$
$k = [\,1.5 \;\; 1.5 \;\; 1.5], \varepsilon = [\;\; 0 \;\;\; 0 \;\;\; 0]$

$\alpha = [-23 \;\; 50 \;\; 55], \beta = [-50 \;\; 70 \;\; 50]$
$\rho = [\,0.1 \;\; 0.2 \;\; 0.1], \xi = [0.4 \;\; -0.15 \;\; 0.425]$
$k = [\,1.5 \;\; 1.5 \;\; 1.5], \varepsilon = [\;\; 0 \;\;\; 0 \;\;\; 0]$

Figure 31 - Time-frequency distribution of the two different samples from realistic simulated EEGs with SNR = -8 dB, along with parameters corresponding to the three sources used for generation of each one. The time-frequency representation is theaverage of TFDs of all channels calculated using Pseudo Wigner-Ville kernel with β=0.01.

5.5.3 Comparison with existing ESL methods (other than MUSIC)

The method was also evaluated by comparing to three distributed sources (imaging) approaches, standardized Low Resolution brain Electromagnetic Tomography (sLORETA) [221], weighted Minimum Norm Estimate (wMNE) [222, 223] and dynamic Statistical Parametric Maps (dSPM) [224]. These comparisons were also performed using realistic simulated EEG datasets which could provide a standard base for the comparison. These algorithms are implemented in the Brainstorm software and the outputs were depicted in the Brainstorm format. Though, the TF-MUSIC algorithm was implemented using scripts in the MATLAB environment and its output was loaded into the

Brainstorm software for the uniformity of illustration.

Although the output of these algorithms is different from TF-MUSIC, this comparison is still meaningful. While the output of the distributed sources methods such as sLORETA or wMNE shows a temporal current density in the brain [10], the output of TF-MUSIC is a metric which indicates merit of each point as the candidate source location. In the case of imaging methods the localization error is calculated based on the properties of the maximums of estimated current source distribution, and in the case of TF-MUSIC also it is the maximum which is the base of calculations (as mentioned in performance metric formulation) [13]. This similarity can be used to establish a common base for the comparison between the two groups. In other words, in both cases the error-less source localization is achieved when the maximum of the output is located in the position of the original sources.

The results of applying the TF-MUSIC algorithm and these distributed sources ESL techniques to typical realistic simulated EEG data (depicted in Figure 32) using three sources and SNR = -5 dB is shown in Figure 33. The TF-MUSIC output is the same as Figure 29 (in which sources are localized without error) except that it is depicted in the Brainstorm format and repeated in two time instances. The output of sLORETA, wMNE and dSPM is also sampled in two different time instances as shown in Figure 32 (with red lines and arrows).

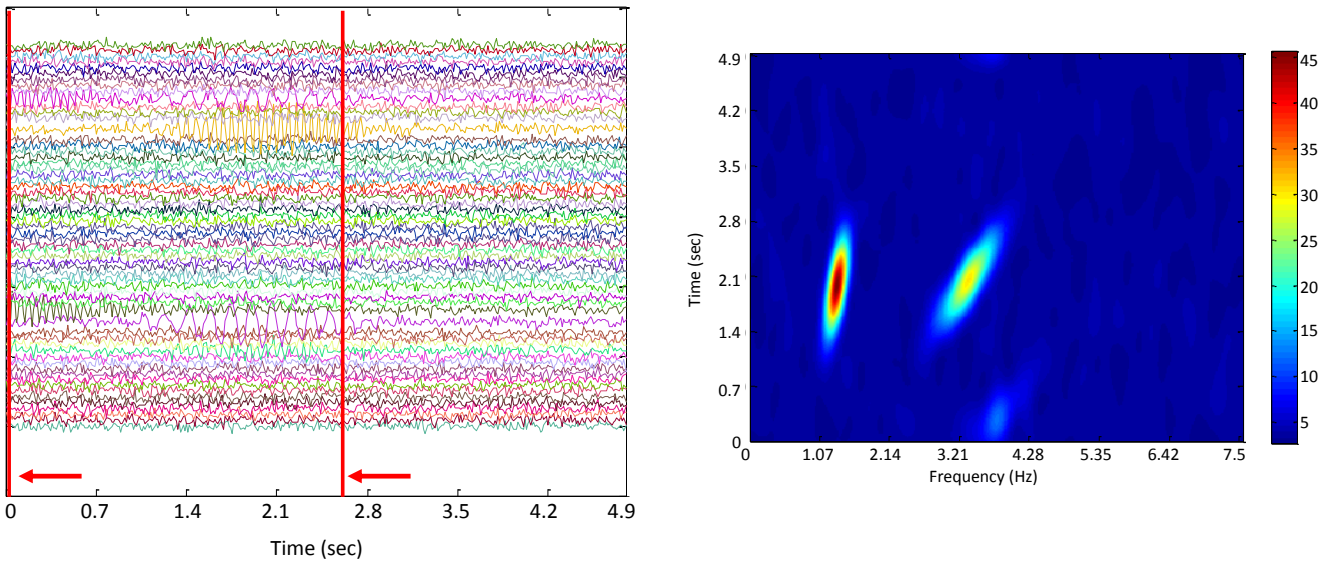

$\alpha = [-13\ 60\ \ 47.5]$, $\beta = [-20\ 80\ 37.5]$, $\rho = [\ 0.1\ \ 0.2\ \ 0.1]$, $\xi = [0.4\ \ -0.15\ \ 0.425]$, $k = [\ 1.5\ \ 1.5\ \ 1.5]$, $\varepsilon = [0\ 0\ 0]$, SNR =-5 dB

Figure 32 - Left) Realistic simulated EEG using three sources with the specified parameters. The red lines and arrows indicating the time instance in which source localization is performed. Right) The time-frequency representation is the average of TFDs of all channels calculated using Pseudo Wigner-Ville kernel and typical kernel parameter (as table 1)

Before interpreting the results it is necessary to mention another difference between the output of the TF-MUSIC algorithm and these distributed sources methods. Owing to the fact that TF-MUSIC is a spatio-temporal technique that uses a period of EEG signals to localize sources, processing a period of signal, rather than a time instance of signal, is necessary for the TF-MUSIC algorithm to function properly and estimate signal and noise subspaces. In other words, TF-MUSIC can simultaneously detect and localize sources with time delay in a single run of the algorithm, while, the distributed sources methods that work based on the time instances of the source signal, rather than a period of signal, need to proceed in time to detect and localize such sources.

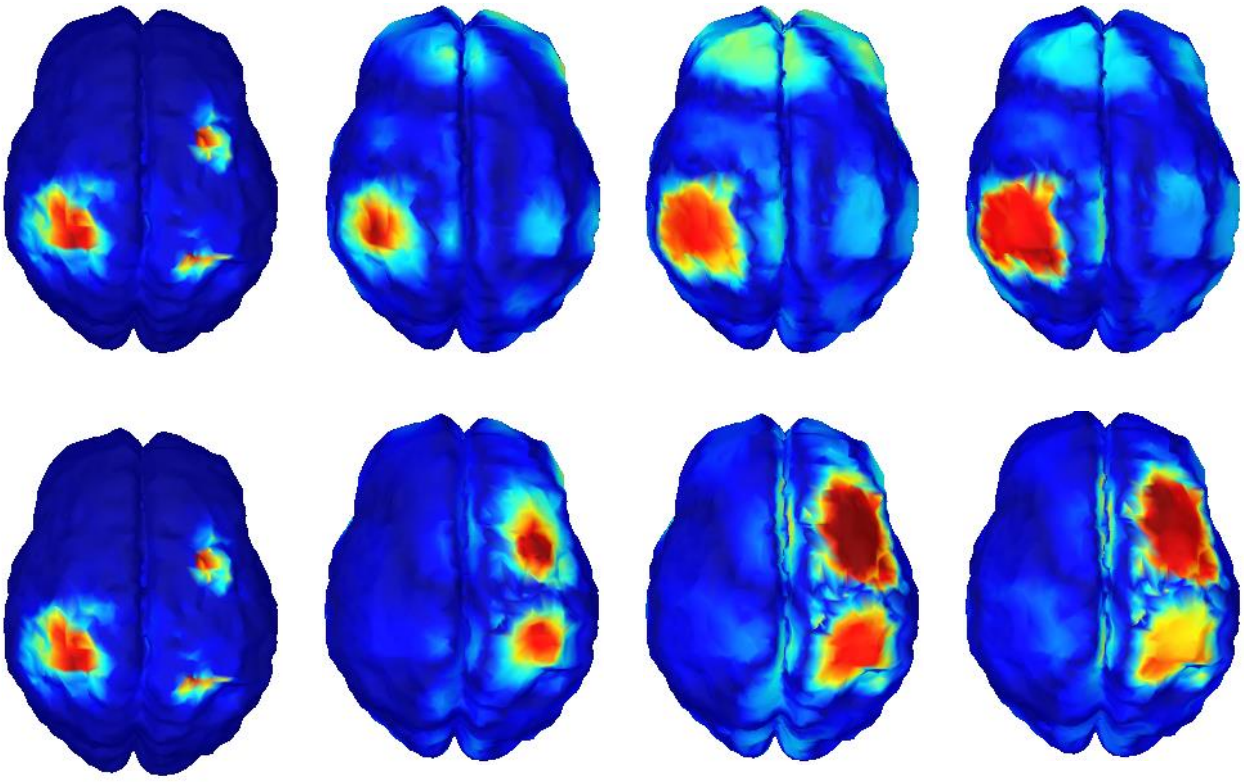

(a) (b) (c) (d)

Figure 33 - Outputs of various source localization methods for a realistic simulated EEG signal generated by three sources and SNR = -5 dB. Results are depicted for two different time instances, top row at t = 0.01 s and the bottom row at t = 2.65 s. a) TF-MUSIC, b) wMNE c) sLORETA and d) dSPM (through Brainstorm software)

Consequently as seen, TF-MUSIC has detected the three sources (which appear with time shift) simultaneously. However, the three distributed sources (imaging) methods process instances of source signal separately as they appear in time. The TF-MUSIC output is the same in t = 0.01 s and t = 2.65 s in Figure 33. The three red regions over the cortex correspond to the three sources and the maximum of the metric value is exactly located at the location of the original sources. As previously explained, the output of wMNE, sLORETA and dSPM are not equivalent to the output of the TF-MUSIC algorithm in terms of their values or colour equivalency, but the location of their maximum can be compared to the location of the TF-MUSIC output's maximum.

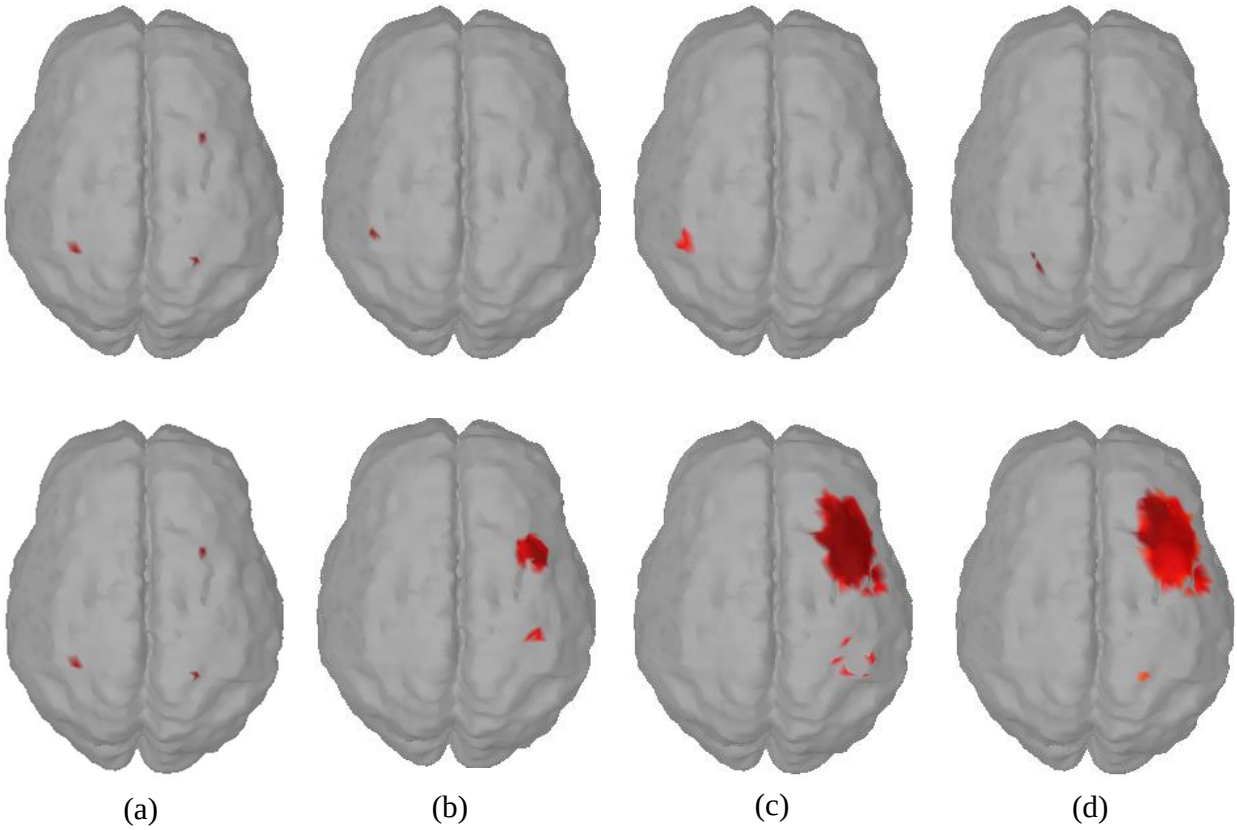

Figure 34 - Manual thresholding of the outputs of ESL methods depicted in Figure 33. The red regions in each image indicate the highest value (the maximum of output). Same as Figure 33, the results are depicted for two different time instances, top row at t = 0.01 s and the bottom row at t = 2.65 s. a) TF-MUSIC, b) wMNE c) sLORETA and d) dSPM

In fact, the colour range is different even between distributed sources techniques, but what is important is the location of the sources which is determined by the maximums of the outputs. A manual thresholding of the outputs depicted in Figure 33 was performed using Brainstorm software which resulted in Figure 34. As seen, after removing colour of the regions with magnitudes lower than maximums, what remains is the location of sources localized by each method (in the specified instance of time). Among the distributed sources methods depicted in Figure 34 sLORETA method has smallest localization error while it designates a large area around one of the sources as the source location. These results are discussed further in the concluding section.

5.5.4 Evaluation using real EEG

Since the main objective of design and implementation of a new ESL technique is to solve a real life problem, i.e., to be applied on real EEG data, the last step in the evaluation of such a method includes localization of sources in the real EEG data. Accordingly, the implemented TF-MUSIC algorithm was also evaluated by being applied to real EEG data as the last step of the evaluation procedure. In order to use a real EEG dataset in the evaluation of an ESL technique, it should have known cortical representation such as evoked potentials. The evoked potentials have helped to study specific brain activities and also have provided an objective indication for the sensory function in infants where perceptual tests are impractical or unreliable [225, 226].

However, these potentials are so weak that they are fully submerged in spontaneous electrical activity of the brain. While the EEG signal amplitude can normally reach to 50~100 μV, evoked potentials may be as small as 0.5~1 μV and often no larger than 5 μV. One of the common methods to enhance evoked potentials is through signal averaging technique. In this method the stimulus is repeated in separated intervals. After a large number of repetitions (e.g. greater than 200), the average value of EEG is calculated for the time instances based on an interval period and the result is presented in the form of a single interval evoked potential. Due to lack of correlation between separate intervals of background brain activity and correlation of the evoked potentials, this summation results in a clear representation of an evoked potential [225, 226].

The visually evoked potential or VEP was the only available neonatal evoked potential to be used in this study. The VEP EEGs are initiated by brief visual stimuli and are represented on the scalp overlying the visual cortex (Occipital lobe) [227]. They are an important means of obtaining reproducible quantitative data about the functional integrity of the optic pathways [228] that can even better quantify its functional integrity than other imaging modalities [227]. The VEP is also a primary tool to evaluate subjects such as neonates that cannot communicate [96].

The TF-MUSIC algorithm was applied on neonatal VEP data and the result is depicted in Figure 35. Since anatomical data was not available for the VEP dataset, the anatomical data used for this

evaluation was the same as that utilized in the generation of realistic simulated EEGs and also evaluations performed in two previous sections. The available VEP data included 21 channels though the results are depicted in the 64-electrode representation for a better illustration of the output. In order to visualize the output, the TF-MUSIC metric (output of the TF-MUSIC algorithm) was mapped to the cortex and the value of metric was designated by colours. Then, a manual thresholding similar to Figure 34 was performed to remove the colour of regions that the value of metric was less than 90% of its maximum. As seen, the maximum of the output (and regions with a value of metric greater than maximum's 90%), are located in the Occipital area of cortex which is in line with the known representation for the visually evoked potential EEG data.

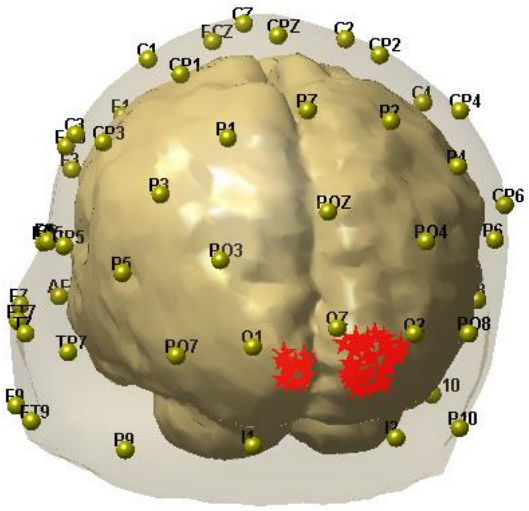

Figure 35 - The results of applying TF-MUSIC on actual neonatal VEP data

The red stars indicate locations where the magnitude of TF-MUSIC metric is bigger than 90% of its maximum.

5.5.5 The effect of ROI-identification and TFD Kernel selection on the enhancement

After validation and evaluation of the proposed algorithm using real and simulated datasets, the final step of this study is dedicated to the analysis of the proposed method. This analysis helps to know the possible future enhancement directions and potentials for later investigation on ESL and neonatal ESL through the TF-MUSIC algorithm. The very first step of such an analysis can be studying the

differences between the TF-MUSIC and MUSIC algorithms. The block diagram in Figure 36 depicts the main implementation steps in the MUSIC algorithm. The comparison between Figure 36 and Figure 21 (implementation of TF-MUSIC) reveals that their two main differences include ROI-identification and STFD blocks. As seen, the procedure in MUSIC and TF-MUSIC is similar except that in TF-MUSIC the noise and signal subspaces are extracted from the regions of TFD of signal (STFD), which is determined by ROI, rather than signal as in the case of MUSIC. Therefore, in order to analyse TF-MUSIC algorithm, it is sufficient to investigate the role of these two blocks in the enhancement achieved by TF-MUSIC over MUSIC (as explained in section 5.5.2 and illustrated in Figure 30).

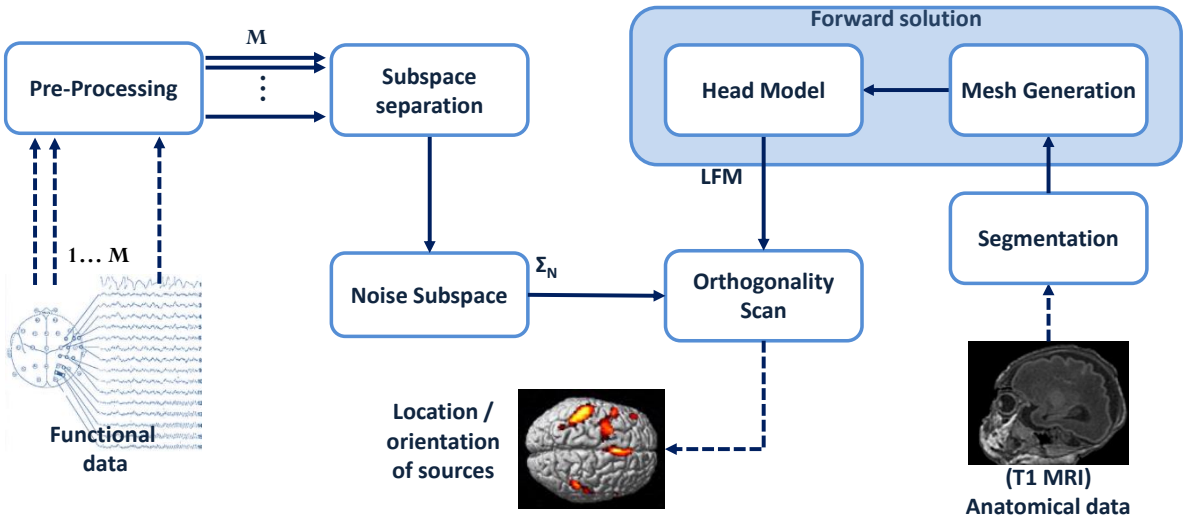

Figure 36 - Implementation of the MUSIC algorithm for EEG source localization

5.5.5.1 The effect of ROI-identification in the enhancement

The same 9 sets of source parameters, $\alpha, \beta, \rho, \xi, \kappa, \varepsilon,$ (for 3 sources) that used to generate realistic simulated EEGs in Figure 30 were applied to generate the same set of EEGs for the analysis of ROI-identification effect. The TF-MUSIC algorithm was implemented using the same kernels and kernel parameters except that the whole time-frequency plane was identified as one ROI, i.e., no specific region of the time-frequency plane was selected as the region of interest. In each SNR value from $\{0, -5, -8, -10, -13, -15\}$ dB, the TF-MUSIC-without-ROI algorithm implemented through each

kernel (and kernel parameter) and applied to the 9 various EEGs generated in the same SNR. The performance value calculated for each kernel in each SNR, as a result, was the average of 9 value, i.e., a total of 54 various performance values were averaged in each SNR (exactly the same procedure to generate Figure 30). The final performance result for the TF-MUSIC-without-ROI identification, calculated in this method, is depicted in Figure 37.

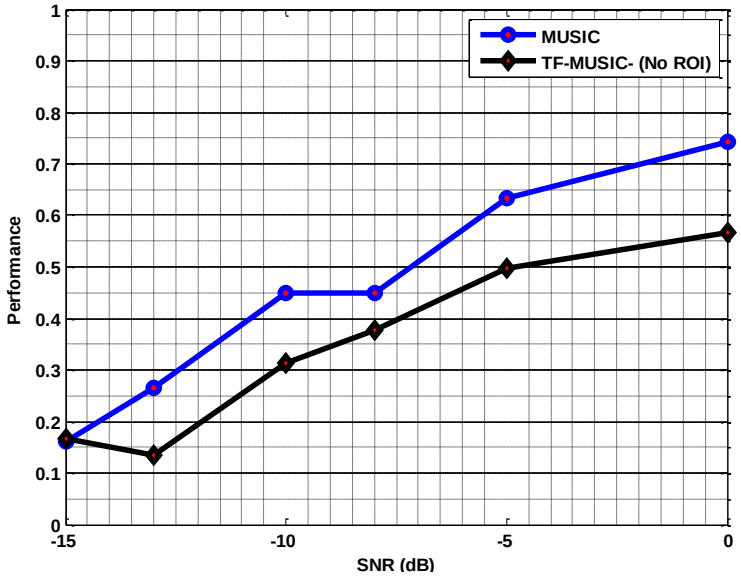

Figure 37 - The averaged performance of the TF-MUSIC algorithm without ROI identification implemented using TFD kernels listed in table 1 and applied on 9 various simulated EEGs compared to the MUSIC algorithm

As seen, the performance of the TF-MUSIC algorithm without identifying ROI is considerably less than MUSIC except in the last point. The most probable reason for the similarity of the performances in the last point is the formulation of the performance metric which limit the further falls at the end of the range. In order to determine the reason of performance degradation, when no ROI is selected in the TF-MUSIC algorithm (compare Figure 36 to Figure 21), the role of ROI in the formulation should be studied. The matrix $\boldsymbol{\Gamma_{XX}}$ in equation (45) which is used to calculate the signal and noise subspaces can be written as

$$\boldsymbol{\Gamma_{XX}} = \begin{bmatrix} \frac{1}{N_\Omega}\sum_{\Omega}\rho_{11}[n,k] & \cdots & \frac{1}{N_\Omega}\sum_{\Omega}\rho_{1M}[n,k] \\ \vdots & \ddots & \vdots \\ \frac{1}{N_\Omega}\sum_{\Omega}\rho_{M1}[n,k] & \cdots & \frac{1}{N_\Omega}\sum_{\Omega}\rho_{MM}[n,k] \end{bmatrix} \tag{61}$$

where $\rho_{ii}[n,k]$ is auto-TFD of channel i and $\rho_{ij}[n,k]$ is cross-TFD of channel i and channel j. If no ROI is selected, i.e., the whole time-frequency plane is chosen as the ROI, the equation will be

$$\boldsymbol{\Gamma_{XX\_noROI}} = \begin{bmatrix} \frac{1}{N_\Psi}\sum_{\Psi}\rho_{11}[n,k] & \cdots & \frac{1}{N_\Psi}\sum_{\Psi}\rho_{M1}[n,k] \\ \vdots & \ddots & \vdots \\ \frac{1}{N_\Psi}\sum_{\Psi}\rho_{1M}[n,k] & \cdots & \frac{1}{N_\Psi}\sum_{\Psi}\rho_{MM}[n,k] \end{bmatrix} \tag{62}$$

in which Ψ represents the whole time-frequency plane and N_Ψ represents its area. The main components of signals are expected to be localized in parts of the time-frequency plane, which are selected as the ROIs Ω, while the white Gaussian noise power is spread throughout the time-frequency plane. Consequently, each component of matrix $\boldsymbol{\Gamma_{XX\_noROI}}$ will contain almost the same amount of signal's power as components of matrix $\boldsymbol{\Gamma_{XX}}$ where it contains more noise power, i.e., the whole noise spread in the time-frequency plane. This means that signal and noise subspace estimation will be weaker from matrix $\boldsymbol{\Gamma_{XX\_noROI}}$ than matrix $\boldsymbol{\Gamma_{XX}}$ and therefore the corresponding accuracy of the EEG source localization will be reduced. A similar analysis can be done to compare each of the above matrices to the MUSIC algorithm. The signal and noise subspaces in the MUSIC algorithm are calculated from a signal time series or more accurately from a period of a signal's time series as

$$\boldsymbol{X}[\mathbf{1}:\boldsymbol{n}] = \begin{bmatrix} x_1[1:n] \\ x_2[1:n] \\ \vdots \\ x_M[1:n] \end{bmatrix} \tag{63}$$

The matrix $\boldsymbol{X}$ contains the whole noise of the time domain, and equivalently the whole noise of time-frequency plane of the signal. Therefore, the subspace separation based on it will result in less

accuracy than the matrix $\boldsymbol{\Gamma_{XX}}$, i.e., the TF-MUSIC that is in line with the results depicted in Figure 30. The comparison of the equations (62) and (63) reveals that

- entries of matrix $\boldsymbol{\Gamma_{XX\_noROI}}$ and $\boldsymbol{X}$ contain a similar amount of noise, i.e., the whole noise of the time-frequency plane,
- entries of matrix $\boldsymbol{\Gamma_{XX\_noROI}}$ are quadratic transformations of signal.

Therefore, the subspace separation is harder based on matrix $\boldsymbol{\Gamma_{XX\_noROI}}$ than matrix $\boldsymbol{X}$ which contains signal. This is in line with the results depicted in Figure 37 where the accuracy of MUSIC is better than TF-MUSIC without ROI identification.

5.5.5.2 Choice of TFD kernels and kernel parameters

As shown in a previous section, the main advantage of TF-MUSIC over MUSIC is achieved through ROI identification stage. It was also shown that TF-MUSIC without ROI identification performs poorer than MUSIC, though, the role of various TFD kernels in representation of signal and therefore determination of ROI still need to be investigated. The TFD kernels listed in table 1, that are utilized in the implementation of TF-MUSIC in this study, are not the only available TFD kernels. There are other distributions such as Levin, Born-Jordan, Zhao-Atlas-Mark, Rihaczek and Page that can be used for this purpose [188]. The applied kernel parameters were also typical values that could be replaced by many other values. Investigating all possibilities for the TFD kernel and kernel parameters in this way is a huge volume of works. However, studying examples from the generated EEGs and the ROI identified by various kernels or kernel parameters will provide a good understanding about the role of TFD kernel in this regard. Figure 38 depicts ROIs in the averaged TFD of a 64-channels simulated EEG dataset identified by four different TFD kernels (with the kernel parameters listed in table 1).
As seen, despite using various TFD kernels the identified ROIs are very similar. This means their resulting estimated noise and signal subspaces are similar. Therefore, it is expected their corresponding sources are localized in similar locations and the localization performance / accuracy is close among these various TFD kernels. This is also illustrated in Table 2 where the ESL

performances of applying the TF-MUSIC algorithm with 5 different TFD kernels are compared to the MUSIC algorithm.

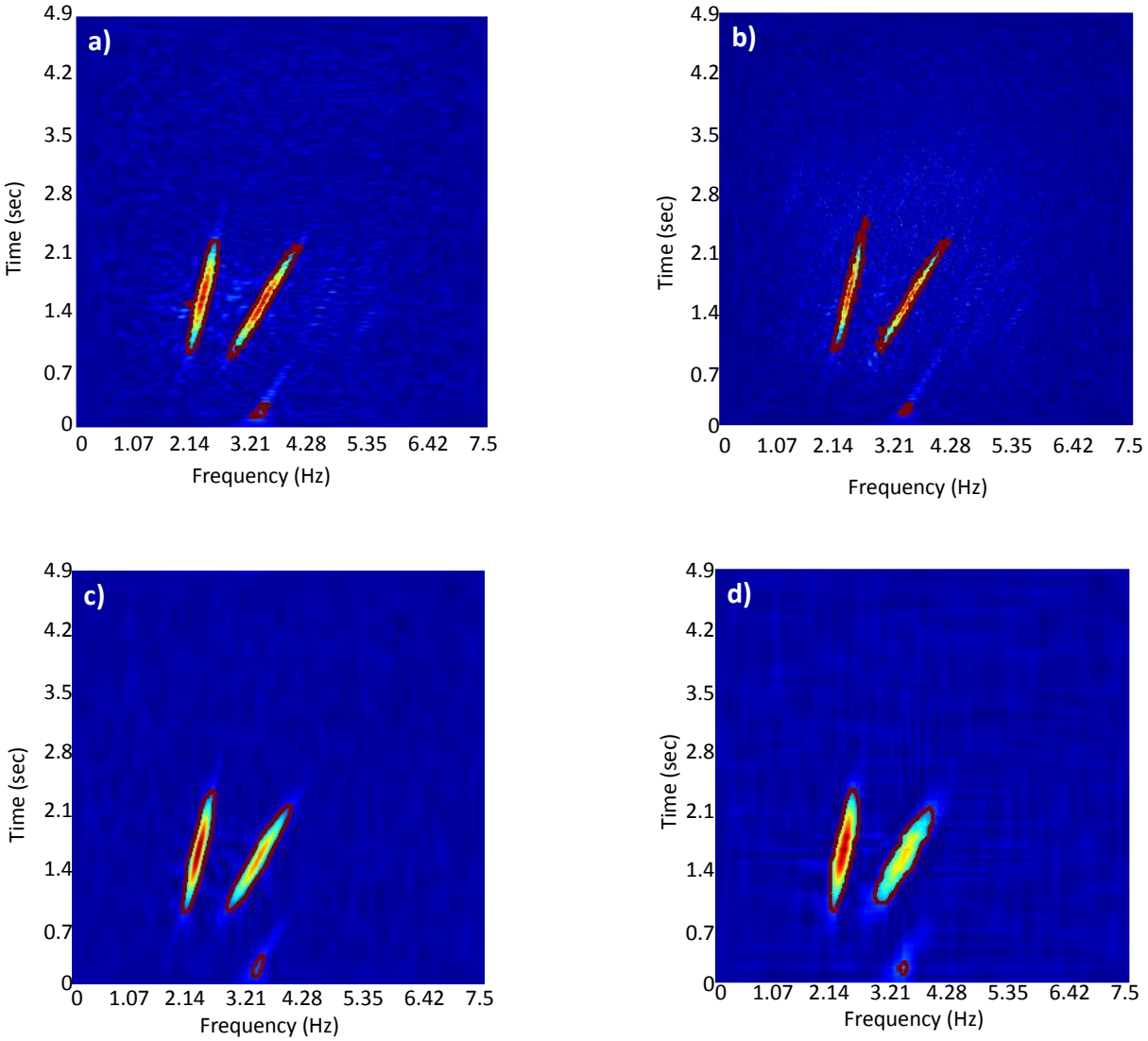

Figure 38 - Comparison between ROIs identified in the averaged TFD of the simulated EEG using 3 sources with parameters $\alpha =$ [-20 53 52.75], β =[-41 73 46.25], ρ =[0.1 0.2 0.1], ξ =[0.325 -0.175 0.3125], k =[1.5 1.5 1.5], ε =[0 0 0] (in SNR=-5 dB) by four TFD as a) PWVD (β=0.01) b) WVD c) EMBD (α=0.1, β=.3) d) CW (σ=11)

Similar to previous experiments, 9 sets of 3 source parameters were applied to generate 9 sets of realistic EEGs in each SNR as listed in Table 2. The TF-MUSIC algorithm was implemented using each listed kernel and applied to all simulated EEGs. The ESL performance value recorded for each

kernel, therefore, calculated as the average of 9 ESL performances. A similar procedure took place for the MUSIC algorithm and it was applied to same 9 sets of realistic simulated EEGs where its recorded performance was the average over 9 performance values.

The averaged ESL performance values listed in Table 2 reveals that

- Except the last column (SNR = -15 dB which can be interpreted as the performance value for the localization of deep sources and all sources are localized with error) the performance of the TF-MUSIC algorithm is better than MUSIC. This superiority is in line with previous results and as explained in a previous section is due to SNR enhancement achieved by ROI identification.

Table 2 - Performance of the TF-MUSIC algorithm implemented using various TFD kernels along with the performance of the MUSIC algorithm. These values are calculated by applying algorithms on 9 different sets of source signals (realistic simulated EEGs by 3 sources with 9 different sets of parameters). Hence, the result in each SNR (both MUSIC and either of TFD kernels) is the average of 9 performance values.

SNR / Kernel	0 dB	-5 dB	-8 dB	-10 dB	-13 dB	-15 dB
WVD	0.9665	0.8546	0.7129	0.5578	0.3211	0.2373
PWVD	0.9402	0.9144	0.7341	0.6136	0.3543	0.2695
SPEC	0.9234	0.8823	0.7499	0.6007	0.3572	0.2044
CW	0.9411	0.9005	0.7940	0.6959	0.4940	0.3220
EMBD	0.8534	0.7879	0.6830	0.5366	0.3643	0.1630
MUSIC	*0.7428*	*0.6329*	*0.4487*	*0.4484*	*0.2656*	*0.1613*

- There is no single kernel (and kernel parameter) which is performing the best or the poorest in all SNR values. Some kernels are performing as the best kernel in some SNRs but not in all SNRs (the CW kernel is the best performing kernel in the SNRs -8 dB, -10 dB, -13 dB and -15 dB) and some kernels are doing the poorest in some SNRs and not in all SNRs (the EMBD

kernel is performing poorer than other implemented TFD kernels in SNRs 0 dB, -5 dB, -8 dB, -10 dB and -15 dB).

This example indicates that although the choice of TFD kernel can affect or improve the ESL performance of the TF-MUSIC algorithm, it cannot pledge its advantage for all signal samples. In other words, it is possible to find or optimize a TFD kernel (or kernel parameters) that performs better than other kernels (or kernel parameters) on a specific EEG dataset or even on several datasets, but it cannot prove its superiority in the case of untested EEG datasets. Furthermore, due to numerous possibilities of TFD kernel - kernel parameters combinations, such an optimization cannot guarantee that there is no better performing set of TFD kernel - kernel parameters combination.

5.6 Conclusion

Neonatal brain function analysis is an important tool to understand the newborn brain and to improve neonatal health. EEG source localization, which is commonly used in adults for functional brain analysis, is not well developed in neonates. This is a multidisciplinary research field by necessity requiring expertise from neurophysiology and neonatology, competencies in signal processing, medical image processing and a sound understanding of physics and mathematics. These skills can hardly be collected in a single research centre, and research in this field requires collaboration between various technical and medical researchers. This is evident from the organization of my two published papers on neonatal EEG which have been extended and included in this thesis. Lack of appropriate functional and anatomical neonatal brain data is another important obstacle in developing such techniques. A significant part of my research has involved looking for an appropriate neonatal MRI dataset to be segmented and converted to a realistic neonatal head model.

The realistic neonatal head model, which is generated based on the true geometry of neonatal brain and other layers of neonatal head, serves as the first building block in any neonatal EEG source localization technique. The true neonatal head model parameters, such as various layers' conductivity

or true source depth which are the other aspects of a realistic neonatal head model, has been the main obstacle in developing neonatal EEG source localization techniques. In order to address the lack of a current method for neonatal EEG source localization, this dissertation has proposed a method which is based on a realistic neonatal head model with true estimation of head model parameters. Acquiring these parameters is discussed in chapters 2 to 4 and this chapter is dedicated to the development and evaluation of a method to solve the inverse EEG problem through signal processing techniques.

When the appropriate neonatal head model parameters and segmented neonatal MRI were provided, the work on generating realistic neonatal head model started. First, the segmented neonatal MRI converted to a 3 dimensional mesh of points, then by assuming a 64-channels EEG cap, the electromagnetic relationships were calculated between putative dipoles in each mesh point of brain and an EEG electrode location. In this way, a realistic neonatal head model or the lead field matrix was acquired. The last step was to solve the inverse EEG problem using the acquired LFM and the proposed method.

A method was proposed in this chapter to enhance the TF-MUSIC algorithm which has been previously applied to localize sources of adult MEG data. The TF-MUSIC algorithm is a signal processing technique that uses subspaces of spatial TFD of a measurement signal such as MEG or EEG and the LFM to estimate the best dipole locations. Not all parts of TFD of EEG signals are used for the signal and noise subspace separation in this technique. Some specific regions of TFD plane (ROIs) are selected which constitute the basis for the subspace estimation. It was shown in this chapter that the identification of ROI plays an important role in the source localization accuracy of an EEG source localization method.

These regions (ROIs) were manually selected in the previous implementation of the TF-MUSIC algorithm. However, manual selection / identification of ROIs is subjective, and the result of source localization and its accuracy can be affected by the competency of the user identifying these regions in the time-frequency plane. Most importantly, identification of these regions in the time-frequency plane is not a skill of a neurophysiologist or clinical / medical experts. Identification of ROIs for a

specific feature of EEG signal in the time-frequency plane relies on knowing the time-frequency representation of that EEG feature. This knowledge depends on an advanced signal processing technique which is not broadly available among neurophysiologists, neonatologists and other clinical / medical people who are not working in the field signal processing. This means the previous implementation of the TF-MUSIC algorithm is not practical in real applications where no signal processing expert is present in clinical / medical practices.

In order to address this deficiency in the previous implementation of the TF-MUSIC algorithm, I proposed to identify the ROIs automatically. This enhancement not only makes usage of the TF-MUSIC algorithm possible in real clinical practices, but it also produces objective results which do not depend on the knowledge of the user. The automatic ROI identification for the TF-MUSIC algorithm was implemented based on the concept of object in the image. EEG datasets are multichannel signals in which events or features of interest may appear in some of the channels only. Therefore, it is necessary to generate a unique image for all multichannel EEG data that can clearly represent the signal for the events or the regions of interest.

In order to produce a unique time frequency representation for multichannel EEG data, TFDs of all channels are calculated and averaged over channels. The averaging procedure fades out the signal of interest's components but it also reduces the noise with a greater factor, as it is assumed that noise or background brain activities are not correlated between EEG electrodes. In the worst case, when the signal of interest appears in one EEG channel / electrode only (which is NOT the case with dense array neonatal EEG recordings or even 64-channels neonatal EEGs); the fading factor is equal for the noise and signal. Otherwise, i.e., when the signal of interest appears in more than one EEG channels / electrodes, the fading factor for signal is smaller than noise as signal components are assumed to be correlated between various EEG electrodes. This means the averaging procedure does not degrade the signal of interest; on the contrary, it enhances the SNR for the signal of interest.

The averaged TFD is converted to a binary image where ROIs are identified as connected areas. In the current implementation, it is assumed the number of ROIs is known in the signal. This assumption

is realistic in many ESL applications such as evoked potentials or any other marked dataset in which each marked area can be assumed as a separate ROI. However, there are many other possibilities in image processing techniques and pattern recognition such as clustering that can be easily implemented for finding the number of ROIs and added to the algorithm. It was also assumed that the areas of ROIs are greater than a minimum which is a realistic assumption where features of EEG are present in time (and frequency) for more than a minimum period. This threshold is set to 50 pixels in the current implementation and objects with smaller areas are assumed noise and are removed. For an EEG dataset with a sampling rate of 256 Hz this means a region of signal with duration of 5 ms or larger can be selected as an ROI if its bandwidth is more than 1 Hz. These dimensions are much smaller than any features investigated in this study, such as focal transients or visually evoked potentials. Consequently the selected threshold worked well in this implementation (none of the marked event removed due to this threshold).

After finishing the implementation of the proposed method, it was necessary to validate and evaluate the implemented algorithm. A common method for the evaluation of ESL algorithms applied in previous studies is to simulate EEG signals using known sources, combine them with different levels of white Gaussian noise and apply the ESL technique to localize sources of the noisy simulated EEGs. These simulated EEGs with different SNRs not only make it possible to evaluate the capacity of an ESL method for recovering weak cortical sources, they have been interpreted as the EEGs generated by deeper sources. Therefore, the capacity of a method to recover sources of an EEG dataset with low SNR values indicates its capacity to reconstruct deep sources in the EEG with higher SNRs.

In order to validate and evaluate the proposed algorithm, simulated EEG datasets were generated using the realistic neonatal head model produced previously, and three sources with 9 sets of parameters. This variety of source parameters was used to study various state of separation of source signatures in time-frequency plane. However, these are not the only possibilities for the source signal parameters and numerous other values are possible which are not tested in this study. Nonetheless, the capacity of the proposed method is illustrated through the applied parameters as explained in this

chapter. Since data was assumed artefact free, the noise collected by EEG acquiring hardware was the only assumed noise. In this way, the above mentioned EEGs were generated in 6 different levels of SNR as {0, -5, -8, -10, -13, -15} dB.

In order to quantify the error of the TF-MUSIC algorithm, a metric was needed. Most of the presented ESL performance metrics allow for only the dipole localization error. Though there are other factors that can be considered for measuring original and reconstructed sources similarities, a new performance metric was introduced in this chapter that takes into account these parameters to enhance the error measurement's accuracy in EEG source localization. These parameters were combined in an empirical formulation which was finalized after a series of experiments using the above mentioned simulated EEGs.

A better calibration of this performance metric will be possible if there are more real artefact free neonatal EEGs with known cortical presentation. A set of exponential weighting functions and coefficients were applied in the proposed formulation of this performance metric to limit the value of performance when the original and reconstructed sources are very different. Though it seems, according to the results achieved using simulated EEGs, the exponential weighting functions need to be revised for better calibration. The value of performance metric is not a unique identifier of an ESL's merit and it is possible to modify it in order to include the effect of source depth. It is possible to include some new coefficients, or modify current coefficients, to allow for such considerations.

The proposed metric allowed the comparing of accuracies of the TF-MUSIC algorithm and other ESL techniques. The performance of the TF-MUSIC algorithm was about 25% better when compared to the MUSIC algorithm if ROIs were identified automatically. This enhancement was achieved in the price of the huge computational cost of the TF-MUSIC algorithm. As it revealed in this chapter, superiority of the TF-MUSIC algorithm is mainly due to SNR enhancement resulted by correct ROI identification. It was also shown that TF-MUSIC without ROI identification performs poorer than MUSIC.

The TF-MUSIC algorithm was also compared to wMNE, sLORETA and dSPM using the realistic

simulated EEGs. The outputs were mapped on the neonatal head model (the brain) and visually compared together. A manual threshold was applied to represent only their maximums. The result indicated the maximums of these distributed sources algorithms were practically close to that of TF-MUSIC. Since these methods are well developed for localizing the sources of brain functions with broad active regions, they do not constitute the ideal rivals for this comparison. However, it is not claimed that the presented method is the best possible source localization algorithm for neonatal EEG, and this comparison indicated the capacity of the proposed method. The method was also applied to localize sources of real neonatal VEP where the results indicated the localization of sources in the Occipital region which is the known representation of the VEP. In the simulations used in this study, source signatures are not overlapping (in time-frequency plane), as the available real data was only included in separate marked events and the VEP which did not include overlapping sources. In other words, the current implementation of the algorithm assumes each ROI include only one source. However, the method can be easily modified to localize multiple sources in one ROI. An example of localizing multiple sources with overlapping signature in the time-frequency plane is illustrated in Appendix 1. This is similar to the procedure of the MUSIC algorithm for localizing multiple sources. This work has opened a door to further studies on neonatal EEG source localization and there are many possibilities that can be investigated in subsequent studies. Future work will attempt to enhance the proposed method through better estimation of subspaces. This can be achieved either through improving the ROI identification procedure or the estimation procedure. It is possible to use other methods to produce a unique representation of multichannel EEG which may improve ROI identification procedure. Methods such as singular value decomposition which has been used in a previous implementation of the TF-MUSIC algorithm or even the principal components of EEG signals are possibilities that can be used for this purpose. The subspaces of the regions of STFD which are selected as ROIs can also be estimated using other subspace techniques rather than MUSIC. FINES [229] is another subspace method which can be combined with time frequency analysis to generate possibly better performances. Contrary to MUSIC which uses the entire estimated noise

subspace, FINES uses closeness criterion to find a small set of particular vectors in the estimated noise subspace [36]. The other aspect of future work will include finding a more accurate measure for the evaluation of ESL methods in the case of real EEG data with unknown cortical representation. Functional Magnetic Resonance Imaging which is commonly used for functional brain analysis could be considered in combination with ESL in these cases.

CHAPTER 6: CONCLUSIONS AND SUGGESTIONS FOR FUTURE WORK

6.1 Thesis summary

The overall objective was to improve neonatal health care through enhancing non-invasive neonatal brain monitoring by developments in neonatal ESL.

Functional brain organization in neonates has been investigated through (i) proposing methodologies to estimate essential neonatal head model parameters such as skull conductivity, source depth and spatial resolution of neonatal EEG, (ii) nominating an algorithm to fulfill prerequisite conditions in the neonatal EEG inverse problem, i.e., estimating neural activity from the scalp potential, and enhancing the selected algorithm, and (iii) validating and evaluating the proposed method through application to simulated and real EEG and quantifying its performance by introducing a new EEG source localization (ESL) performance metric.

Source localization performance is strongly affected by accuracy of the head model, including head model geometry and the chosen values of relevant parameters. Lack of accurate knowledge on the structural parameters in the neonatal head model has been an obstacle in the development of neonatal ESL. Neonatal skull conductivity, an essential component of the head volume conductor model, cannot be measured directly due to ethical restrictions. The spatial patterning of the neonatal EEG has also been hampered by the common use of 10 to 20 electrodes for neonatal EEG recordings. Insufficient knowledge of the cortex-scalp distance in neonates and children has also hampered the determination of source depth which is a prerequisite for solving the EEG inverse problem.

This thesis has addressed these requirements and made contributions in both practical and theoretical aspects of neonatal EEG source localization by:

- Applying empirical methods along with realistic simulations to indirectly estimate the unknown *in vivo* neonatal head model parameters, namely
    - the effect of fontanelles on the neonatal skull conductivity profile,
    - the number of electrodes needed to capture full spatial details of neonatal EEG

    - the proper neonatal skull conductivity value
    - the appropriate source depth in the neonatal head model
- Proposing and enhancing an algorithm to compute the neonatal EEG inverse solution. The chosen algorithm was chosen from adult EEG source localization literature to fulfill several requirements in the neonatal ESL environment. The technique uses a current dipole to model neural activity in the brain and the whole source space is scanned for the dipole location that minimizes a cost function. The cost function is minimized where the orthogonality between the estimated EEG noise subspace and the lead field matrix (LFM) is at a maximum. The LFM is calculated in the EEG forward model and the noise subspace is estimated from manually identified regions of the spatial time frequency distribution (STFD) of EEG signals. The manual identification of regions of interest (ROI) necessitated a knowledge of the time frequency representation of EEG signals which is not practical. In order to address this limitation the subjective manual ROI identification was replaced by image processing techniques to objectively determine these regions. Thus the enhanced algorithm is suitable for application in clinical practice because knowledge of the time frequency representation of the EEG signals is not required.
- Introducing an improved performance metric that quantifies the correspondence between the estimated and original source distributions. Since the original sources in real EEGs are unknown, most of the ESL evaluation methods use simulated EEGs where known source locations are used to generate EEG signals. After applying ESL to the simulated EEGs, the distance between original and estimated source locations can be defined as dipole localization error. A new performance metric is proposed that takes into account other factors in addition to dipole localization error to enhance the ESL error measurement accuracy. The two parameters effective in measuring original and reconstructed source similarities are addressed in this new performance metric as current intensity in the location of the original source and presence of other sources.

6.2 Major conclusions of the thesis

The major conclusions from the empirical and theoretical implementations, simulations, algorithm development, implementation and evaluation include:

A) A clear difference is evident between adults and neonates in terms of spatial decay of signal's correlations. The spatial decays were approximately three times steeper in neonates than in 256 channel recordings in adult subjects.

B) The amount of unique information in neonatal scalp EEG is much richer than commonly assumed. The Nyquist frequency for spatial EEG sampling is ~0.5-0.8 c/cm., equivalent to a wavelength of 1.25-2 cm. Thus in the neonate a 3-5mm interelectrode spacing is needed to capture full spatial detail.

C) A hdEEG neonatal study using 64 electrodes, showed that each electrode covers roughly about 3cm of scalp (a circle with 3 cm diameter). This implies that in practical terms the conventional neonatal EEG using 10 to 20 electrodes gives a significant spatial under sampling, and consequently will lead to an underestimation of brain events and their EEG amplitudes.

D) The conventional "full neonatal array" of 10-20 electrodes ignores large parts of brain activity. In particular, electrode coverage of the parietal and centro-temporal areas, the areas with the most developmentally significant rapid oscillations, is so poor that even a majority of focal events may go undetected.

E) An experiment with a spherical head model clearly established how source depth dramatically affects spatial power spectral density (PSDx). Simulation experiments show also that skull conductivity strongly affects PSDx. This observation implies that building a source analysis paradigm using EEG from deep brain lesions as the anatomical reference is inappropriate when aiming to develop and validate source localization paradigms for cortical EEG activity.

F) EEG amplitude spatial decay is not statistically significant different in over skull and fontanelles. Thus a neonatal head model can be constructed without any special consideration for fontanelles.

G) Comparing skull conductivities in the range 0.003 to 0.3 S/m in head models showed the spatial decays of real neonatal EEG data are best reproduced when skull conductivities around 0.06-0.2 S/m are assumed. These conductivity values are orders of magnitude higher than used in adult head models.

H) The TF-MUSIC algorithm with automatically identified ROIs adequately reconstructed original source distributions in realistic simulated neonatal EEGs with different time-frequency domain signatures, even in low signal to noise situations. The realistic simulated neonatal EEGs were generated using the neonatal head model based on segmented neonatal brain MRI and the estimated parameters. The performance of the TF-MUSIC algorithm was characterised using the newly proposed performance metric. Visual evoked potentials (VEP) EEG data was also used to evaluate the TF-MUSIC algorithm in its application to real neonatal VEP EEG and the source was localised bilaterally to the occipital lobes, the expected site of cortical representation of VEP data.

6.3 Suggestions for future work

This work has provided significant advances in neonatal EEG source localization with many possibilities to be investigated in subsequent studies. Future work should attempt to enhance the proposed method through improved estimation of signal and noise subspaces which could be achieved either through improving the objective ROI identification procedure or the estimation procedure. It is also required that a more accurate measurement to be performed for the evaluation of ESL methods in the case of real EEG data with unknown cortical representation. Functional Magnetic Resonance Imaging which is commonly used for functional brain analysis could be considered in combination with ESL in these cases.

The observation of highly varying spatial patterning is consistent with the idea that the development of infant cognition may be studied by analysis of the formation of spatiotemporal patterns like cinematic frames that in some respects resemble “neural avalanches”. Capturing these with novel dense array EEG devices, may open a novel window to capturing the details of development and their functional correlates. These steps are essential to the new opportunities for source level connectivity analysis of emerging large scale brain processes involved in the development of perception and cognition through to providing tools to study pathological conditions such as neonatal brain seizures and the effectiveness of interventions to improve brain outcomes.

References

[1] S. Baillet, J. C. Mosher, and R. M. Leahy, "Electromagnetic brain mapping," *Signal Processing Magazine, IEEE,* vol. 18, pp. 14-30, 2001.

[2] G. Lantz, L. Spinelli, R. G. Menendez, M. Seeck, and C. M. Michel, "Localization of distributed sources and comparison with functional MRI," *Epileptic Disord,* vol. Special Issue, pp. 45-58, Jul 2001.

[3] C. Phillips, M. D. Rugg, and K. J. Friston, "Anatomically Informed Basis Functions for EEG Source Localization: Combining Functional and Anatomical Constraints," *Neuroimage,* vol. 16, pp. 678-695, 2002.

[4] A. Messe, D. Rudrauf, H. Benali, and G. Marrelec, "Relating structure and function in the human brain: relative contributions of anatomy, stationary dynamics, and non-stationarities," *PLoS Comput Biol,* vol. 10, p. e1003530, Mar 2014.

[5] C. M. Michel, G. Thut, S. Morand, A. Khateb, A. J. Pegna, R. Grave de Peralta, *et al.*, "Electric source imaging of human brain functions," *Brain Res Rev,* vol. 36, pp. 108-118, 2001.

[6] M. M. Mesulam, "From sensation to cognition," *Brain,* vol. 121, pp. 1013-1052, June 1, 1998 1998.

[7] Baillet Sylvain. (2014, 22/5/2014). *MEG Clinical & Research Program,* . Available: http://www.mcw.edu/MEG.htm

[8] A. R. McIntosh, "Mapping cognition to the brain through neural interactions," *Memory,* vol. 7, pp. 523-48, Sep-Nov 1999.

[9] R. S. Menon and S. G. Kim, "Spatial and temporal limits in cognitive neuroimaging with fMRI," *Trends Cogn Sci,* vol. 3, pp. 207-216, Jun 1999.

[10] F. Darvas, D. Pantazis, E. Kucukaltun-Yildirim, and R. M. Leahy, "Mapping human brain function with MEG and EEG: methods and validation," *Neuroimage,* vol. 23, Supplement 1, pp. S289-S299, 2004.

[11] C. Grova, J. Daunizeau, J. M. Lina, C. G. Bénar, H. Benali, and J. Gotman, "Evaluation of EEG localization methods using realistic simulations of interictal spikes," *Neuroimage,* vol. 29, pp. 734-753, 2006.

[12] R. Srinivasan, "Methods to Improve the Spatial Resolution of EEG," *INTERNATIONAL JOURNAL OF BIOELECTROMAGNETISM,* vol. 1, pp. 102-111, // 1999.

[13] C. M. Michel, M. M. Murray, G. Lantz, S. Gonzalez, L. Spinelli, and R. Grave de Peralta, "EEG source imaging," *Clinical Neurophysiology,* vol. 115, pp. 2195-2222, 2004.

[14] L. Hesheng, P. H. Schimpf, D. Guoya, G. Xiaorong, Y. Fusheng, and G. Shangkai, "Standardized shrinking LORETA-FOCUSS (SSLOFO): a new algorithm for spatio-temporal EEG source reconstruction," *Biomedical Engineering, IEEE Transactions on,* vol. 52, pp. 1681-1691, 2005.

[15] N. Roche-Labarbe, A. Aarabi, G. Kongolo, C. Gondry Jouet, M. Dümpelmann, R. Grebe, *et al.*, "High-Resolution Electroencephalography and Source Localization in Neonates," *Human Brain Mapping,* vol. 29, pp. 167-176, 2008.

[16] J. Dudink, S. J. Counsell, M. H. Lequin, and P. P. Govaert, "DTI reveals network injury in perinatal stroke," *Archives of Disease in Childhood - Fetal and Neonatal Edition,* vol. 97, pp. F362-F364, September 1, 2012 2012.

[17] P. Fransson, U. Åden, M. Blennow, and H. Lagercrantz, "The Functional Architecture of the Infant Brain as Revealed by Resting-State fMRI," *Cerebral Cortex,* vol. 21, pp. 145-154, January 1, 2011 2011.

[18] G. A. Lodygensky, L. Vasung, S. V. Sizonenko, and P. S. Huppi, "Neuroimaging of cortical development and brain connectivity in human newborns and animal models," *J Anat,* vol. 217, pp. 418-28, Oct 2010.

[19] M. Colonnese and R. Khazipov, "Spontaneous activity in developing sensory circuits: Implications for resting state fMRI," *NeuroImage,* vol. 62, pp. 2212-2221, 10/1/ 2012.

[20] I. L. Hanganu-Opatz, "Between molecules and experience: role of early patterns of coordinated activity for the development of cortical maps and sensory abilities," *Brain Res Rev,* vol. 64, pp. 160-76, Sep 2010.

[21] K. K. Sampsa Vanhatalo, "Spontaneous and Evoked Activity in the Early Human Brain," in *The Newborn Brain: Neuroscience & Clinical Applications*, H. Lagercrantz, Hanson, M.A., Ment, L.R., Peebles, D.M., Ed., 2nd ed: Cambridge University Press, 2010, pp. 229–243.

[22] M. André, M. D. Lamblin, A. M. d'Allest, L. Curzi-Dascalova, F. Moussalli-Salefranque, S. Nguyen The Tich, *et al.*, "Electroencephalography in premature and full-term infants. Developmental features and glossary," *Neurophysiologie Clinique/Clinical Neurophysiology,* vol. 40, pp. 59-124, 5// 2010.

[23] R. J. Ellingson and J. F. Peters, "Development of EEG and daytime sleep patterns in normal full-term infants during the first 3 months of life: Longitudinal observations," *Electroencephalography and Clinical Neurophysiology,* vol. 49, pp. 112-124, 1980.

[24] C. Dreyfus-Brisac and N. Monod, "The electroencephalogram of full-term newborns and premature infants," in *Handbook of electroencephalography and clinical neurophysiology*. vol. 6, ed, 1975, pp. 6-23.

[25] N. Roche-Labarbe, A. Aarabi, G. Kongolo, C. Gondry-Jouet, M. Dümpelmann, R. Grebe, *et al.*, "High-Resolution Electroencephalography and Source Localization in Neonates," *Human Brain Mapping,* vol. 29, pp. 167-176, 2008.

[26] Maryam Odabaee, Siamak Layeghy, Mostefa Mesbah, Ghasem Azemi, Boualem Boashash, Paul B. Colditz, *et al.*, "EEG amplitude and correlation spatial decay analysis for neonatal head modelling," in *Information Science, Signal Processing and their Applications (ISSPA), 2012 11th International Conference on*, 2012, pp. 882-887.

[27] M. Fuchs, J. Kastner, M. Wagner, S. Hawes, and J. S. Ebersole, "A standardized boundary element method volume conductor model," *Clinical Neurophysiology,* vol. 113, pp. 702-712, 2002.

[28] C. E. Acar and N. G. Gencer, "Sensitivity of EEG and MEG to conductivity perturbations," in *Engineering in Medicine and Biology Society, 2003. Proceedings of the 25th Annual International Conference of the IEEE,* 2003, pp. 2834-2837 Vol.3.

[29] C. Ramon, P. Schimpf, J. Haueisen, M. Holmes, and A. Ishimaru, "Role of Soft Bone, CSF and Gray Matter in EEG Simulations," *Brain Topography,* vol. 16, pp. 245-248, 2004.

[30] I. Despotovic, P. J. Cherian, M. De Vos, H. Hallez, W. Deburchgraeve, P. Govaert, *et al.*, "Relationship of EEG sources of neonatal seizures to acute perinatal brain lesions seen on MRI: a pilot study," *Hum Brain Mapp,* vol. 34, pp. 2402-17, Oct 2013.

[31] M. S. Beauchamp, M. R. Beurlot, E. Fava, A. R. Nath, N. A. Parikh, Z. S. Saad, *et al.*, "The Developmental Trajectory of Brain-Scalp Distance from Birth through Childhood: Implications for Functional Neuroimaging," *PLoS ONE,* vol. 6, p. e24981, 2011.

[32] M. Odabaee, A. Tokariev, S. Layeghy, M. Mesbah, P. B. Colditz, C. Ramon, *et al.*, "Neonatal EEG at scalp is focal and implies high skull conductivity in realistic neonatal head models," *Neuroimage,* vol. 96, pp. 73-80, 2014.

[33] W. J. Freeman, M. D. Holmes, B. C. Burke, and S. Vanhatalo, "Spatial spectra of scalp EEG and EMG from awake humans," *Clin Neurophysiol,* vol. 114, pp. 1053-68, Jun 2003.

[34] R. Srinivasan, D. Tucker, and M. Murias, "Estimating the spatial Nyquist of the human EEG," *Behavior Research Methods, Instruments, & Computers,* vol. 30, pp. 8-19, 1998/03/01 1998.

[35] M. Odabaee, W. J. Freeman, P. B. Colditz, C. Ramon, and S. Vanhatalo, "Spatial patterning of the neonatal EEG suggests a need for a high number of electrodes," *Neuroimage,* vol. 68, pp. 229-235, 2013.

[36] R. Grech, T. Cassar, J. Muscat, K. P. Camilleri, S. G. Fabri, M. Zervakis, *et al.*, "Review on solving the inverse problem in EEG source analysis," *Journal of NeuroEngineering and Rehabilitation,* vol. 5, p. 25, 2008.

[37] J. C. Mosher, S. Baillet, and R. M. Leahy, "EEG Source Localization and Imaging Using Multiple Signal Classification Approaches," *Journal of Clinical Neurophysiology,* vol. 16, pp. 225-238, 1999.

[38] R. Menendez, S. Andino, G. Lantz, C. Michel, and T. Landis, "Noninvasive Localization of Electromagnetic Epileptic Activity. I. Method Descriptions and Simulations," *Brain Topography,* vol. 14, pp. 131-137, 2001/12/01 2001.

[39] C. Phillips, J. Mattout, M. D. Rugg, P. Maquet, and K. J. Friston, "An empirical Bayesian solution to the source reconstruction problem in EEG," *Neuroimage,* vol. 24, pp. 997-1011, 2005.

[40] C. M. Michel and M. M. Murray, "Towards the utilization of EEG as a brain imaging tool," *Neuroimage,* vol. 61, pp. 371-385, 2012.

[41] L. Gavit, S. Baillet, J. F. Mangin, J. Pescatore, and L. Garnero, "A multiresolution framework to MEG/EEG source imaging," *Biomedical Engineering, IEEE Transactions on,* vol. 48, pp. 1080-1087, 2001.

[42] J. C. Mosher and R. M. Leahy, "Source localization using recursively applied and projected (RAP) MUSIC," *Signal Processing, IEEE Transactions on,* vol. 47, pp. 332-340, 1999.

[43] H. Buchner, C. Kauert, and I. Radermacher, "Short-term changes of finger representation at the somatosensory cortex in humans," *Neuroscience Letters,* vol. 198, pp. 57-59, 1995.
[44] G. L. Barkley and C. Baumgartner, "MEG and EEG in Epilepsy," *Journal of Clinical Neurophysiology,* vol. 20, pp. 163-178, 2003.
[45] K. Kobayashi, H. Yoshinaga, M. Oka, Y. Ohtsuka, and J. Gotman, "A simulation study of the error in dipole source localization for EEG spikes with a realistic head model," *Clinical Neurophysiology,* vol. 114, pp. 1069-1078, 2003.
[46] I. Merlet and J. Gotman, "Reliability of dipole models of epileptic spikes," *Clinical Neurophysiology,* vol. 110, pp. 1013-1028, 1999.
[47] H. Hallez, B. Vanrumste, R. Grech, J. Muscat, W. De Clercq, A. Vergult, *et al.*, "Review on solving the forward problem in EEG source analysis," *Journal of NeuroEngineering and Rehabilitation,* vol. 4, p. 46, 2007.
[48] H. Buchner, T. Waberski, M. Fuchs, H.-A. Wischmann, M. Wagner, and R. Drenckhahn, "Comparison of realistically shaped boundary-element and spherical head models in source localization of early somatosensory evoked potentials," *Brain Topography,* vol. 8, pp. 137-143, 1995/12/01 1995.
[49] K. A. Awada, D. R. Jackson, J. T. Williams, D. R. Wilton, S. B. Baumann, and A. C. Papanicolaou, "Computational aspects of finite element modeling in EEG source localization," *Biomedical Engineering, IEEE Transactions on,* vol. 44, pp. 736-752, 1997.
[50] K. Uutela, M. Hamalainen, and R. Salmelin, "Global optimization in the localization of neuromagnetic sources," *Biomedical Engineering, IEEE Transactions on,* vol. 45, pp. 716-723, 1998.
[51] R. Grave de Peralta Menendez and S. L. Gonzalez Andino, "Single dipole localization: some numerical aspects and a practical rejection criterion for the fitted parameters," *Brain Topogr,* vol. 6, pp. 277-82, Summer 1994.
[52] M. Scherg and D. V. Cramon, "Evoked dipole source potentials of the human auditory cortex," *Electroencephalography and Clinical Neurophysiology/Evoked Potentials Section,* vol. 65, pp. 344-360, 9// 1986.
[53] S. Baillet, "Toward Functional Brain Imaging of Cortical Electrophysiology Markovian Models for Magneto and Electroencephalogram Source Estimation and Experimental Assessments," 1998.
[54] S. Kirkpatrick, C. D. Gelatt, and M. P. Vecchi, "Optimization by Simulated Annealing," *Science,* vol. 220, pp. 671-680, May 13, 1983 1983.
[55] M. I. Miga, T. E. Kerner, and T. M. Darcey, "Source localization using a current-density minimization approach," *Biomedical Engineering, IEEE Transactions on,* vol. 49, pp. 743-745, 2002.
[56] M. S. Hämäläinen and R. J. Ilmoniemi, *Interpreting measured magnetic fields of the brain: estimates of current distributions*: Helsinki University of Technology, Department of Technical Physics, 1984.
[57] H. Olaf, "Keep it simple: a case for using classical minimum norm estimation in the analysis of EEG and MEG data," *Neuroimage,* vol. 21, pp. 1612-1621, 2004.
[58] A. Dale, "Improved Localization of Cortical Activity By Combining EEG and MEG with MRI Cortical Surface Reconstruction: A Linear Approach," 1993.
[59] S. Komssi, J. Huttunen, H. J. Aronen, and R. J. Ilmoniemi, "EEG minimum-norm estimation compared with MEG dipole fitting in the localization of somatosensory sources at S1," *Clinical Neurophysiology,* vol. 115, pp. 534-542, 2004.
[60] I. F. Gorodnitsky, J. S. George, and B. D. Rao, "Neuromagnetic source imaging with FOCUSS: a recursive weighted minimum norm algorithm," *Electroencephalogr Clin Neurophysiol,* vol. 95, pp. 231-51, Oct 1995.
[61] S. Baillet, "Evaluation of inverse methods and head models for EEG source localization using a human skull phantom," *Physics in Medicine and Biology,* vol. 46 77, pp. 77-96, 2001.
[62] R. D. Pascual-Marqui, C. M. Michel, and D. Lehmann, "Low resolution electromagnetic tomography: a new method for localizing electrical activity in the brain," *International Journal of Psychophysiology,* vol. 18, pp. 49-65, 10// 1994.
[63] R. Grave, "Linear Inverse Solutions With Optimal Resolution Kernels Applied to Electromagnetic Tomography," 1997.
[64] S. G. A. R. Grave de Peralta, "Comparison of algorithms for the localization of focal sources: evaluation with simulated data and analysis of experimental data " *INTERNATIONAL JOURNAL OF BIOELECTROMAGNETISM,* vol. 4, 2002.
[65] R. Grave de Peralta Menendez, M. M. Murray, C. M. Michel, R. Martuzzi, and S. L. Gonzalez Andino, "Electrical neuroimaging based on biophysical constraints," *Neuroimage,* vol. 21, pp. 527-539, 2004.

[66] L. Hesheng, G. Xiaorong, P. H. Schimpf, Y. Fusheng, and G. Shangkai, "A recursive algorithm for the three-dimensional imaging of brain electric activity: shrinking LORETA-FOCUSS," *Biomedical Engineering, IEEE Transactions on,* vol. 51, pp. 1794-1802, 2004.
[67] B. D. Van Veen and K. M. Buckley, "Beamforming: a versatile approach to spatial filtering," *ASSP Magazine, IEEE,* vol. 5, pp. 4-24, 1988.
[68] R. O. Schmidt, "Multiple emitter location and signal parameter estimation," *Antennas and Propagation, IEEE Transactions on,* vol. 34, pp. 276-280, 1986.
[69] J. C. Mosher, P. S. Lewis, and R. M. Leahy, "Multiple dipole modeling and localization from spatio-temporal MEG data," *Biomedical Engineering, IEEE Transactions on,* vol. 39, pp. 541-557, 1992.
[70] J. C. Mosher and R. M. Leahy, "Recursive MUSIC: A framework for EEG and MEG source localization," *Biomedical Engineering, IEEE Transactions on,* vol. 45, pp. 1342-1354, 1998.
[71] K. Sekihara, S. S. Nagarajan, D. Poeppel, A. Marantz, and Y. Miyashita, "Reconstructing spatio-temporal activities of neural sources using an MEG vector beamformer technique," *Biomedical Engineering, IEEE Transactions on,* vol. 48, pp. 760-771, 2001.
[72] K. Sekihara, S. S. Nagarajan, D. Poeppel, S. Miyauchi, N. Fujimaki, H. Koizumi, *et al.*, "Estimating neural sources from each time-frequency component of magnetoencephalographic data," *Biomedical Engineering, IEEE Transactions on,* vol. 47, pp. 642-653, 2000.
[73] K. Sekihara, S. Nagarajan, D. Poeppel, and Y. Miyashita, "Time-frequency MEG-MUSIC algorithm," *IEEE Trans Med Imaging,* vol. 18, pp. 92-7, Jan 1999.
[74] K. Sakuma, K. Sekihara, and I. Hashimoto, "Neural source estimation from a time-frequency component of somatic evoked high-frequency magnetic oscillations to posterior tibial nerve stimulation," *Clin Neurophysiol,* vol. 110, pp. 1585-8, Sep 1999.
[75] E. Rodriguez, N. George, J. P. Lachaux, J. Martinerie, B. Renault, and F. J. Varela, "Perception's shadow: long-distance synchronization of human brain activity," *Nature,* vol. 397, pp. 430-3, Feb 4 1999.
[76] L. Cohen, *Time-frequency analysis* vol. 778: Prentice Hall PTR Englewood Cliffs, NJ:, 1995.
[77] B. Boashash, *Time frequency signal analysis and processing: a comprehensive reference* Amsterdam; Boston: Elsevier, 2003.
[78] J. R. Castro Conde, E. D. Martínez, C. G. Campo, A. M. Pérez, and M. L. McLean, "Positive temporal sharp waves in preterm infants with and without brain ultrasound lesions," *Clinical Neurophysiology,* vol. 115, pp. 2479-2488, 2004.
[79] A. Okumura, F. Hayakawa, T. Kato, K. Maruyama, T. Kubota, M. Suzuki, *et al.*, "Abnormal sharp transients on electroencephalograms in preterm infants with periventricular leukomalacia," *The Journal of Pediatrics,* vol. 143, pp. 26-30, 2003.
[80] M. Hämäläinen, R. Hari, R. J. Ilmoniemi, J. Knuutila, and O. V. Lounasmaa, "Magnetoencephalography—theory, instrumentation, and applications to noninvasive studies of the working human brain," *Reviews of Modern Physics,* vol. 65, pp. 413-497, 04/01/ 1993.
[81] S. Baillet, "Problem Inverse MEG/EEG," 2001.
[82] Li Z, Zeki R, Hilder L, and Sullivan EA, "Australia's mothers and babies 2010," Australian Institute of Health and Welfare, Canberra, Australia2012.
[83] G. Ball, L. Srinivasan, P. Aljabar, S. J. Counsell, G. Durighel, J. V. Hajnal, *et al.*, "Development of cortical microstructure in the preterm human brain," *Proc Natl Acad Sci U S A,* vol. 110, pp. 9541-6, Jun 4 2013.
[84] Y. Noble and R. Boyd, "Neonatal assessments for the preterm infant up to 4 months corrected age: a systematic review," *Dev Med Child Neurol,* vol. 54, pp. 129-39, Feb 2012.
[85] Chiara Nosarti, Abraham Reichenberg, Robin M. Murray, Sven Cnattingius, Mats P. Lambe, Li Yin, *et al.*, "Preterm birth and psychiatric disorders in young adult life," *Archives of General Psychiatry,* vol. 69, pp. 610-617, 2012.
[86] J. L. Y. Cheong and L. W. Doyle, "Increasing rates of prematurity and epidemiology of late preterm birth," *Journal of Paediatrics and Child Health,* vol. 48, pp. 784-788, 2012.
[87] S. Beck, D. Wojdyla, L. Say, A. P. Betran, M. Merialdi, J. H. Requejo, *et al.*, "The worldwide incidence of preterm birth: a systematic review of maternal mortality and morbidity," *Bulletin of the World Health Organization,* vol. 88, p. 31, 2010.
[88] Li Z, McNally L, Hilder L, and Sullivan EA, "Australia's Mothers and Babies 2009," Australian Institute of Health and Welfare, Sydney, Australia2011.
[89] G. Boylan, L. Burgoyne, C. Moore, B. O'Flaherty, and J. Rennie, "An international survey of EEG use in the neonatal intensive care unit," *Acta Paediatr,* vol. 99, pp. 1150-5, Aug 2010.

[90] J. M. Rennie, G. Chorley, G. B. Boylan, R. Pressler, Y. Nguyen, and R. Hooper, "Non-expert use of the cerebral function monitor for neonatal seizure detection," *Arch Dis Child Fetal Neonatal Ed,* vol. 89, pp. F37-40, Jan 2004.

[91] R. A. Shellhaas, A. I. Soaita, and R. R. Clancy, "Sensitivity of amplitude-integrated electroencephalography for neonatal seizure detection," *Pediatrics,* vol. 120, pp. 770-7, Oct 2007.

[92] B. H. Walsh, D. M. Murray, and G. B. Boylan, "The use of conventional EEG for the assessment of hypoxic ischaemic encephalopathy in the newborn: A review," *Clinical Neurophysiology,* vol. 122, pp. 1284-1294, 2011.

[93] S. Sanei and J. A. Chambers, "EEG Source Localization," in *EEG Signal Processing*, ed: John Wiley & Sons Ltd, 2007, pp. 197-218.

[94] C.-G. Bénar, C. Grova, E. Kobayashi, A. P. Bagshaw, Y. Aghakhani, F. Dubeau, *et al.*, "EEG–fMRI of epileptic spikes: Concordance with EEG source localization and intracranial EEG," *NeuroImage,* vol. 30, pp. 1161-1170, 5/1/ 2006.

[95] J. Dubois, M. Benders, C. Borradori-Tolsa, A. Cachia, F. Lazeyras, R. Ha-Vinh Leuchter, *et al.*, "Primary cortical folding in the human newborn: an early marker of later functional development," *Brain,* vol. 131, pp. 2028-2041, August 1, 2008 2008.

[96] M. Aminoff, "Electroencephalography: general principles and clinical applications," in *Electrodiagnosis in Clinical Neurology*, Third ed: Harcourt Health Sciences Group, 1992, pp. 41-91.

[97] T. C. Ferree, K. J. Eriksen, and D. M. Tucker, "Regional head tissue conductivity estimation for improved EEG analysis," *Biomedical Engineering, IEEE Transactions on,* vol. 47, pp. 1584-1592, 2000.

[98] T. C. Ferree, M. T. Clay, and D. M. Tucker, "The spatial resolution of scalp EEG," *Neurocomputing,* vol. 38–40, pp. 1209-1216, 6// 2001.

[99] T. F. Oostendorp, J. Delbeke, and D. F. Stegeman, "The conductivity of the human skull: results of in vivo and in vitro measurements," *Biomedical Engineering, IEEE Transactions on,* vol. 47, pp. 1487-1492, 2000.

[100] R. Hoekema, G. H. Wieneke, F. S. S. Leijten, C. W. M. van Veelen, P. C. van Rijen, G. J. M. Huiskamp, *et al.*, "Measurement of the Conductivity of Skull, Temporarily Removed During Epilepsy Surgery," *Brain Topography,* vol. 16, pp. 29-38, Fall 2003.

[101] M. Dannhauer, B. Lanfer, C. H. Wolters, and T. R. Knösche, "Modeling of the human skull in EEG source analysis," *Human Brain Mapping,* vol. 32, pp. 1383-1399, 2011.

[102] I. Despotovic, P. J. Cherian, M. D. Vos, H. Hallez, P. Govaert, M. Lequin, *et al.*, "Influence of volume conductor model errors on EEG dipole source localization in neonates," in *20th Annual Meeting & Exhibition: International Society for Magnetic Resonance in Medicine (ISMRM-2012)*, 2012.

[103] R. Srinivasan, P. L. Nunez, and R. B. Silberstein, "Spatial filtering and neocortical dynamics: estimates of EEG coherence," *Biomedical Engineering, IEEE Transactions on,* vol. 45, pp. 814-826, 1998.

[104] I. Despotovic, W. Deburchgraeve, H. Hallez, E. Vansteenkiste, and W. Philips, "Development of a Realistic Head Model for EEG Event-Detection and Source Localization in Newborn Infants," *31st Annual International Conference of the IEEE EMBS Minneapolis, Minnesota, USA, September 2-6, 2009*, 2009.

[105] C. H. Wolters, A. Anwander, X. Tricoche, D. Weinstein, M. A. Koch, and R. S. MacLeod, "Influence of tissue conductivity anisotropy on EEG/MEG field and return current computation in a realistic head model: A simulation and visualization study using high-resolution finite element modeling," *NeuroImage,* vol. 30, pp. 813-826, 2006.

[106] H. Gert Van, C. Jeremy De, V. Bart, W. Rik Van de, L. Ignace, D. H. Michel, *et al.*, "EEG dipole source localization using artificial neural networks," *Physics in Medicine and Biology,* vol. 45, p. 997, 2000.

[107] S. Rush and D. A. Driscoll, "Current distribution in the brain from surface electrodes," *Anesth Analg,* vol. 47, pp. 717-23, Nov-Dec 1968.

[108] C. Tang, F. You, G. Cheng, D. Gao, F. Fu, G. Yang, *et al.*, "Correlation between structure and resistivity variations of the live human skull," *IEEE Trans Biomed Eng,* vol. 55, pp. 2286-92, Sep 2008.

[109] P. L. Nunez, R. B. Silberstein, Z. Shi, M. R. Carpenter, R. Srinivasan, D. M. Tucker, *et al.*, "EEG coherency II: experimental comparisons of multiple measures," *Clin Neurophysiol,* vol. 110, pp. 469-86, Mar 1999.

[110] A. Adeloye, K. R. Kattan, and F. N. Silverman, "Thickness of the normal skull in the American Blacks and Whites," *Am J Phys Anthropol,* vol. 43, pp. 23-30, Jul 1975.

[111] C. F. Hansman, "Growth of interorbital distance and skull thickness as observed in roentgenographic measurements," *Radiology,* vol. 86, pp. 87-96, Jan 1966.
[112] M. Letts, D. Kaylor, and G. Gouw, "A biomechanical analysis of halo fixation in children," *J Bone Joint Surg Br,* vol. 70, pp. 277-9, Mar 1988.
[113] P. G. Grieve, R. G. Emerson, W. P. Fifer, J. R. Isler, and R. I. Stark, "Spatial correlation of the infant and adult electroencephalogram," *Clinical Neurophysiology,* vol. 114, pp. 1594-1608, 2003.
[114] R. Plonsey and D. Heppner, "Considerations of quasi-stationarity in electrophysiological systems," *The bulletin of mathematical biophysics,* vol. 29, pp. 657-664, 1967/12/01 1967.
[115] K. Jerbi, S. Baillet, J. C. Mosher, G. Nolte, L. Garnero, and R. M. Leahy, "Localization of realistic cortical activity in MEG using current multipoles," *NeuroImage,* vol. 22, pp. 779-793, 2004.
[116] R. Plonsey and R. E. Collin, *Principles and applications of electromagnetic fields*. Newyork, NY: McGraw-Hill, 1961.
[117] M. Sun, "An efficient algorithm for computing multishell spherical volume conductor models in EEG dipole source localization," *IEEE Trans Biomed Eng,* vol. 44, pp. 1243-52, Dec 1997.
[118] T.-H. Li and G. North, "Aliasing Effects and Sampling Theorems of Spherical Random Fields when Sampled on a Finite Grid," *Annals of the Institute of Statistical Mathematics,* vol. 49, pp. 341-354, 1997/06/01 1997.
[119] A. Gevins, M. E. Smith, L. McEvoy, and D. Yu, "High-resolution EEG mapping of cortical activation related to working memory: effects of task difficulty, type of processing, and practice," *Cerebral Cortex,* vol. 7, pp. 374-385, June 1, 1997 1997.
[120] A. Gevins, "The future of electroencephalography in assessing neurocognitive functioning," *Electroencephalography and Clinical Neurophysiology,* vol. 106, pp. 165-172, 2// 1998.
[121] S. S. Shapiro, "An Analysis of Variance Test for Normality (complete samples)," *Biometrika,* vol. 52, pp. 591-611, 1965 1965.
[122] W. P. Fifer, P. G. Grieve, J. Grose-Fifer, J. R. Isler, and D. Byrd, "High-Density Electroencephalogram Monitoring in the Neonate," *Clinics in Perinatology,* vol. 33, pp. 679-691, 9// 2006.
[123] S. Vanhatalo, M. Metsäranta, and S. Andersson, "High-fidelity recording of brain activity in the extremely preterm babies: Feasibility study in the incubator," *Clinical Neurophysiology,* vol. 119, pp. 439-445, 2// 2008.
[124] S. Stjerna, J. Voipio, M. Metsaranta, K. Kaila, and S. Vanhatalo, "Preterm EEG: a multimodal neurophysiological protocol," *J Vis Exp,* 2012.
[125] P. G. Grieve, R. G. Emerson, J. R. Isler, and R. I. Stark, "Quantitative analysis of spatial sampling error in the infant and adult electroencephalogram," *NeuroImage,* vol. 21, pp. 1260-1274, 4// 2004.
[126] J. S. Ebersole, "Cortical Generators and EEG Voltage Fields," in *Current practice of clinical electroencephalography*, J. S. Ebersole and T. A. Pedley, Eds., 3rd ed Philadelphia: Lippincott Williams & Wilkins, 1997, pp. 107–38.
[127] M. Scherg, N. Ille, H. Bornfleth, and P. Berg, "Advanced tools for digital EEG review: Virtual source montages, whole-head mapping, correlation, and phase analysis," *Journal of Clinical Neurophysiology,* vol. 19, pp. 91-112, 2002.
[128] D. M. Tucker, M. Brown, P. Luu, and M. D. Holmes, "Discharges in ventromedial frontal cortex during absence spells," *Epilepsy & Behavior,* vol. 11, pp. 546-557, 12// 2007.
[129] M. Beauchemin, B. González-Frankenberger, J. Tremblay, P. Vannasing, E. Martínez-Montes, P. Belin, *et al.*, "Mother and stranger: An electrophysiological study of voice processing in newborns," *Cerebral Cortex,* vol. 21, pp. 1705-1711, 2011.
[130] W. J. Freeman and R. Q. Quiroga, *Imaging Brain Function With EEG : Advanced Temporal and Spatial Analysis of Electroencephalographic Signals*. New York, NY: Springer New York, 2013.
[131] S. Vanhatalo, J. Matias Palva, S. Andersson, C. Rivera, J. Voipio, and K. Kaila, "Slow endogenous activity transients and developmental expression of K +-Cl- cotransporter 2 in the immature human cortex," *European Journal of Neuroscience,* vol. 22, pp. 2799-2804, 2005.
[132] W. J. Freeman, L. J. Rogers, M. D. Holmes, and D. L. Silbergeld, "Spatial spectral analysis of human electrocorticograms including the alpha and gamma bands," *Journal of Neuroscience Methods,* vol. 95, pp. 111-121, 2/15/ 2000.
[133] A. Tokariev, K. Palmu, A. Lano, M. Metsäranta, and S. Vanhatalo, "Phase synchrony in the early preterm EEG: Development of methods for estimating synchrony in both oscillations and events," *NeuroImage,* vol. 60, pp. 1562-1573, 4/2/ 2012.
[134] W. J. Freeman, "Origin, structure, and role of background EEG activity. Part 3. Neural frame classification," *Clinical Neurophysiology,* vol. 116, pp. 1118-1129, 5// 2005.

[135] M. T. Colonnese, A. Kaminska, M. Minlebaev, M. Milh, B. Bloem, S. Lescure, *et al.*, "A Conserved Switch in Sensory Processing Prepares Developing Neocortex for Vision," *Neuron,* vol. 67, pp. 480-498, 8/12/ 2010.
[136] A. Clauset, C. R. Shalizi, and M. E. J. Newman, "Power-law distributions in empirical data," *SIAM Review,* vol. 51, pp. 661-703, 2009.
[137] J. S. Barlow, *The electroencephalogram: its patterns and origins*: MIT press, 1993.
[138] C. Ramon, W. J. Freeman, M. Holmes, A. Ishimaru, J. Haueisen, P. H. Schimpf, *et al.*, "Similarities between simulated spatial spectra of scalp EEG, MEG and structural MRI," *Brain Topography,* vol. 22, pp. 191-196, 2009.
[139] S. Toyama, K. Takano, and K. Kansaku, "A non-adhesive solid-gel electrode for a non-invasive brain-machine interface," *Front Neurol,* vol. 3, p. 114, 2012.
[140] G. Drost, D. F. Stegeman, B. G. M. van Engelen, and M. J. Zwarts, "Clinical applications of high-density surface EMG: A systematic review," *Journal of Electromyography and Kinesiology,* vol. 16, pp. 586-602, 12// 2006.
[141] B. Esler, T. Lyons, S. Turovets, and D. Tucker, "Instrumentation for low frequency EIT studies of the human head and its validation in phantom experiments," *Journal of Physics: Conference Series,* vol. 224, p. 012007, 2010.
[142] S. I. Turovets, P. Poolman, A. Salman, A. D. Malony, and D. M. Tucker, "Conductivity analysis for high-resolution EEG," in *BioMedical Engineering and Informatics: New Development and the Future - Proceedings of the 1st International Conference on BioMedical Engineering and Informatics, BMEI 2008*, 2008, pp. 386-393.
[143] R. Kozma, M. Puljic, and W. J. Freeman, "Thermodynamic model of criticality in the cortex based on EEG/ECOG data," *Criticality in Neural Systems,* pp. 153-176, 2012.
[144] D. Plenz and T. C. Thiagarajan, "The organizing principles of neuronal avalanches: cell assemblies in the cortex?," *Trends in Neurosciences,* vol. 30, pp. 101-110, 3// 2007.
[145] A. J. Brockmeier, M. K. Hazrati, W. J. Freeman, L. Lin, and J. C. Principe, "Locating spatial patterns of waveforms during sensory perception in scalp EEG," in *Engineering in Medicine and Biology Society (EMBC), 2012 Annual International Conference of the IEEE*, 2012, pp. 2531-2534.
[146] H. Panagiotides, W. J. Freeman, M. D. Holmes, and D. Pantazis, "Behavioral states may be associated with distinct spatial patterns in electrocorticogram," *Cogn Neurodyn,* vol. 5, pp. 55-66, Mar 2011.
[147] Y. Ruiz, S. Pockett, W. J. Freeman, E. Gonzalez, and G. Li, "A method to study global spatial patterns related to sensory perception in scalp EEG," *Journal of Neuroscience Methods,* vol. 191, pp. 110-118, 8/15/ 2010.
[148] S. L. Bressler and V. Menon, "Large-scale brain networks in cognition: emerging methods and principles," *Trends in Cognitive Sciences,* vol. 14, pp. 277-290, 6// 2010.
[149] U. Zwiener, M. Rother, D. Hoyer, H. Witte, M. Eiselt, and M. Funke, "Experimental and clinical studies of neonatal eeg mapping--methodical prerequisites and data interpretation," *Journal of physiology and pharmacology: an official journal of the Polish Physiological Society,* vol. 42, pp. 235-248, 1991.
[150] P. G. Grieve, J. R. Isler, A. Izraelit, B. S. Peterson, W. P. Fifer, M. M. Myers, *et al.*, "EEG functional connectivity in term age extremely low birth weight infants," *Clinical Neurophysiology,* vol. 119, pp. 2712-2720, 2008.
[151] M. Odabaee, S. Layeghy, M. Mesbah, G. Azemi, B. Boashash, P. Colditz, *et al.*, "EEG amplitude and correlation spatial decay analysis for neonatal head modelling," in *Information Science, Signal Processing and their Applications (ISSPA), 2012 11th International Conference on*, 2012, pp. 882-887.
[152] S. Stjerna, J. Voipio, M. Metsäranta, K. Kaila, and S. Vanhatalo, "Preterm EEG: a multimodal neurophysiological protocol," *Journal of visualized experiments: JoVE,* p. e3774, 2012.
[153] M. Beauchemin, B. González-Frankenberger, J. Tremblay, P. Vannasing, E. Martínez-Montes, P. Belin, *et al.*, "Mother and Stranger: An Electrophysiological Study of Voice Processing in Newborns," *Cerebral Cortex,* vol. 21, pp. 1705-1711, August 1, 2011 2011.
[154] Freeman Walter J., Holmes Mark D. , Burke Brian C., and V. Sampsa, "Spatial spectra of scalp EEG and EMG from awake humans," vol. 114, pp. 1053-1068, June 2003 2003.
[155] A. M. Silau, B. Fischer Hansen, and I. Kjaer, "Normal prenatal development of the human parietal bone and interparietal suture," *Journal of craniofacial genetics and developmental biology,* vol. 15, pp. 81-86, 1995.

[156] B. Esler, T. Lyons, S. Turovets, and D. Tucker, "Instrumentation for low frequency EIT studies of the human head and its validation in phantom experiments," *Journal of Physics: Conference Series,* vol. 224, p. 4, 2010.
[157] S. I. Turovets, P. Poolman, A. Salman, A. D. Malony, and D. M. Tucker, "Conductivity Analysis for High-Resolution EEG," in *BioMedical Engineering and Informatics, 2008. BMEI 2008. International Conference on*, 2008, pp. 386-393.
[158] S. Pant, T. Te, A. Tucker, and R. J. Sadleir, "The conductivity of neonatal piglet skulls," *Physiological Measurement,* vol. 32, pp. 1275-1283, 2011.
[159] S. Vanhatalo, J. Voipio, and K. Kaila, "Full-band EEG (FbEEG): an emerging standard in electroencephalography," *Clinical Neurophysiology,* vol. 116, pp. 1-8, 2005.
[160] J. R. Castro Conde, E. D. Martínez, C. G. Campo, A. M. Pérez, and M. L. McLean, "Positive temporal sharp waves in preterm infants with and without brain ultrasound lesions," *Clinical neurophysiology : official journal of the International Federation of Clinical Neurophysiology,* vol. 115, pp. 2479-2488, 2004.
[161] P. L. Nunez, R. B. Silberstein, Z. Shi, M. R. Carpenter, R. Srinivasan, D. M. Tucker, *et al.*, "EEG coherency II: experimental comparisons of multiple measures," *Clinical Neurophysiology,* vol. 110, pp. 469-486, 1999.
[162] S. Vanhatalo, J. Voipio, A. Dewaraja, M. D. Holmes, and J. W. Miller, "Topography and elimination of slow EEG responses related to tongue movements," *NeuroImage,* vol. 20, pp. 1419-1423, 2003.
[163] S. M. Smith, M. Jenkinson, M. W. Woolrich, C. F. Beckmann, T. E. J. Behrens, H. Johansen-Berg, *et al.*, "Advances in functional and structural MR image analysis and implementation as FSL," *Neuroimage,* vol. 23, Supplement 1, pp. S208-S219, 2004.
[164] C. Ramon, P. Schimpf, and J. Haueisen, "Influence of head models on EEG simulations and inverse source localizations," *Biomedical engineering online,* vol. 5, p. 10, 2006.
[165] F. Tadel, S. Baillet, J. C. Mosher, D. Pantazis, and R. M. Leahy, "Brainstorm: a user-friendly application for MEG/EEG analysis," *Intell. Neuroscience,* vol. 2011, pp. 1-13, 2011.
[166] A. Gramfort, T. Papadopoulo, E. Olivi, and M. Clerc, "OpenMEEG: opensource software for quasistatic bioelectromagnetics," *Biomedical engineering online,* vol. 9, pp. 1-20, 2010.
[167] I. Despotovic, P. J. Cherian, M. De Vos, H. Hallez, W. Deburchgraeve, P. Govaert, *et al.*, "Relationship of EEG sources of neonatal seizures to acute perinatal brain lesions seen on MRI: A pilot study," *Human Brain Mapping,* vol. 34, pp. 2402-2417, 2013.
[168] L. M. Ernst, E. D. Ruchelli, and D. S. Huff, "Color Atlas of Fetal and Neonatal Histology," ed New York, NY: Springer, 2011, pp. 323-336.
[169] M. S. Beauchamp, R. Beurlot Michelle, Fava Eswen, R. Nath Audrey, A. Parikh Nehal, S. Saad Ziad, *et al.*, "The Developmental Trajectory of Brain-Scalp Distance from Birth through Childhood: Implications for Functional Neuroimaging," *PLoS ONE,* vol. 6, p. e24981, 2011.
[170] H. T. Epstein, "Phrenoblysis: Special brain and mind growth periods. I. Human brain and skull development," *Developmental Psychobiology,* vol. 7, pp. 207-216, 1974.
[171] A. Christie, "Prevalence and distribution of ossification centers in the newborn infant," *Am J Dis Child,* vol. 77, pp. 355-61, Mar 1949.
[172] J. J. González, S. Mañas, L. De Vera, L. D. Méndez, S. López, J. M. Garrido, *et al.*, "Assessment of electroencephalographic functional connectivity in term and preterm neonates," *Clinical Neurophysiology,* vol. 122, pp. 696-702, 2011.
[173] A. Omidvarnia, P. Fransson, M. Metsäranta, and S. Vanhatalo, "Functional Bimodality in the Brain Networks of Preterm and Term Human Newborns," *Cerebral Cortex,* 2013 May 5 2013.
[174] J. M. Palva, S. Monto, S. Kulashekhar, and S. Palva, "Neuronal synchrony reveals working memory networks and predicts individual memory capacity," *Proceedings of the National Academy of Sciences,* vol. 107, pp. 7580-7585, April 20, 2010 2010.
[175] J.-M. Schoffelen and J. Gross, "Source connectivity analysis with MEG and EEG," *Human Brain Mapping,* vol. 30, pp. 1857-1865, 2009.
[176] S. Vanhatalo, A. Alnajjar, V. T. Nguyen, P. Colditz, and P. Fransson, "Safety of EEG–fMRI recordings in newborn infants at 3T: A study using a baby-size phantom," *Clinical Neurophysiology,* 2013.
[177] B. Hellström, B. Karlsson, and H. Müssbichler, "Electrode placement in EEG of infants and its anatomical relationship studied radiographically," *Electroencephalography and Clinical Neurophysiology,* vol. 15, pp. 115-117, 1963.

[178] M. G. Welch, M. M. Myers, P. G. Grieve, J. R. Isler, W. P. Fifer, R. Sahni, *et al.*, "Electroencephalographic activity of preterm infants is increased by Family Nurture Intervention: A randomized controlled trial in the NICU," *Clinical Neurophysiology,* vol. 125, pp. 675-684, 4// 2014.
[179] S. Vanhatalo and K. Kaila, "Development of neonatal EEG activity: From phenomenology to physiology," *Seminars in Fetal and Neonatal Medicine,* vol. 11, pp. 471-478, 2006.
[180] R. Khazipov and H. J. Luhmann, "Early patterns of electrical activity in the developing cerebral cortex of humans and rodents," *Trends in Neurosciences,* vol. 29, pp. 414-418, 7// 2006.
[181] M. D. Brockmann, B. P. schel, N. Cichon, and I. L. Hanganu-Opatz, "Coupled Oscillations Mediate Directed Interactions between Prefrontal Cortex and Hippocampus of the Neonatal Rat," *Neuron,* vol. 71, pp. 332-347, 7/28/ 2011.
[182] W. Kilb, S. Kirischuk, and H. J. Luhmann, "Electrical activity patterns and the functional maturation of the neocortex," *Eur J Neurosci,* vol. 34, pp. 1677-1686, 2011/11// 2011.
[183] E. A. Tolner, A. Sheikh, A. Y. Yukin, K. Kaila, and P. O. Kanold, "Subplate neurons promote spindle bursts and thalamocortical patterning in the neonatal rat somatosensory cortex," *J Neurosci,* vol. 32, pp. 692-702, Jan 11 2012.
[184] K. Gröchenig, *Foundations of time-frequency analysis*. Boston, MA: Springer, 2001.
[185] P. Flandrin, *Time-frequency / time-scale analysis* vol. 10. London: Academic Press, 1999.
[186] L. Cohen, "Time-frequency distributions-a review," *Proceedings of the IEEE,* vol. 77, pp. 941-981, 1989.
[187] F. Hlawatsch and G. F. Boudreaux-Bartels, "Linear and quadratic time-frequency signal representations," *Signal Processing Magazine, IEEE,* vol. 9, pp. 21-67, 1992.
[188] B. Boashash, Ed., *Time frequency signal analysis and processing: A comprehensive reference* (Elsevier Amsterdam, Boston, 2003, p.^pp. Pages.
[189] W. Martin and P. Flandrin, "Wigner-Ville spectral analysis of nonstationary processes," *Acoustics, Speech and Signal Processing, IEEE Transactions on,* vol. 33, pp. 1461-1470, 1985.
[190] T. Classen and W. F. G. Mecklenbrauker, "The Wigner Distribution: A Tool for Time-Frequency Signal Analysis - Part 1: -Time Signals," *Philips Journal of Research,* vol. 35, pp. 276-350, 1980 1980.
[191] F. Auger and É. Chassande-Mottin, "Quadratic Time-Frequency Analysis I: Cohen's Class," in *Time-Frequency Analysis*, ed: ISTE, 2010, pp. 131-163.
[192] A. V. Oppenheim, A. S. Willsky, and S. H. Nawab, *Signals and systems* vol. 2. Englewood Cliffs, NJ, USA: Prentice-Hall 1983.
[193] B. Boashash, "Note on the use of the Wigner distribution for time-frequency signal analysis," *Acoustics, Speech and Signal Processing, IEEE Transactions on,* vol. 36, pp. 1518-1521, 1988.
[194] S. L. Hahn, *Hilbert Transforms in Signal Processing*. London: Artech House, 1996.
[195] J. Ville, "Théorie et applications de la notion de signal analytique," *Cables et transmission,* vol. 2, pp. 61-74, 1948.
[196] L. Cohen, *Time-frequency analysis: theory and applications*: Prentice-Hall, Inc., 1995.
[197] T. Classen and W. F. G. Mecklenbrauker, "The Wigner Distribution: A Tool for Time-Frequency Signal Analysis - Part 2: Discrete-Time Signals," *Philips Journal of Research,* vol. 35, pp. 276-350, // 1980.
[198] F. Hlawatsch and W. Kozek, "The Wigner distribution of a linear signal space," *Signal Processing, IEEE Transactions on,* vol. 41, pp. 1248-1258, 1993.
[199] P. K. Banerjee and R. Butterfield, *Boundary element methods in engineering science* vol. 17: McGraw-Hill London, 1981.
[200] O. C. Zienkiewicz and P. Morice, *The finite element method in engineering science* vol. 1977: McGraw-hill London, 1971.
[201] C. M. Michel, M. Seeck, and M. M. Murray, "The speed of visual cognition," *Supplements to Clinical neurophysiology,* vol. 57, pp. 617-627, 2003.
[202] J. J. Foxe, M. E. McCourt, and D. C. Javitt, "Right hemisphere control of visuospatial attention: line-bisection judgments evaluated with high-density electrical mapping and source analysis☆," *Neuroimage,* vol. 19, pp. 710-726, 2003.
[203] O. Seong Keun and U. Chong, "A Sequential Estimation Approach for Performance Improvement of Eigenstructure-Based Methods in Array Processing," *Signal Processing, IEEE Transactions on,* vol. 41, p. 457, 1993.
[204] P. Stoica, P. Handel, and A. Nehoral, "Improved sequential MUSIC," *Aerospace and Electronic Systems, IEEE Transactions on,* vol. 31, pp. 1230-1239, 1995.

[205] S. L. Gonzalez Andino, R. Grave de Peralta Menendez, C. M. Lantz, O. Blank, C. M. Michel, and T. Landis, "Non-stationary distributed source approximation: An alternative to improve localization procedures," *Human brain mapping*, vol. 14, pp. 81-95, 2001.

[206] Z. Yimin, M. Weifeng, and M. G. Amin, "Subspace analysis of spatial time-frequency distribution matrices," *Signal Processing, IEEE Transactions on*, vol. 49, pp. 747-759, 2001.

[207] S. Vanhatalo, J. Voipio, and K. Kaila, "Full-band EEG (FbEEG): an emerging standard in electroencephalography," *Clinical neurophysiology : official journal of the International Federation of Clinical Neurophysiology*, vol. 116, pp. 1-8, 2005.

[208] S. Haufe, V. V. Nikulin, K.-R. Müller, and G. Nolte, "A critical assessment of connectivity measures for EEG data: A simulation study," *NeuroImage*, vol. 64, pp. 120-133, 1/1/ 2013.

[209] J. C. Mosher, S. Baillet, F. Darvas, D. Pantazis, and R. M. Leahy, "Brainstorm electromagnetic imaging software," *International Journal of Bioelectromagnetism* vol. 7, p. 2, 2005.

[210] A. Gramfort, T. Papadopoulo, E. Olivi, and M. Clerc, "OpenMEEG: opensource software for quasistatic bioelectromagnetics," *BioMedical Engineering OnLine*, vol. 9, p. 45, 2010.

[211] B. Boashash and T. Ben-Jabeur, "Design of a high-resolution separable-kernel quadratic TFD for improving newborn health outcomes using fetal movement detection," in *Information Science, Signal Processing and their Applications (ISSPA), 2012 11th International Conference on*, 2012, pp. 354-359.

[212] J. M. O'Toole, M. Mesbah, and B. Boashash, "A computationally efficient implementation of quadratic time-frequency distributions," in *Signal Processing and Its Applications, 2007. ISSPA 2007. 9th International Symposium on*, 2007, pp. 1-4.

[213] J. M. O' Toole and B. Boashash, "Fast and memory-efficient algorithms for computing quadratic time–frequency distributions," *Applied and Computational Harmonic Analysis*, vol. 35, pp. 350-358, 2013.

[214] J. Yao and J. P. A. Dewald, "Evaluation of different cortical source localization methods using simulated and experimental EEG data," *NeuroImage*, vol. 25, pp. 369-382, 4/1/ 2005.

[215] J. C. Mosher, M. E. Spencer, R. M. Leahy, and P. S. Lewis, "Error bounds for EEG and MEG dipole source localization," *Electroencephalogr Clin Neurophysiol*, vol. 86, pp. 303-21, May 1993.

[216] B. Neil Cuffin and D. Cohen, "Comparison of the magnetoencephalogram and electroencephalogram," *Electroencephalography and Clinical Neurophysiology*, vol. 47, pp. 132-146, 8// 1979.

[217] D. Cohen and B. N. Cuffin, "Demonstration of useful differences between magnetoencephalogram and electroencephalogram," *Electroencephalography and Clinical Neurophysiology*, vol. 56, pp. 38-51, 7// 1983.

[218] B. N. Cuffin, "Effects of measurement errors and noise on MEG moving dipole inverse solutions," *IEEE Trans Biomed Eng*, vol. 33, pp. 854-61, Sep 1986.

[219] J. C. Mosher, P. Lewis, and R. Leahy, "Spatial localization of neural sources using the magnetoencephalogram," in *Spectrum Estimation and Modeling, 1990., Fifth ASSP Workshop on*, 1990, pp. 289-293.

[220] O. Oshiro, M. Mukai, F. Takeuchi, and S. Kuriki, "Analysis of errors in neuromagnetic localization of multiple current dipole sources," *Physics in Medicine and Biology*, vol. 37, p. 845, 1992.

[221] R. Pascal-Marqui, "Standardized low-resolution brain electromagnetic tomography (sLORETA): Technical details," *Methods Findings Exp Clin Pharmacol*, p. 8, 2002.

[222] T. Kohler, M. Wagner, M. Fuchs, H. Wischmann, x, A, *et al.*, "Depth normalization in MEG/EEG current density imaging," in *Engineering in Medicine and Biology Society, 1996. Bridging Disciplines for Biomedicine. Proceedings of the 18th Annual International Conference of the IEEE*, 1996, pp. 812-813 vol.2.

[223] B. Jeffs, R. Leahy, and M. Singh, "An Evaluation of Methods for Neuromagnetic Image Reconstruction," *Biomedical Engineering, IEEE Transactions on*, vol. BME-34, pp. 713-723, 1987.

[224] A. M. Dale, A. K. Liu, B. R. Fischl, R. L. Buckner, J. W. Belliveau, J. D. Lewine, *et al.*, "Dynamic Statistical Parametric Mapping: Combining fMRI and MEG for High-Resolution Imaging of Cortical Activity," *Neuron*, vol. 26, pp. 55-67, 4// 2000.

[225] D. Regan, "Electrical responses evoked from the human brain," *Scientific American*, vol. 241, pp. 134-146, 1979/12// 1979.

[226] M. P. Regan and D. Regan, "A frequency domain technique for characterizing nonlinearities in biological systems," *Journal of Theoretical Biology*, vol. 133, pp. 293-317, 8/7/ 1988.

[227] D. J. Creel, "Visually Evoked Potentials," in *Webvision: The Organization of the Retina and Visual System*, ed US: National Library of Medicine, 2007.

[228] M. J. Aminoff and D. S. Goodin, "Visual evoked potentials," *J Clin Neurophysiol*, vol. 11, pp. 493-9, Sep 1994.
[229] X. Xiao-Liang, X. Bobby, and H. Bin, "An alternative subspace approach to EEG dipole source localization," *Physics in Medicine and Biology*, vol. 49, p. 327, 2004.

Appendix -1

The procedure for localizing multiple sources with overlapping signature in the time-frequency plane necessitates knowing the number of sources in the ROI. The averaged TFD of a 64-channels EEG with overlapping signature in time-frequency domain is depicted in Figure A1-a. The ROI was identified by the TF-MUSIC algorithm automatically which is depicted in Figure A1-b.

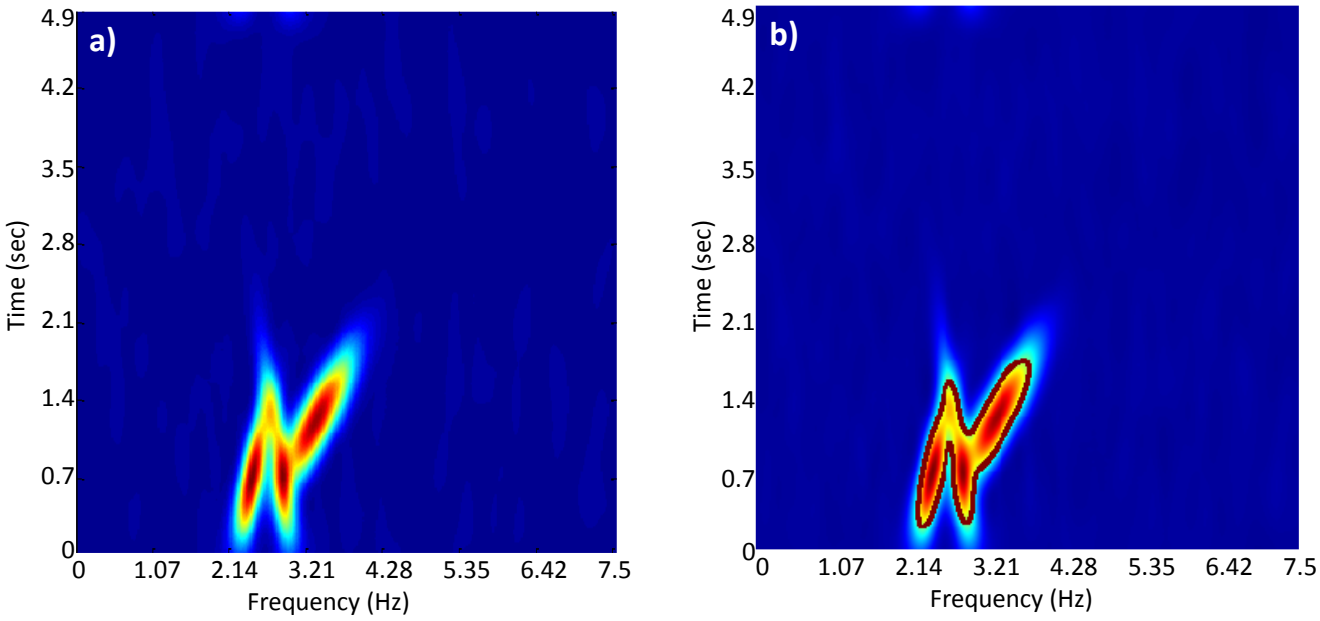

Figure A1 - a) The averaged TFD of a 64-channels simulated EEG using 3 sources with SNR = 0 dB and source parameters Kesi =[0.15 0.14 0.25], Alpha =[-23 -13 55], Rho =[0.1 0.2 0.1], Beta =[-50 70 50], K =[2.2 1.6 2.6] and Epsilon =[0 0 0] b) The ROI identified automatically includes the 3 sources whose signatures are overlapping

The result of applying the TF-MUSIC algorithm on the above simulated EEG is depicted in Figure A2. The magnitude of the TF-MUSIC output, i.e., the localization function was normalized by dividing on its maximum and mapped over source space. This means the value of TF-MUSIC metric for each source location (nodes of the mesh which spanned over the brain) was directly illustrated using a color as depicted in Figure A2.

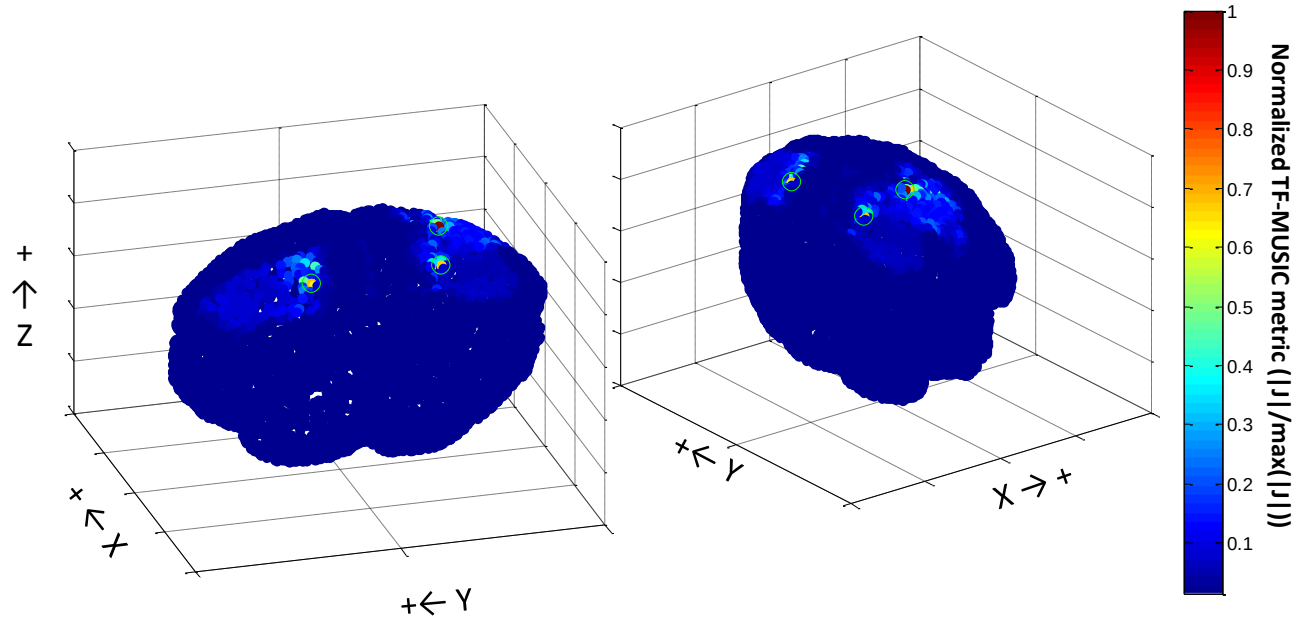

Figure A2 - The output of TF-MUSIC algorithm from two different view angles. Results for the EEG generated using 3 sources with overlapping signature in the time-frequency plane. The magnitude of the TF-MUSIC metric was normalized and mapped to the source space (the mesh spanned over the brain). The green circles indicate the location of the original sources.

As seen, the first three values of the TF-MUSIC metric has happened in the location of the original sources (designated using green circles).